REDUCTION OF DEXTRAN CONTAMINATION IN RAW SUGAR PRODUCTION

Arwut Promraksa

A Thesis Submitted in Partial Fulfillment of the Requirements for the

Degree of Doctor of Philosophy in Chemical Engineering

Suranaree University of Technology

Academic Year 2008

การลดปริมาณการเจือปนของเดกซ์แทรนในกระบวนการผลิตน้ำตาลทรายดิบ

นายอาวุธ พรหมรักษา

วิทยานิพนธ์นี้เป็นส่วนหนึ่งของการศึกษาตามหลักสูตรปริญญาวิศวกรรมศาสตรดุษฎีบัณฑิต
สาขาวิชาวิศวกรรมเคมี
มหาวิทยาลัยเทคโนโลยีสุรนารี
ปีการศึกษา 2551

REDUCTION OF DEXTRAN CONTAMINATION IN RAW SUGAR PRODUCTION

Suranaree University of Technology has approved this thesis submitted in partial fulfillment of the requirements for the Degree of Doctor of Philosophy.

Thesis Examining Committee

_____

(Dr. Terasut Sookkumnerd)

Chairperson

_____

(Assoc. Prof. Dr. Adrian Flood)

Member (Thesis Advisor)

_____

(Assoc. Prof. Dr. Kenneth Haller)

Member

_____

(Asst. Prof. Dr. Chalongsri Flood)

Member

_____

(Asst. Prof. Dr. Sopark Sonwai)

Member

_____

(Prof. Dr. Pairote Sattayatham)

Vice Rector for Academic Affairs

_____

(Assoc. Prof. Dr. Vorapot Khompis)

Dean of Institute of Engineering

อาวุธ พรหมรักษา : การลดปริมาณการเจือปนของเดกซ์แทรนในกระบวนการผลิตน้ำตาลทรายดิบ (REDUCTION OF DEXTRAN CONTAMINATION IN RAW SUGAR PRODUCTION) อาจารย์ที่ปรึกษา : รศ. ดร.เอเดรียน ฟลัด, 238 หน้า.

ผลึกน้ำตาลเจือปนด้วยเดกซ์แทรนได้เป็นปัญหาที่สำคัญประการหนึ่งในกระบวนการผลิตน้ำตาลทรายดิบ งานวิจัยนี้จึงได้พยายามลดการเจือปนนี้โดยวิธีการกรองน้ำอ้อยใส (Clarified juice) ที่ซึ่งจะถูกทำให้เข้มข้นเพื่อใช้ในการตกผลึกต่อไปด้วยเยื่อเลือกผ่าน (Membrane) และโดยการหาสภาวะที่เหมาะสมในกระบวนการตกผลึก การวิจัยเริ่มจากการพัฒนาวิธีการตรวจวัดเดกซ์แทรนในตัวอย่างด้วยเทคนิคทางนิวเคลียร์แมกเนติกเรโซแนนซ์ (Nuclear Magnetic Resonance) แต่ปรากฏว่าวิธีการนี้ไม่เหมาะสมที่จะตรวจวัดเดกซ์แทรนที่ความเข้มข้นต่ำ จึงไม่ได้ถูกนำไปใช้ในการทดลองอื่นที่เกี่ยวเนื่องกับการหาวิธีการลดการเจือปนของเดกซ์แทรนโดยการกรองหรือการตกผลึก การกรองด้วยเยื่อเลือกผ่านถูกใช้ในระบบเดดเอนด์ (Dead-end) โดยที่การกวนภายในเครื่องกรองถูกนำมาใช้เพื่อลดการอุดตันของเยื่อเลือกผ่าน (Fouling) และการเกิดปรากฏการณ์คอนเซนเทรชันโพลาไรเซชัน (Concentration polarization) สารละลายจำลองน้ำอ้อยใสถูกเตรียมโดยการละลายน้ำตาลซูโครส 15% บริกซ์ (Brix) เจือปนด้วยเดกซ์แทรน 5,000 ส่วนในล้านส่วนของบริกซ์ (ppm/Brix) เยื่อเลือกผ่านพอลิอิเทอร์ซัลโฟน (Polyethersulfone) และ รีเจนเนอเรตเตดเซลลูโลส (Regenerated cellulose) ขนาดรูเลือกผ่าน (MWCO) ตั้งแต่ 5,000 ดาลตัน ถึง 30,000 ดาลตัน ถูกใช้ในการกรองนี้ สภาวะต่าง ๆ ในการกรองถูกปรับเปลี่ยน เช่น ความดันผ่านเยื่อเลือกผ่านปรับในช่วง 1 ถึง 3 บาร์, อัตราการกวน 100 รอบต่อนาทีและ 200 รอบต่อนาที จากผลทดลองพบว่าเยื่อเลือกผ่านรีเจนเนอเรตเตดเซลลูโลสขนาดรูเลือกผ่าน 5,000 ดาลตัน มีความสามารถแยกเดกซ์แทรนออกจากสารละลายน้ำตาลสูงที่สุด โดยที่อัตราการไหลผ่านเยื่อเลือกผ่านสามารถยอมรับได้ ทั้งความสามารถในการแยกเดกซ์แทรนและอัตราการไหลผ่านเยื่อเลือกผ่าน สามารถปรับปรุงให้ดีขึ้นด้วยการเพิ่มอัตราเร็วในการกวน ในขณะที่การเพิ่มความดันผ่านเยื่อเลือกผ่านทำได้เพียงเพิ่มอัตราการไหล ทั้งเยื่อเลือกผ่านพอลิอิเทอร์ซัลโฟนและรีเจนเนอเรตเตดเซลลูโลสขนาดรูเลือกผ่าน 5,000 ดาลตันถูกนำมาใช้ในการทดลองในระบบการกรองแบบเดดเอนด์ ทั้งที่มีการกวนและปราศจากการกวนเพื่อศึกษากลไกการอุดตัน จากการทดลองพบว่าระบบการกรองที่ปราศจากการกวนการอุดตันเป็นแบบการสะสมของเดกซ์แทรนบนผิวของเยื่อเลือกผ่าน (Cake formation) ส่วนระบบการกรองที่มีการกวนการอุดตันเป็นแบบการปิดรูเลือกผ่านอย่างสนิท (Complete pore blocking) ในการทดลองโดยการปรับเปลี่ยนสภาวะในการตกผลึกน้ำตาลจากสารละลายจากการปรับเปลี่ยนอุณหภูมิ ความเข้มข้นของสารละลายน้ำตาลและ ความเข้มข้นของการเจือปนด้วยเดกซ์แทรน จากการวิเคราะห์หาค่าสัมประสิทธิ์การเข้าไปเจือปนในผลึกโดยเดกซ์แทรนจากสารละลาย พบว่าค่า

สัมประสิทธิ์การเข้าไปเจือปนในผลึกระหว่างการตกผลึก มีความสัมพันธ์กับอัตราการตกผลึกอย่างชัดเจน ได้ความสัมพันธ์ว่า $K_{eff}[\%] = (9.8 \pm 1.0) \times \left(1 - \exp^{(-1.7 \pm 0.4)G}\right)$ กลไกการเข้าไปเจือปนของเดกซ์แทรนในผลึกน้ำตาลสามารถอธิบายด้วยกลไกการดูดซับโดยผิวของผลึก (Surface adsorption) และการแทรกตัวภายในผลึกด้วยของเหลว (Liquid inclusion) กลไกการดูดซับโดยผิวของผลึกจะเกิดได้ง่ายสำหรับการตกผลึกด้วยอัตราการตกผลึกสูงเนื่องจากผลึกที่ได้จากการตกผลึกด้วยอัตรานี้จะมีผิวไม่เรียบทำให้พื้นที่ในการดูดซับเดกซ์แทรนมีมาก

สาขาวิชาวิศวกรรมเคมี ลายมือชื่อนักศึกษา _____

ปีการศึกษา 2551 ลายมือชื่ออาจารย์ที่ปรึกษา _____

ARWUT PROMRAKSA : REDUCTION OF DEXTRAN CONTAMINATION IN RAW SUGAR PRODUCTION.
THESIS ADVISOR : ASSOC. PROF. ADRIAN FLOOD, Ph.D., 238 PP.

SUGAR PRODUCTION/SUCROSE/DEXTRAN/IMPURITY/ MEMBRANE SEPARATION/ULTRAFILTRATION/ CRYSTALLIZATION

The problems relating to the presence of dextran in the sugar production process have been a concern for many years. The major concern is raw sugar product contaminated with dextran, and this study aims to reduce this contamination. The objective of the study is dextran reduction either in a stage after the clarification of the juice or in the stage of sugar crystallization. Both membrane filtration and crystallization are expected to be possible techniques for dextran reduction in the sugar production process. In the first part of the study a Nuclear Magnetic Resonance (NMR) technique for the determination of dextran content is developed, however since there is a constraint in its detection limit, it is not considered for further use in the studies on dextran reduction. Membrane separation was performed using a dead-end ultrafiltration operation with a stirring bar placed just above the surface of the membrane to reduce fouling and concentration polarization. Ultrafiltration (UF) was investigated to separate dextran from a synthetic clarified juice made by dissolving 15% Brix of sucrose containing 5,000 ppm/Brix of dextran. Commercial polyethersulfone (PES) and regenerated cellulose (RC) membranes with a variety of pore sizes (MWCO 5,000 Da-30,000 Da) were used in the filtration. The operating

conditions were adjusted, including transmembrane pressures (TMP) in the range of 1-3 bar, and agitation speeds of 100 rpm and 200 rpm. It was found that the 5,000 MWCO RC membrane has a larger dextran rejection than that of the other membranes, while its flux is suitable. Both percent rejection and flux can be improved by increasing agitation, while increasing the TMP improves only the flux. Both membrane materials with 5,000 MWCO were used in a membrane fouling study for unstirred and stirred dead-end filtration. It is seen that the mechanism of membrane fouling for unstirred filtration is controlled by cake filtration, while fouling for the filtration with agitation at 100 rpm is described by the complete pore blocking model. Temperature, supersaturation, and dextran concentration were varied for the study of dextran partition during sucrose crystallization. It is seen that the dextran partition coefficient between the liquid phase and the crystalline phase has a significant correlation with the crystal growth rate. The relationship between the partition coefficient and the growth rate is $K_{eff}[\%] = (9.8 \pm 1.0) \times \left(1 - \exp^{(-1.7 \pm 0.4)G}\right)$. The dextran incorporation mechanism is described by both the crystal surface adsorption and the liquid inclusion. Adsorption becomes more significant at higher growth rates since higher growth rates lead to a rougher crystal surface, resulting in increased surface area and sites for adsorption.

School of Chemical Engineering Student's signature _____

Academic Year 2008 Advisor's signature _____

ACKNOWLEDGEMENTS

I wish to thank many people who have contributed through the duration of my Ph.D. study. Firstly, grateful thanks and appreciation are given to the thesis advisor, Assoc. Prof. Dr. Adrian Flood for providing me with the opportunity to undertake the Royal Golden Jubilee (RGJ) Ph.D. Program, and for giving suggestions in the research planning through the thesis preparation. Secondly the thanks go to Dr. Philip Schneider who is co-advisor for his valuable suggestions and guidance during my study at James Cook University (JCU), Townsville, Australia. Thanks also go to the thesis examination committees, Dr. Terasut Sookkumnerd, Asst. Prof. Dr. Sopark Sonwai, Asst. Prof. Dr. Chalongsri Flood, Assoc. Prof. Dr. Kenneth Haller, and my advisor for good commenting during the examination. Finally, I would like to thank all academic staff in the School of Chemical Engineering, Suranaree University of Technology (SUT). Special appreciation goes to Asst. Prof. Dr. Chalongsri Flood for giving me a good background in mass transport that is essential for applying to the research.

I would like to thank the School of Chemical Engineering, SUT, and JCU, for supporting the equipment required for the research. Essentially, I would like to acknowledge the financial support of the Thailand Research Fund (TRF) through the RGJ, scholarship number 1.C.TS/46/B.1 for supporting me and for research funding.

Arwut Promraksa

TABLE OF CONTENTS

Page

TABLE OF CONTENTS (Continued)

Page

TABLE OF CONTENTS (Continued)

Page

TABLE OF CONTENTS (Continued)

Page

TABLE OF CONTENTS (Continued)

Page

TABLE OF CONTENTS (Continued)

Page

TABLE OF CONTENTS (Continued)

Page

TABLE OF CONTENTS (Continued)

Page

LIST OF TABLES

Table **Page**

LIST OF TABLES (Continued)

Table **Page**

LIST OF TABLES (Continued)

LIST OF TABLES (Continued)

LIST OF FIGURES

Figure **Page**

LIST OF FIGURES (Continued)

Figure **Page**

LIST OF FIGURES (Continued)

Figure **Page**

LIST OF FIGURES (Continued)

Figure **Page**

SYMBOLS AND ABBREVIATIONS

Symbols

A = membrane area, m^2

A_b = the blocked area of membrane per volume of filtrate, m^{-1}

A_c = the crystal surface area, m^2

a = the open pore area of membrane, m^2

a_0 = the open pore area of membrane at time = 0, m^2

B = the removal rate of solute above the membrane surface, s^{-1}

C = concentration of supersaturated solution, g of solute/g of solution

C^* = the solubility, g of solute/g of solution

C_B = bulk concentration, g/m^3

C_C = the concentration at cake solution interface, g/m^3

C_b = bulk concentration, g/m^3

C_f = concentration of the feed solution, g/m^3

C_i = concentration at the crystal-solution interface, g/m^3

C_p = concentration of the permeate, g/m^3

C_{sp} = dextran concentration in the sugar product, ppm

C_m = dextran concentration in the solution, ppm/Brix

C_s = the concentration of the solute, g/m^3

c_i = the concentration of component i, g/m^3

D = dextran concentration, ppm

D_i = the diffusion coefficient of component i, m^2/s

SYMBOLS AND ABBREVIATIONS (Continued)

D_s = the diffusion coefficient of the solute, m^2/s

d = membrane pore diameter, m

E_A = the activation energy, kJ/ mol

G = growth rate of the crystal, m/s

I = the NMR Peak integral

J = the permeate flux, m/s

J^* = a critical flux, m/s

J_0 = the initial flux, m/s

J_a = the flux after long-term fouling, m/s

J_i = the mass flux of component i, $g/m^2 \cdot s$

J_{lim} = the limiting flux, m/s

J_s = the mass flux of solute, $g/m^2 \cdot s$

K = the equilibrium thermodynamic, -

K' = a coefficient reflecting of the membrane pore and the solute, $m^4/N \cdot s$

K_{eff} = the partition coefficient between the solution and the crystal, -

k = fitting parameter for membrane fouling model, (s/m^2, m^{-1}, $(m \cdot s)^{-0.5}$, and s^{-1} depending on the mechanism of fouling)

k_0 = fitting parameter for cake filtration, s/m^2

k_1 = fitting parameter for partial pore blocking, m^{-1}

$k_{1.5}$ = fitting parameter for internal pore blocking, $(m \cdot s)^{-0.5}$

k_2 = fitting parameter for complete pore blocking, s^{-1}

SYMBOLS AND ABBREVIATIONS (Continued)

k_c	=	the cake filtration constant, g/m^3
k_d	=	the ratio of diffusion coefficient and boundary thickness, m/s
k_r	=	surface reaction rate constant, m/s
k_s	=	the mass transfer coefficient of the solute, m^2/s
$\bar{L}$	=	mean size of product crystal, μm
m_c	=	the crystal mass, g
m_{dc}	=	the dry cake mass accumulation per unit area, g/m^2
N	=	number of crystal, -
n	=	the exponent for membrane fouling model or the power for power-law of crystal growth rate, -
ΔP	=	the transmembrane pressure, N/m^2
p	=	pressure, N/m^2
R	=	the ideal gas constant, 8.314 kJ·K/mol
R_c	=	the resistance of the cake layer, m^{-1}
R_{cp}	=	the resistance due to concentration polarization, m^{-1}
R_f	=	the resistance due to fouling, m^{-1}
R_m	=	the membrane resistance, m^{-1}
s	=	the cake compressibility, -
T	=	temperature, °C
t	=	time, s
v	=	the volume of filtrate, m^3
W	=	weight of crystal product, g

SYMBOLS AND ABBREVIATIONS (Continued)

x	=	position from the membrane surface or the crystal surface, m
α	=	the specific cake resistance per unit mass, m/g
α_0	=	constant
δ	=	boundary layer thickness, m
ε	=	porosity, -
ε_0	=	the clean membrane porosity, -
ℓ	=	membrane pore length, m
μ	=	viscosity, $N/m^2 \cdot s$
$\Delta\pi$	=	the transmembrane pressure, N/m^2
ρ_c	=	the crystal density, g/m^3
σ	=	relative supersaturation, -
σ_c	=	a complex temperature dependent constant, -

SYMBOLS AND ABBREVIATIONS (Continued)

Abbreviations

ACS	=	American chemical society
ASI	=	Audubon sugar institute
BCF	=	Burton-Cabrera-Frank
CCG	=	constant crystal growth
CSD	=	crystal size distribution
CSR	=	commonwealth sugar refineries
Da	=	Daltons
DS	=	dry substance
ED	=	electrodialysis
GPC	=	Gel permeation chromatography
GRD	=	growth rate dispersion
I	=	impurity
L	=	liquid
MAU	=	milliabsorbance units
MF	=	microfiltration
MW	=	molecular weight
MWCO	=	molecular weight cut-off
NF	=	nanofiltration
NMR	=	nuclear magnetic resonance
OCA	=	optical contact angle

SYMBOLS AND ABBREVIATIONS (Continued)

PES	=	polyethersulfone
PV	=	pervaporation
ppm	=	part per million
RC	=	regenerated cellulose
RF	=	random fluctuation
RFR	=	relative flux reduction
RO	=	reverse osmosis
rpm	=	revolution per minute
S	=	Sucrose
SD	=	standard deviation
SEM	=	scanning electron microscopy
SNT	=	the secondary nucleation thresholds
SW	=	sugar to water ratio
TMP	=	transmembrane pressure
UF	=	ultrafiltration
W	=	water

CHAPTER I

INTRODUCTION

1.1 Sugar Manufacturing and Dextran Contamination

Sugar manufacturing and refining plants are usually located near the centre of crop growing areas. Sugar cane and sugar beet are the main sources of sugar production in the world. In more than 60% of the sugar manufacture in the world, the sugar is produced from extraction of sugar from sugar cane; the balance is produced from sugar beet. In the first stage of the cane sugar production processes, the sucrose-rich juice is extracted from sugar cane which contains approximately 70% water, 14% fiber, 13.3% saccharose (mostly sucrose), and 2.7% soluble impurities (World Bank Group, 2009). These impurities have an affect on the production processes and present problems in sugar production processes. Normally, production of sucrose from cane sugar is performed exclusively in tropical and subtropical countries (Wikipedia, 2009). Sugar cane cultivation is usually propagated from cuttings rather than seed growth. The cane is often planted from cutting by hand then the cane will make up new stalks, called ratoons (Wikipedia, 2009). Sugar cane is harvested either by hand, or mechanically depending on the level of development of the country and the wage levels of the necessary laborers. When the cane is harvested by hand, the cane field is sometimes burned, so the standing cane can be easily cut just above ground level, and then the harvested cane is delivered to the mill. This practice is falling out of favor as it reduces the amount of nutrients that are returned to the soil. Delays between harvesting and milling should be as short as possible since delays

result in loss of sucrose due to cane deterioration.

Sugar cane deterioration is caused by enzymatic, chemical, and microbial processes (Irvine, 1993). For example, invert sugars (glucose and fructose) are usually produced by inversion of sucrose under acidic conditions by enzyme invertase. Microbial deterioration is mostly caused by bacteria of the *Leuconostoc* species that are common in soil. *Leuconostoc* bacteria can invade the cane stalk tissue where it is exposed by cutting or mechanical damage in the harvesting season. The degradation of sucrose and the formation of dextran are caused by the enzyme dextransucrase, which is produced in harvested cane by the *Leuconostoc* bacteria (Chen and Chou, 1993). Dextran formation usually occurs during the period of cane cutting and grinding (Irvine, 1993). In practice, a minimum time for delivery of harvested cane to the mill and initiation of the milling process is required to reduce the formation of dextran.

There are many problems in cane sugar production processes that are caused or made worse by the presence of dextran in syrup (Cuddihy *et al.*, 2001). Since dextran is formed by polymerization of a large number of glucose molecules from degraded sucrose, hence the chain propagation of dextran molecules results in a large sucrose loss. There are many processes such as evaporation of cane juice and crystallization of sucrose that operate at lower expected efficiency if dextran is present, due to increased viscosity in the syrup or mesquite. A low quality raw sugar product contaminated with dextran is often blamed for poor quality refined sugar, both by domestic and overseas customers, because dextran changes the relative facial growth rates resulting in a significant elongation of crystals during sugar refining. The elongated crystals, needle-shape grain are primarily caused by dextran (Vaccari

and Mantovani, 1995). Since it is necessary to reduce the dextran content in the raw sugar product, purification operations such as membrane filtration and crystallization have been studied in order to obtain reasonable improvement in the raw sugar production processes.

1.2 Study Motivation and Research Objectives

Most of the impurities in the raw sugar production process can be eliminated by sedimentation of mud, in the clarifier. The waste product containing various types of large impurities, called mud, is formed by flocculating the juice with lime. However, some remaining polysaccharides, such as starch and dextran, may not be totally removed, and may have a detrimental effect on the downstream processes. There are many publications involving the effect of dextran presence on sugar production, and test methods that have been developed to analyze dextran in sugar.

In this study, test methods from the literature were reviewed and improved for the research. Carbon-13 nuclear magnetic resonance (^{13}C NMR) is the fundamental technique used in dextran analysis method improvement. Two main purification methods, ultrafiltration and crystallization, were investigated for the reduction of dextran contamination in raw sugar product. A reasonable membrane (in terms of material type and pore size) is necessary to test the flux and the rejection of dextran during ultrafiltration process. In addition, membrane fouling and cake compressibility were also determined to fully characterize the viability of the process for removing dextran from raw juice. In the sucrose crystallization process, possible mechanisms of impurity (dextran) incorporation into sugar crystal during the process were explained in order that the study on dextran partition coefficient between the mother liquor and

the sugar crystal can be modeled. The dextran partition in crystallization is investigated under various conditions of dextran level, supersaturation, and temperature to determine the feasibility of dextran reduction in the crystallization process.

1.3 Research Development

The problem of dextran presence in sugar production process has been a concern for several decades, however it has not been studied in sufficient detail to be able to overcome the problem in the industrial process, except via addition of an expensive enzyme, dextranase. Therefore dextran reduction methods have been studied in lab-scale processes to enhance our knowledge of methods to remove dextran from the process, in order to apply this knowledge in commercial sugar production. The first set of experiments is to determine a dextran analysis method that is suitable for use in the following experiments. Many dextran analysis methods have been developed, including the haze test, CSR method, and Roberts test, among others. In this study, carbon-13 nuclear magnetic resonance (^{13}C NMR) is used to improve the methods currently under use. In Chapter II, details of the sugar manufacturing process and problems caused by dextran are introduced. Moreover, the theoretical details necessary as a background to the ultrafiltration and crystallization experiments are also reviewed in this chapter. Chapter III presents a discussion of the dextran analysis methods development based on ^{13}C NMR. Chapter IV discusses the theory and experiments performed in order to determine the feasibility of separation of dextran from raw juices using ultrafiltration. Various membranes have been used to separate dextran from a synthetic juice. Permeate fluxes and dextran rejections for

each membrane are determined to specify a reasonable membrane that can be used to reduce the dextran content in the juice. Likewise, the fouling characteristics of the membranes during dextran separation are discussed in Chapter V. Mechanisms of dextran incorporation into the sugar crystal during sucrose crystallization and the relationship between the dextran partition coefficient and the crystal growth rate are analyzed in Chapter VI and VII, respectively. Finally, the conclusions for the work and some recommendations for further work are proposed in Chapter VIII.

1.4 Expected Results from the Study

There are many dextran analysis methods already reported in the literature. The early method is widely known as the Haze method. It depends on the precipitation of dextran in sucrose-rich juice by addition of alcohol followed by spectrophotometric turbidity measurement to determine the dextran content. Subsequently, the CSR method and the Roberts test have been developed. These methods also required a separation of concentrated dextran by precipitation with alcohol. In this research the ^{13}C NMR will be developed for measuring dextran content in a sample instead of using spectrophotometer. However, a large amount of dextran sample is required for concentrating before measuring with NMR since the detection with ^{13}C NMR is restricted by the low abandance of ^{13}C isotope in unenriched materials. The NMR method will not be used in the further study for dextran reduction due to the constraint of its detection limit. For the purpose of reduction of dextran content, ultrafiltration will be used to separate dextran from raw sugar juice. Reasonable membranes can be selected by consideration of the permeate flux, the membrane rejection, and fouling of the membrane. In the case of the sucrose

crystallization process improvement, the study of dextran incorporation into sugar crystal during the process will be performed to examine the possibility of dextran removal during the crystallization process by analyzing the dextran partition coefficient between the mother liquor and the sugar crystal. The variation of the partition coefficient due to the crystallization conditions and the growth kinetics can enable the design of the crystallization process for the purpose of reduction of the dextran content.

1.5 References

Chen, J. C. P. and Chou, C. C. (1993). Microbiological control in sugar manufacturing and refining. In J. C. P., Chen and C. C., Chou, (eds.). **Cane Sugar Handbook** (12th ed. pp. 641-658). New York: John Wiley and Sons.

Cuddihy, J. A., Porro, M. E., and Rauh, J. S. (2001). The presence of total polysaccharides in sugar production and methods for reducing their negative effects. **J. Amer. Soc. Sugarcane Technol**. 21: 73–91.

World Bank Group. (2009). Environmental Guidelines for Sugar Manufacturing [On-line]. Available: www.miga.org/documents/SugarManufacturing.pdf

Irvine, J. E. (1993). Sugarcane. In J. C. P., Chen and C. C., Chou, (eds.). **Cane Sugar Handbook** (12th ed. pp. 1-20). New York: John Wiley and Sons.

Wikipedia. (2009). Sugarcane [On-line]. Available: http://en.wikipedia.org/wiki/Sugarcane.

Vaccari, G., and Mantovani, G. (1995). Sucrose crystallization. In M. Mathlouthi, and P. Reiser (ed.). **Sucrose Properties and Applications** (pp. 33-74). Great Britain: Blackie Academic and Professional.

CHAPTER II

REVIEW OF THE LITERATURE

2.1 Introduction

2.1.1 Raw Sugar Processing

Raw and refined sugar is produced worldwide for the purpose of human consumption. Significant sugar production occurs in every continent. Cold climate countries, particularly in Europe and North America, produce sugar mainly form sugar beet. In Thailand, as well as in many large sugar exporting countries such as Brazil, Australia, and South Africa, raw sugar crystals are produced from the tropical plant, sugarcane.

The process of raw sugar production from sugarcane is illustrated in Figure 2.1. It initially involves processes of cane chopping, shredding, or crushing, and after one or a combination of these processes is completed, the sucrose-rich juice is extracted from the pieces of cane with water at 80°C in a series of mills containing three to five rollers. The products from the mills are a liquid stream of relatively low dissolved solids concentration, and a solid waste stream that contains the insoluble parts of cane called bagasse. The bagasse can be burned as the fuel in boilers in the power plant to produce the heat required later in the process. Bagasse can also be sold to manufacturers of plaster board, as an animal feed, or for other uses.

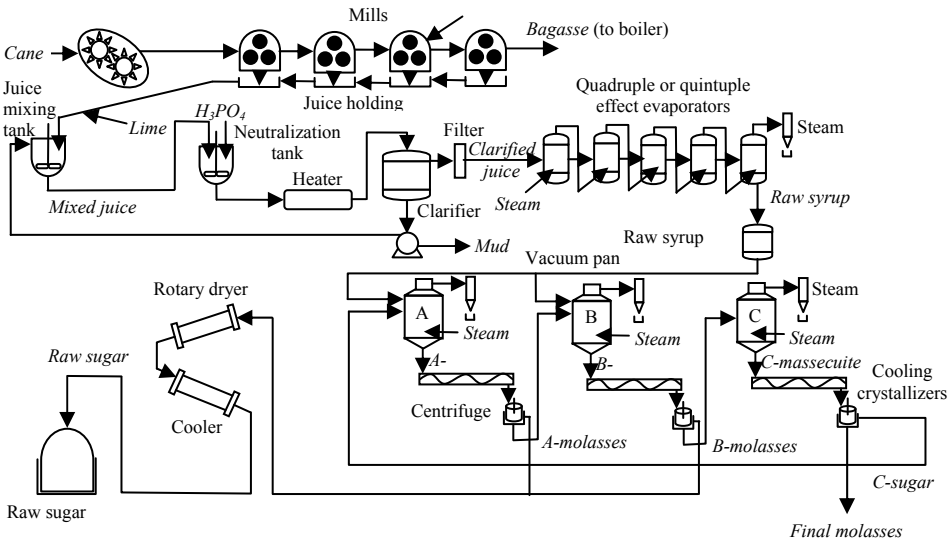

Figure 2.1 Flow chart for the raw sugar manufacturing process. Process streams are named using italic font and equipment with nonitalic font.
Some auxiliary equipment has been omitted for clarity.
(from Flood, C. and Flood, A. E., 2006).

The liquid product from the mills is called juice. The juice is quite turbid since it contains suspended insoluble particles. It also contains a number of organic and inorganic impurities. The organic impurities vary from small molecules such as fructose and glucose from the inversion of sucrose, oligosaccharides (such as raffinose), polysaccharides (particularly dextran and starch); up to vary large molecules such as albumins, fats, waxes, and gums (Chen, 1993). Since it is required to remove both the insoluble and soluble impurities from the juice, it is treated by addition of lime and by heating in the clarifiers. The clarifying process of the juice involves the addition of lime (CaO) into the juice, and then heating the juice to its boiling point to coagulate and entrap the impurities such as albumins and some of fats, waxes, and gums. The process produces a precipitate called “mud” that settles to the

bottom of the clarifiers and can be used as an agicultural fertilizer (Chen, 1993; Andreis *et al.*, 1990). The clarified juice overflowing the clarifiers is sent to evaporators, while the juice containing the precipitate is sent to rotary-drum vacuum filters to extract the juice (to avoid loss of valuable product), leaving the filter cake for disposal.

The clarified juice is concentrated from approximately 15 percent dissolved solids (largely sucrose) up to approximately 65 percent dissolved solids in a series of four or five multiple effect evaporators prior to the crystallization process. The concentrated juice, called syrup, is then passed into a series of evaporative batch crystallizers ("vacuum pans") in which the raw sugar crystals are produced from the solution seeded with small (< 10 μm) milled refined sugar seed crystals. Additional syrup can also be added and evaporated so that the growing crystals are allowed to grow in size. The batch is completed when the crystal suspension is sufficiently dense. The dense mixture of syrup and suspended sugar crystals (called massecuite) is discharged into large containers known as cooling crystallizers. The massecuite is slowly stirred and cooled in the crystallizers resulting in additional crystallization to exhaust the batch. At the end of the process, the raw sugar crystals are separated from the remaining mother liquor, known as molasses, by centrifugal force. The separation of the crystalline product from the molasses is performed in batch centrifuges, where the raw sugar is retained in the centrifuge baskets on a fine screen while the molasses passes through the screen. The crystals in the centrifuge are usually sprayed with a fine spray of water to remove mother liquor adhering to the surfaces of the crystals. The A-sugar crystals are quality high-grade raw sugar, and the mother liquor from this process is returned to the production lines of the B-sugar and the C-Sugar. The C-

sugar crystal is commonly used as seed crystals required later in the next batch. The final mother liquor from the C-sugar production is known as blackstrap molasses that can be used as cattle feed and in the production of industrial alcohol, organic chemicals, and yeast (Chen, 1993; Andreis *et al.*, 1990).

2.1.2 Sucrose (Saccharose; α-D-glucopyranosyl-(1,2)-β-D fructofuranoside)

Sucrose is the main soluble component of sugarcane. The sucrose molecule is composed of twelve atoms of carbon, twenty two atoms of hydrogen, and eleven atoms of oxygen, having a molecular formula $C_{12}H_{22}O_{11}$. The molecular weight of sucrose is 342.3. Pure sucrose is colorless, odorless, and sweet tasting (Clarke, 1993; Knecht, 1990). Sucrose crystals are monoclinic prisms having a density of 1.588 g/cm^3. Sucrose is optically active with the specific rotation $[\alpha]_D^{20} + 66.53$ (Clarke, 1993; Knecht, 1990). α is specific rotation, by convention at 20°C, measured with a polarimeter using a 100-millimeter cell length and the 589 nm wavelength of the sodium-D light. The positive sign indicates that the plane of polarization rotates to the right, which is dextrorotatory (Clarke, 1993; Knecht, 1990). Due to optical activity of sucrose, a polarimetric measurement results in a Pol-reading that can be used to determine the sucrose content. The sucrose molecule consists of glucose and fructose molecules bonded at their anomeric carbons, as indicated by the IUPAC name α-D-glucopyranosyl-(1,2)-β-D-fructofuranoside. The two monosaccharides are much more reactive than sucrose due to their unbound anomeric carbons, and such sugars are known as reducing sugars. Conversely, sucrose is a non reducing sugar that is stable in heat, normally up to 100°C. However sucrose can be hydrolyzed by water either in the presence of acid or the enzyme invertase to yield

one molecule of glucose and one molecule of fructose by means of the inversion reaction (Knecht, 1990). More descriptive molecular structures of sucrose, glucose, and fructose are shown in Figure 2.2 (Cayle, 1990).

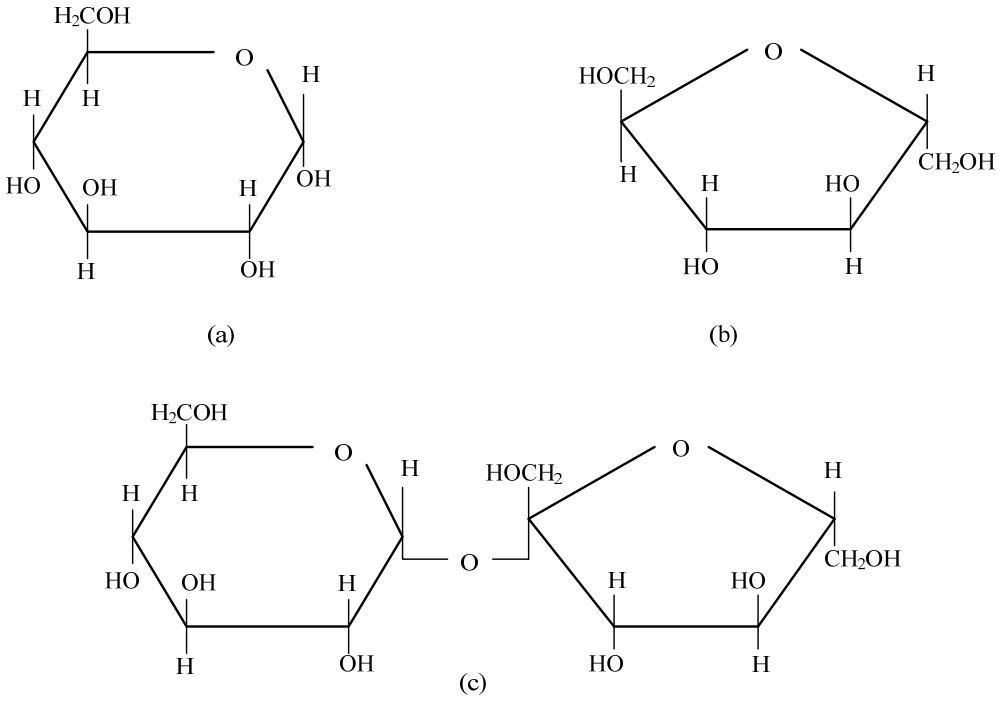

Figure 2.2 (a) α-D-glucose, (b) α-D-fructose, and (c) α-D-sucrose (Cayle, 1990).

The concentrations of sucrose are usually defined in terms of the weight percent of sucrose in the solution (% *S*, g sucrose/100 g solution), or the sucrose to water ratio, *SW* (g of sucrose per g of water) (Bubnik and Kadlec, 1995).

For pure solution:

$$SW = \frac{S}{100 - S} \tag{2.1}$$

For impure solution:

$$SW = \frac{S}{100 - DS} \tag{2.2}$$

where *DS* is dry substance (%)

2.1.3 Polysaccharides

Besides soluble solids (mostly sucrose) and insoluble solids (fiber for example), other soluble nonsugars such polysaccharides are commonly found in sugarcane. These nonsugars are considered as impurities in the process of sugar production. Dextran and starch are the two main polysaccharide impurities, and will be discussed in this section due to their relevance to the research.

1. Dextrans

Dextrans are a series of polymers of glucans containing at least 50% $\alpha(1-6)$ glucosidic linkages in a molecular backbone chain. Dextrans in sugarcane are usually formed by the polymerization of many glucose molecules that form from degradation of sucrose molecules due to the action of the enzyme dextransucrase. Dextransucrase is produced by bacteria of *Leuconostoc* species that can enter the cane stalk from the soil. The mechanism of sucrose degradation and dextran formation is described in Figure 2.3 (Chen and Chou, 1993). The structure and properties of dextrans vary widely according to the strain of the microorganism producing the enzyme and the conditions of cane cultivation such as sucrose concentration, pH, temperature, and aeration. There is a variety of dextran structures produced, which will also contain $\alpha(1-2), \alpha(1-3)$ and/or $\alpha(1-4)$ glucosidic bonds. The molecular weight of dextrans varies in the range from 15,000 to more than 2,000,000 Daltons and they are gummy/slimy substances (Clarke, 1993; Cuddihy *et al*, 2001).

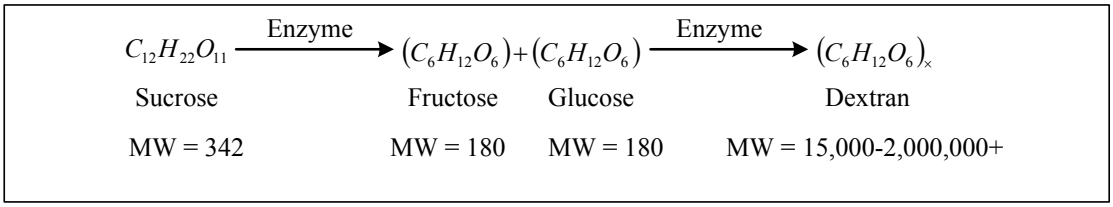

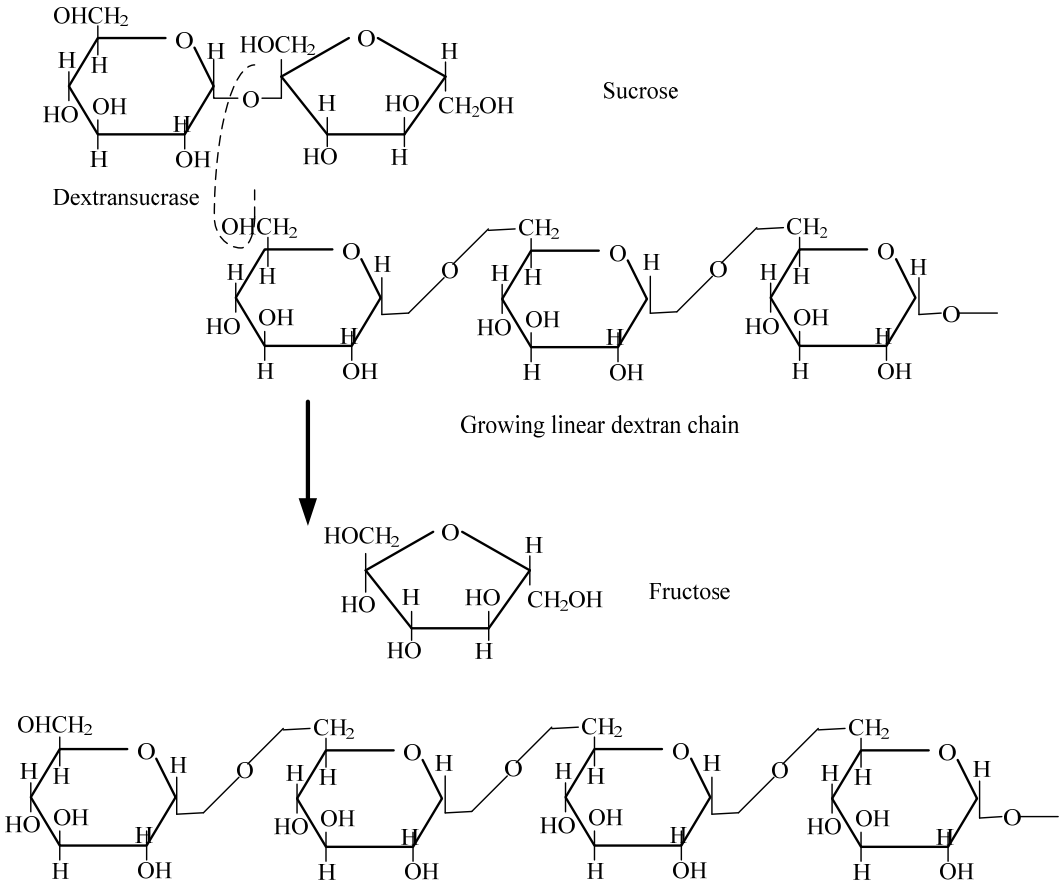

Figure 2.3 Degradation of sucrose and the formation of dextran by dextransucrase (Chen and Chou, 1993).

2. Starch

Sugarcane and juice contain small amounts (between 0.001-0.1%) starch, as shown in Table 2.1. Starch exists in two forms, amylose and amylopectin, both of which are polymers of glucose units with a backbone of $\alpha(1-4)$ linkages. Amylose is essentially a linear and helical structure, while amylopectin is a highly branched polymer in which branches are linked along the backbones by $\alpha(1-6)$ bonding. Normally starch is insoluble in cold water, but it becomes partially soluble in hot water. Most starch is removed from the process of sugar production in raw juice clarifying, however the remainder may be sufficient to have an effect on the rate of evaporation and crystallization (Clarke, 1993; Cuddihy *et al*, 2001).

Table 2.1 Composition of sugarcane and the dissolved solids in the juice (Clarke, 1993).

Millable	**Cane (%)**
Water	73-76
Solids	24-27
Soluble solids	10-16
Fiber (dry)	11-16
Juice constituents	**Soluble solid (%)**
Sugars	75-92
Sucrose	70-88
Glucose	2-4
Fructose	2-4
Salts	3.0-4.5
Inorganic acids	1.5-4.5
Organic acids	1.0-3.0
Organic acids	1.5-5.5
Carboxylic acids	1.1-3.0
Amino acids	0.5-2.5
Other organic nonsugars	
Protein	0.5-0.6
Starch	0.001-0.100
Gums	0.30-0.60
Waxes, fats, phosphatides	0.05-0.15
Other	3.0-5.0

2.1.4 Dextran Contamination in Sugar Processing

It has long been known that dextran is produced in the process of harvested cane deterioration, mainly due to the Leuconostoc bacterium. The deterioration rates commonly depend on the degree of damage to the cane where it has been exposed to the atmosphere, cut-to-crush delay, ambient conditions, degree of burning damage, and delay of burned cane harvesting, degree of frost or freeze damage, and combinations of these factors. It has been estimated that dextran content in harvested cane will result in significant problems in the process of sugar production for periods in excess of 18 hours of deterioration in cool and dry weather, or within 14 hours of deterioration in hot and wet weather (Cuddihy *et al.*, 2001). Although dextran content can increase progressively from the extracted juice to final molasses of sugar production, most dextran that causes process problems is produced in the period between burnt cane harvesting and the preparation prior to the milling.

Dextran levels in each stream of raw sugar manufacturing processes at different factory locations are shown in Table 2.2. The distribution of dextran content in some raw sugar sample analyzed by the Modified Haze method is shown in Table 2.3. According to these data, dextran can not be removed by the clarification process and there is some dextran partitioning into the raw sugar product during the crystal growth.

Table 2.2 Dextran in process streams. Measured at four different Louisiana sugar factories (Rauh *et al.*, 2001).

Dextran, ppm/Brix (Dextran measured by ASI 2 method)				
Samples	**1**	**2**	**3**	**4**
Mixed juice	2690	1094	1928	4650
Clarified juice	2181	1094	1928	4560
Syrup	2602	1239	1986	3858

Table 2.3 Dextran content of some raw sugars. Analyzed by the modified haze method (Chou and Wnukowski, 1981).

Dextran concentration, ppm	**Numbers of cargos**	**Cargo in percentage**
Over 1000	11	10
Between 700-1000	14	13
Between 300-700	33	29
Less than 300	54	49

2.1.5 Problems in Sugar Production Caused by Dextran

There are many processing difficulties in sugar manufacturing caused or exacerbated by the presence of dextran. The presence of dextran in the process not only causes problems in process operation, but also in process control, and in crystal product quality. Minimum levels of dextran contents which would result in problems in the process, and in the product, are listed in Table 2.4.

Table 2.4 Threshould dextran concentration at which problems manifest (Chou and Wnukowski, 1981).

Problem parameters	Dextran in raw sugar (T-40 MW), ppm
Raw sugar polarization	300
Raw sugar crystal elongation	600
Remelt sugar crystal elongation*	400
Washed sugar liquor turbidity	350
Cordial product quality	250
Remelt massecuite viscosity*	400
Soft sugar packaging*	700
Blackstrap molasses purity	100

* Data based on a carbonation refinery. The threshold concentrations may be lower for non carbonation refinery. T-40 MW indicates the molecular weight of 40,000 Daltons.

1. Sucrose loss

Since the dextransucrase enzyme degrades one sucrose molecule to one glucose molecule and one fructose molecule, and many molecules of glucose are used in dextran formation, a significant number of sucrose molecules are degraded for dextran chain propagation. For example, for 1 mole of T-40 dextran formation (average MW 40,000) 222 moles of glucose (MW 180) are required, and this must be equal to number of moles of sucrose lost (Chen and Chou, 1993)

2. *Pol analysis interference*

Traditionally, Pol analysis is used for sucrose content and purity determinations in process control. Since the optical activity of dextran is highly dextrorotatory $[\alpha]_D^{20} +199$, the polarization reading of the sample is highly inflated (Clarke, 1993; Cuddihy *et al.*, 2001).

3. *Effect on juice clarification*

Increases in dextran content increases the viscosity of the juice, which retards the mud setting rate in clarifiers and results in the suspension of precipitated impurities in the clarified juice. Consequently the clarified juice is turbid, resulting in a higher mud volume on the rotary screen in the filtration process (Chen and Chou, 1993; Cuddihy *et al.*, 2001), making screen cleaning more difficult.

4. *Effect on evaporation and crystallization rates*

The primary harmful effects of dextran contamination on evaporation and crystallization rates are increases in the juice and syrup viscosities which lowers mass transfer rates, thus slowing the two mass transfer operations. Secondary effects are a decrease in the rate of evaporation in boilers, a decrease in the crystallization rate in the vacuum pan, and increased scaling of equipment surfaces which results in lower heat transfer efficiency (Cuddihy *et al.*, 2001).

5. *False crystal grain growth*

Dextran contamination and crystal elongation not only reduce crystal growth, but also increase the formation of needle-shaped crystals known as false grain. The false shape is a result of enhanced relative growth along the *c* axis of the sugar crystal due to retardation of growth along the *a* and *b* axes of the crystal by dextran. Needle-shaped raw sugar crystals are undesirable product for many reasons.

Firstly, the efficiency of massecuite purging is reduced due to the combination of the high viscosity of the mother liquor and the reduced settling rate of the needle-shaped crystals. Secondly, the false crystal product is less acceptable to the customer from an aesthetic viewpoint. Lastly, and more seriously, the raw sugar crystals are often contaminated with dextran in high levels which causes many problems in the sugar refinery processes (Chen and Chou, 1993; Cuddihy *et al.*, 2001).

2.1.6 Dextran Elimination Study for Refining Processes

A study on dextran reduction in laboratory-scale processes has been undertaken to examine if it might be possible to reduce dextran through processes generally available to most refineries. The study investigated affination, clarification, adsorption, and crystallization (Chou and Wnukowski, 1981). All the experimental procedures for the study are described in Appendix A.

1. Affination

The study investigated the effect of mingling of sugar samples with affination syrup to remove dextran which was mostly contained in the molasses film that coated onto the crystal surface. Table 2.5 shows that about 20% by weight of dextran was removed from the sugar crystal by the affination process. The remaining dextran in raw sugar will have an influence on the refining process.

Table 2.5 Separation of dextran by the affination process (Chou and Wnukowski, 1981).

Samples	Dextran, ppm		% Remained
	Raw sugar	Washed raw sugar	
1	556	486	78.7
2	663	597	81.0
3	550	495	81.0
4	578	550	85.6

2. Clarification

The clarification processes include carbonation treatment, phosphatation treatment, and phosphatation treatment using cationic surfactants. None of these treatments reduced the dextran content in the treated liquid samples, as shown in Table 2.6.

Table 2.6 Investigation of the clarification process for dextran removal (Chou and Wnukowski, 1981).

Processes	Dextran, ppm	
	Before treatment	After treatment
Clarification	860	962
Phosphatation	858	886
Phosphatation with cationic surfactants	1676	1662

3. Adsorption

Feed liquor samples were passed through a column containing various types of adsorbents to reduce dextran contamination in the liquor. It is seen that no significant amount of dextran was adsorbed by any adsorbent, as shown in Table 2.7.

Table 2.7 Failure of dextran adsorption by carbonaceous adsorbents (Chou and Wnukowski, 1981).

Adsorbents	**Dextran, ppm**	
	Feed	**Effluent**
Char (3rd displacement)	1200	1215
Granular carbon (3rd displacement)	1200	1200
Powdered carbon (batch test)	1200	1225

4. Crystallization

Table 2.8 shows the dextran occlusion during crystallization from syrups made from raw sugar containing various dextran contents. It can be seen that on average 24% of the dextran in the syrups incorporate into the crystallized sugar products.

Table 2.8 Occlusion of dextran during crystallization (Chou and Wnukowski, 1981).

Samples*	Dextran, ppm		% Dextran retained in sugar
	Starting liquor	Crystallized sugar	
Sample 1	1245	548	17.7
Sample 2	538	375	27.9
Sample 3	581	384	26.4

* Raw sugars with widely different dextran content were used.

2.2 General Considerations in Membrane Filtration

Membrane filtration is widely used for many separation processes. Although the mechanisms involved in each type of membrane operation vary, most membrane separation processes such as microfiltration (MF), ultrafiltration (UF), nanofiltration (NF), reverse osmosis (RO), electrodialysis (ED), and pervaporation (PV), can be defined as the separation of two or more components from feed streams based on differences in molecular size or properties of the components involved (Cheryan, 1998a; Baker, 2004a). In this section, a general theory of the separation processes based on size difference, especially considering MF and UF are described, since these processes are the only ones significant in the research described in this thesis.

2.2.1 Definition of a Membrane and Its Applications.

The term “membrane” includes a great variety of materials and structures that can be used as a selective barrier in filtration processes. A membrane should prevent mass movement when the regulated components attempt to pass through it. The primary role of a selective barrier involves passage of selected components through the barrier while other components are rejected. Consequently,

both the permeate stream and the retentate stream are enriched in one or more components (Cheryan 1998a; Strathmann, 1990).

Figure 2.4 shows typical membrane applications in various classes based on the molecular size of the separated components. In MF processes, the size of the membrane is commonly specified directly by the pore size of the MF membrane in micron units. However, with UF membranes, the commercial characterization of membrane size usually refers to the "molecular weight cut off" (MWCO). The MWCO is normally characterized by studying the % rejection of globular proteins or dextrans of various molecular weights by the membrane. In practice, the MWCO is defined as the molecular weight of compound which would have a rejection by the membrane of 90% (Cheryan, 1998a; Porter, 1990).

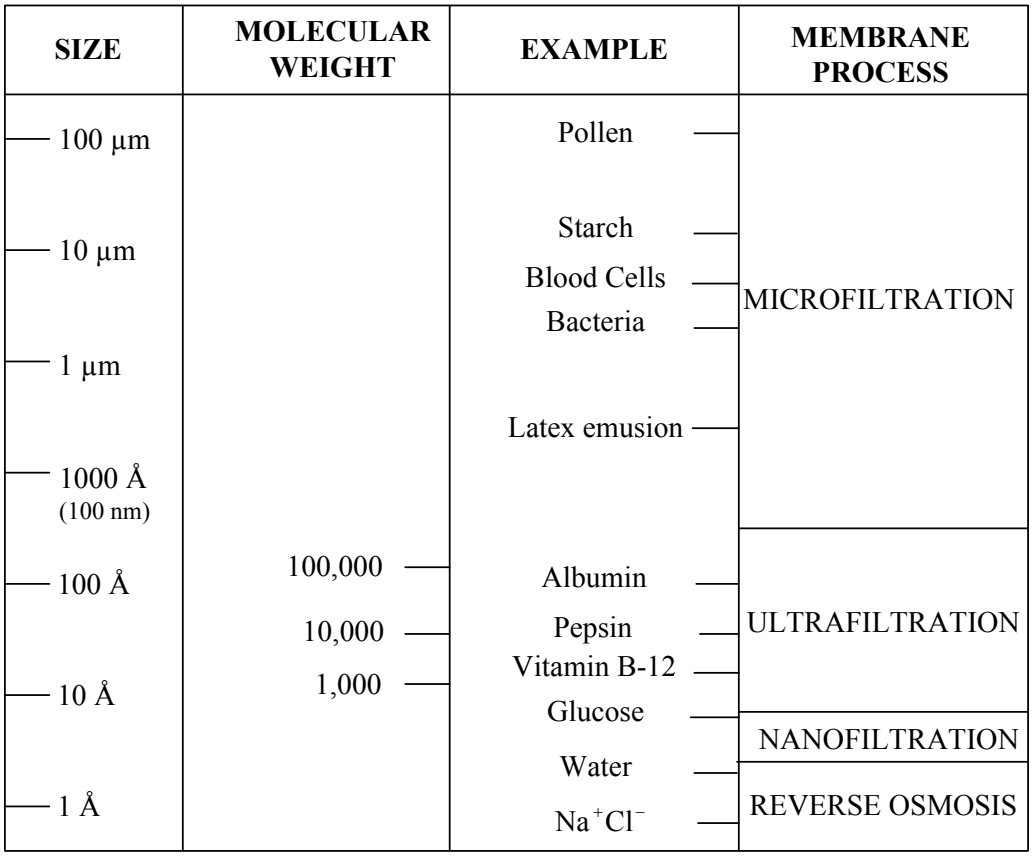

Figure 2.4 Typical applications of membrane filtration processes on solute examples (Cheryan, 1998a).

2.2.2 Mode of Membrane Configuration

The intrinsic selectivity and permeate flux of a membrane separation are important characteristics required for any membrane filtration design. These characteristics can be determined by studies on the mass transfer of solute in the process. For high performance operation, the rates of solute mass transfer should be high while the accumulation of solutes at the upstream surface of membrane is low (Zydney, 1996a).

In order to obtain a high flux in the process, high shear rates or turbulent flows are necessary to achieve a suitable rate of mass transfer and to remove

solutes accumulated on the membrane surface. This is easy to achieve using the cross flow geometry in which the feed flow is parallel to the membrane and perpendicular to the filtrate flow as shown in Figure 2.5. It can be seen that the cross flow operation design is more complex than the dead end mode design since there are three distinct process streams necessary in the cross flow system, while the dead end mode has only two process streams. However, there are many disadvantages in dead end operation of membranes including concentration polarization, variation in the concentration on the retentate side during the experiment, and lack of effective temperature control (Zydney, 1996a). Concentration polarization is caused by an accumulation of solutes on the membrane surface due to their rejection by the membrane, as discussed later. For many laboratory applications as well as the experiments performed in the current research, a magnetic stirrer is used in dead end filtration for the purpose of high shear rate generation. This can achieve a fairly effective solute mass transfer (Zydney, 1996a)

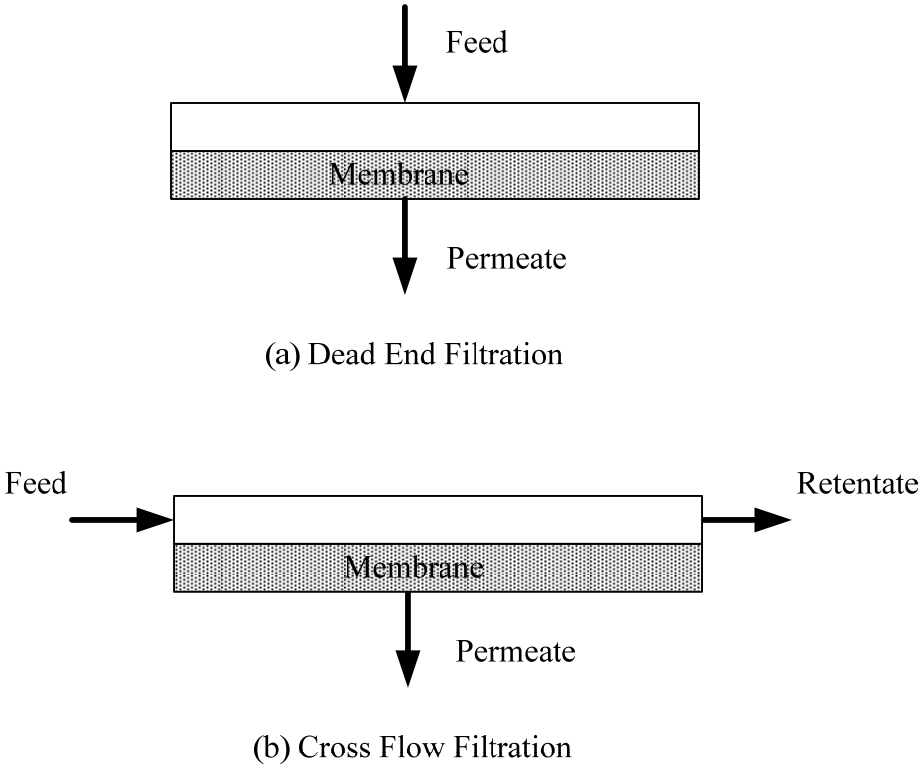

Figure 2.5 Comparison of (a) Dead end filtration and (b) Cross flow filtration.

2.2.3 Types of Membrane Material Used

Although, there are many polymer materials used in the manufacture of membranes, the families of cellulose acetate and polysulfone or polyethersulfone are most commonly used in MF and UF processes (Cheryan, 1998b). Common commercial membranes are made from two materials, regenerated cellulose (RC) and polyethersulfone (PES), and membranes from these materials will be investigated in this study. The chemical structure of both membrane materials are shown in Figure 2.6.

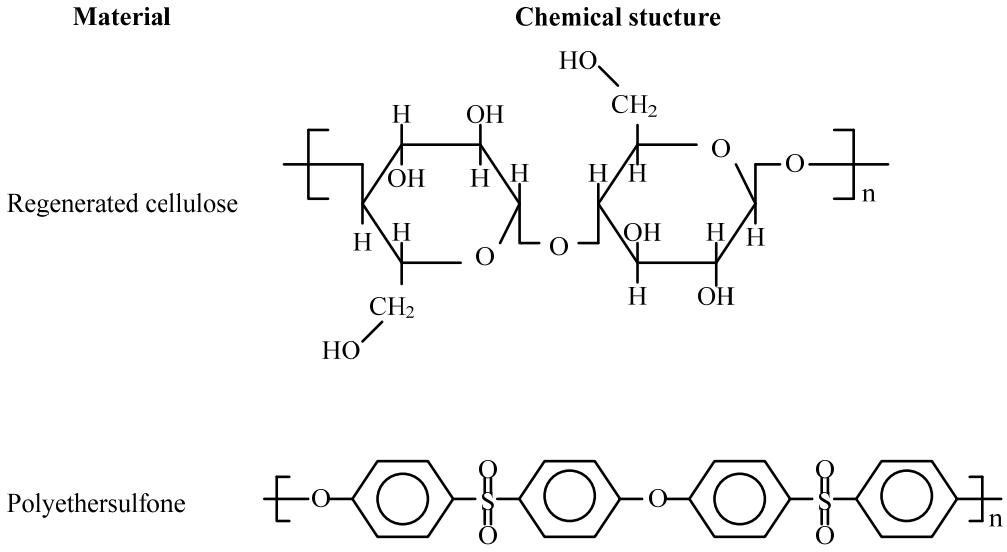

Figure 2.6 Chemical structures of regenerated cellulose and polyethersulfone.

In comparing the performance of RC and PES membranes, the following factors should be considered (Cheryan, 1998b).

1. Range of operating temperatures: The PES membranes can be routienly operated up to 75°C, although some manufacturers are claiming they can be used up to 125°C. In contrast, a maximum temperature of 30°C is recommended for RC membranes by most manufacturers. Since RC membrane use is restricted to low temperature, the flux of the membrane is low due to low diffusivity and high viscosity.

2. Wide pH tolerance: The PES membrane can be continuously operated in a pH range between 1 and 13, while the RC membrane can only be used in the more restricted range of 2-8. A wider range of pH is usually required for membrane cleaning.

Disadvantages of the PES membranes are the pressure limits of the membranes and their hydrophobicity. Firstly, the PES membranes can be typically used in the flat sheet configuration at a pressure less than 7 bar, and 1.7 bar for the

hollow fiber configuration. Secondly, PES is a hydrophobic material, which tends to interact strongly with a variety of solutes. Therefore PES membranes have greater tendency to foul due to solute accumulation compared to more hydrophilic polymers such as cellulose and regenerated cellulose.

2.2.4 Microfiltration and Ultrafiltration

Microfiltration (MF) and Ultrafiltration (UF) are separation processes using microporous membranes. In contrast, most types of membrane separation, including pervaporation and reverse osmosis, use nonporous or dense membranes, and electrodialysis requires a charged membrane. Although microporous membranes are very similar in structure and function to a conventional filter, they have highly voided structures with randomly distributed pores, they are different with respect to their pore size, since they have extremely small pores (Baker, 2004a). Ultrafiltration is usually used to separate water and microsolutes from macromolecules and colloids. The average pore size of UF membranes is in the range of 10-1000 Å. Microfiltration is used to separate suspended particles, and microfiltration membranes have average pore diameters between 0.1 and 10 μm. Thus, microfiltration processes fall between ultrafiltration processes (which mainly separate chemical species) and conventional filters (which separate phases) (Baker, 2004b; Baker, 2004c).

2.2.5 Mass Transfer in Membrane Separation

Membrane separation processes require differences in the rate of permeation of different solutes. The mechanism of permeation in the process can be described with two popular models: the solution diffusion model and the pore flow model, illustrated schematically in Figure 2.7.

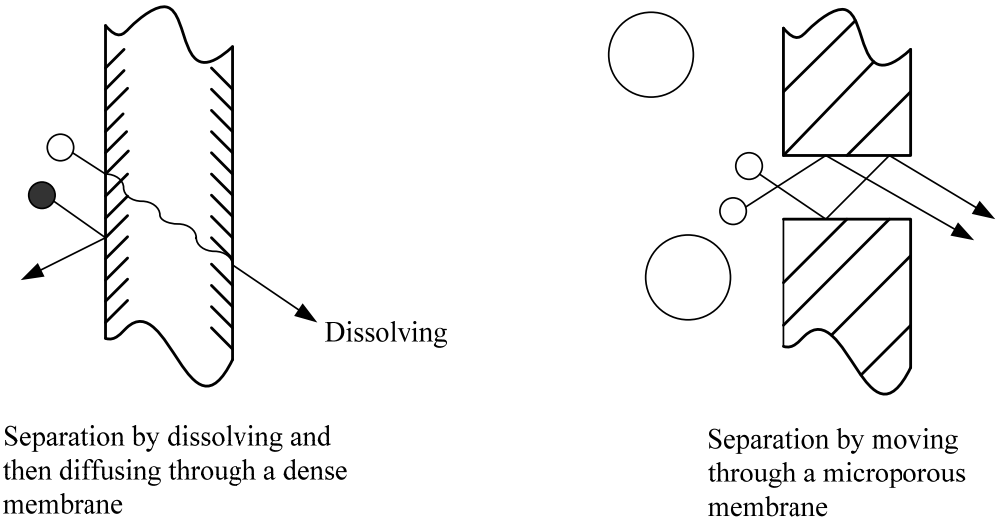

Figure 2.7 Molecular transport through a microporous membrane in the pore flow model and a dense membrane in the solution diffusion model (adapted from Baker, 2004d).

1. The solution-diffusion model

The solution-diffusion model is commonly used to explain the mass transport in nonporous or dense membranes where permeants can dissolve and then diffuse through the membrane due to a concentration gradient. Since there are differences in the solubility and mobility of the permeants in the membrane they can be separated by the membrane process. The concept of the model was proposed based on Fick's theory, which can be expressed in the following equation called Fick's law of diffusion.

$$J_i = -D_i \frac{dc_i}{dx} \tag{2.3}$$

where J_i is the flux of component i (g/m^2·s) and dc_i/dx is the concentration gradient of component i (g/m^4). D_i is the diffusion coefficient (m^2/s) that refers to the mobility of the individual molecules. The solution diffusion model is usually applied to reverse osmosis, pervaporation, and gas permeation in polymer films (Baker, 2004d).

2. The pore-flow model

The pore-flow model is used to describe molecular transport through microporous membranes by pressure-driven convective flow. In this model, the membrane separates species based on differences in molecular size and shape. Molecules smaller than the pore diameter flow through the pore due to the pressure gradient across the membrane, while larger molecules are rejected by the membrane, thus resulting in separation of the different species. The basic equation used in the model is Darcy's law, which can be written as

$$J_i = -K' c_i \frac{dp}{dx} \tag{2.4}$$

where dp/dx is the pressure gradient existing in the porous membrane (N/m^3), c_i is the concentration of component i (g/m^3), and K' is a coefficient reflecting the nature of the membrane pore and the solute (m^4/N·s). The pore-flow model is most commonly used in ultrafiltration and microfiltration processes (Baker, 2004d).

2.2.6 Flux Predicting Models

The mass transfer model and the resistance model are widely used for both ultrafiltration and microfiltration. Both models are typically described as possible mechanisms of flow through the membrane.

1. The mass transfer (film theory) model

One of the simplest and most widely used models to describe transport in the boundary layer is known as film theory. The flux model in this theory is based on a mass transfer controlled system (Cheryan, 1998c). A schematic representation of the mass transfer between the bulk feed and the permeate is shown in Figure 2.8.

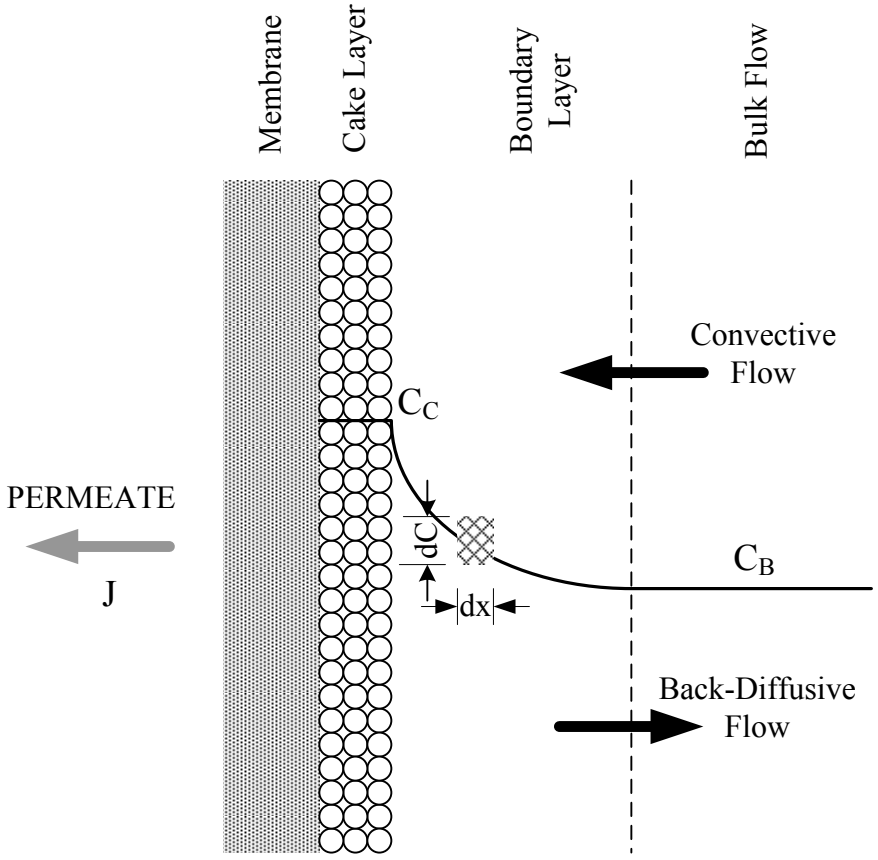

Figure 2.8 Schematic of mass transfer in membrane separation with the phenomenon of concentration polarization (adapted from Cheryan, 1998c).

The solute is brought to the membrane surface by convective mass transport at a flux of J_s (g/m^2·s) which may be defined as

$$J_s = JC_s \tag{2.5}$$

where J is the permeate flux in units of ($m^3/m^2 \cdot s$) and C_s is the solute concentration (g/m^3). During ultrafiltration or microfiltration the rejected solutes normally accumulate at the membrane surface where the concentration becomes higher than the bulk concentration causing the solutes to diffuse back into the bulk solution. The rate of back-transport of solute can be given by

$$J_s = D_s \frac{dC_s}{dx} \tag{2.6}$$

where D_s is the diffusion coefficient of the rejected solute (m^2/s) and dC_s / dx is the concentration gradient over a differential element in the boundary layer at x, the position from the membrane surface (m). At steady state, the forward and back transport mechanisms are in balance with each other. Therefore, the two above equations can be equated and integrated over the boundary layer to give

$$J = \frac{D_s}{\delta} \ln \frac{C_C}{C_B} = k_s \ln \frac{C_C}{C_B} \tag{2.7}$$

where k_s is the mass transfer coefficient of the rejected solute having the same units as the flux J, C_B is the bulk concentration, and C_C is the concentration at the cake-solution interface and δ is the thickness of the boundary layer over which the concentration gradient exists.

This model can be used with the assumption that there is no pressure effect on the flux so it will be valid only in the pressure-independent region.

A pressure independent region can be assumed if the pressure differential is small enough to be neglected (Cheryan, 1998c).

2. The resistance model

In contrast, the mechanism of solute flow through the membrane is dominated by the transmembrane pressure, so that a better approach is to describe the flow by a resistance model. A suitable model for flow through a porous solid is the equation of Hagen-Poiseuille, that is commonly used to describe fluids flowing through channels or membrane pores (Cheryan, 1998c). The equation representing the permeate flux is

$$J = \frac{\Delta P}{\mu(R_m + R_c)} \tag{2.8}$$

where ΔP is the total transmembrane pressure drop, and R_m and R_c are the membrane resistance and the resistance of the cake layer respectively (Cheryan, 1998c; Zydney, 1996b). R_m is dependant on the properties of the membrane, and is often determined by using the flux of water through the membrane. R_c usually includes the resistance due to membrane fouling and the formation of the cake layer. The variable μ represents the viscosity of the permeate.

2.2.7 Concentration Polarization

During ultrafiltration and microfiltration processes, large solutes are usually rejected by the membrane while the solvent and some small molecules (molecules smaller than the membrane pore size) pass through the pores of the membrane. The concentration at the membrane surface increases due to the accumulation of rejected solutes, a phenomenon which is called “concentration

polarization". If the solutes have accumulated to the extent where the concentration at the membrane surface is higher than that in the bulk stream, the solutes adjacent to the membrane surface can back diffuse into the bulk due to a concentration gradient (Porter, 1990; Cheryan, 1998c). This occurs most often in dead-end filtration but also in some case of cross-flow filtration, where the solute accumulation is disturbed by the cross-flow velocity so that the concentration at the membrane surface is lower.

2.2.8 Membrane Fouling

A major factor limiting the use of ultrafiltration and microfiltration in many applications is membrane fouling. Membrane fouling is characterized as an "irreversible" decline in flux caused by physical and/or chemical interactions between the membrane and various solutes. It is due to the deposition and accumulation of solutes on the membrane surface or on the membrane pore wall depending on the interactions and the size of the molecules causing the fouling (Zydney, 1996c).

The effects of membrane fouling on the flux are often similar to those associated with the phenomenon of concentration polarization; however concentration polarization is a different mechanism since it is a reversible phenomenon in the boundary layer. Therefore, the concentration polarization effect can be decreased by adjusting the process design and operating conditions so that the solute accumulation near the interface due to membrane rejection is reduced or eliminated. This can be achieved by lowering the feed concentration or increasing the cross-flow velocity or turbulence in the system, for example (Zydney, 1996c; Cheryan, 1998d).

Membrane fouling can not be eliminated simply by increasing the rate of rejected solute mass transfer. Therefore, the flux decline over the membrane process cycle is irreversible, and this necessitates cleaning of the membrane after

each cycle (Zydney, 1996c). There are several models which have been developed to explain the mechanisms of membrane fouling, including pore blocking, internal pore plugging, and cake filtration moles; these will be more discussed in more detail in Chapter V.

2.2.9 Factors Affecting Fouling

Membrane fouling is a result of specific interactions between various solutes in the feed solution and the membrane. Variation of the fouling process is caused by the differences in membrane material property, solute type, and operating parameters (Cheryan, 1998d). Hydrophilicity is one property of the membrane which has an important influence on fouling. The membrane can be distinguished as hydrophilic (water-attracting) and hydrophobic (water-repelling, but organic- or oil-attracting). The hydrophilic membrane is typically fouled more slowly than the hydrophobic membrane because hydrophobic material tends to attract the organic solutes that are often present in feed stream. The most widely used measurement to characterize the relative hydrophilicity is the contact angle of the membrane surface with a water drop. The measurement is illustrated in Figure 2.9.

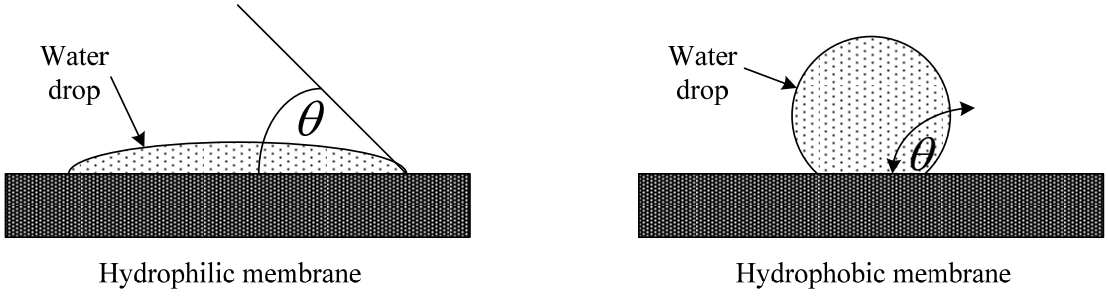

Figure 2.9 Contact angle (adapted from Cheryan, 1998d).

2.3 General Considerations in Crystallization

Crystallization is a widely used technique for separation and purification in many industrial processes. It may be defined as a phase change from a liquid or gaseous state to a typically very pure crystalline product with the remaining liquid or gaseous solution containing the bulk of the impurities. Most crystallization in the chemical process industries are crystallizations from solution. In this short review, the theories necessary to analyze crystallization from solution will be briefly discussed. The crystallization process depends primarily on supersaturation caused by cooling (where, as in most cases, the solubility increases with increasing temperature), concentrating the solution by evaporation, adding non solvents or other solutes to alter the solubility of the solute, and methods involving simultaneous applications of more than one of these processes. They may be known as cooling crystallization, evaporative crystallization, non solvent crystallization, or salting out crystallization (Mersmann, 1995; Schwartz and Myerson, 2002; Strickland-Constable, 1968). Many crystallization process designs improve the rate of production by using crystallizers with agitation either by stirring or pumping of the solution. The concept of ideal crystallizers, such continuous mixed-suspension, mixed-product-removal (MSMPR) crystallizers and ideal mixed batch crystallizers are often applied for use in crystallizer design. The batch crystallizer system is used in the experiments in the current study since it is typically used in sugar manufacturing and is simpler to obtain crystal growth parameters from than other types of crystallizer.

2.3.1 Solubility and Supersaturation

It has been well known that a solution can be prepared by adding a solid solute to the solvent. At a given temperature there is a maximum amount of

solute that can dissolve in a given amount of solvent. The solution containing this maximum amount of dissolved solid is called a saturated solution. Solubility refers to the amount of solid solute required for making a saturated solution at a given set of conditions (Schwartz and Myerson, 2002). A saturated solution can be converted to a supersaturated solution (containing an excess of the solute required for saturating the solution) by four main methods;

1. temperature change,
2. evaporation of solvent,
3. chemical reaction, and
4. changing solvent composition.

Supersaturation is the magnitude by which the solute composition exceeds the saturation point, and is the fundamental driving force for the crystallization process. It can be expressed in various forms, but in crystallization from solution, supersaturation can be defined by the relative supersaturation (σ);

$$\sigma = \frac{C - C^*}{C^*} \tag{2.9}$$

where C is the concentration of the supersaturated solution and C^* is the solubility (Schwartz and Myerson, 2002).

2.3.2 Phase Equilibrium for Crystallization from Solution

The phase diagram for crystallization from solution is shown in Figure 2.10. There are two lines that divide the diagram into three regions. Above the line of the supersaturation limit is an unstable region where phase change occurs without difficulty by mechanisms of both crystal growth and nucleation. Nucleation is

possible in this region because the supersaturation is sufficient to overcome the relatively high energy barrier required for the nucleation. Below the solubility curve, crystals dissolve instead of grow. The metastable region is located between the two lines, where nucleation usually does not occur but seed crystals can grow under a small driving force (Strickland-Constable, 1968). The metastable zone can be specified for various types or mechanisms of nucleation, which will be discussed later.

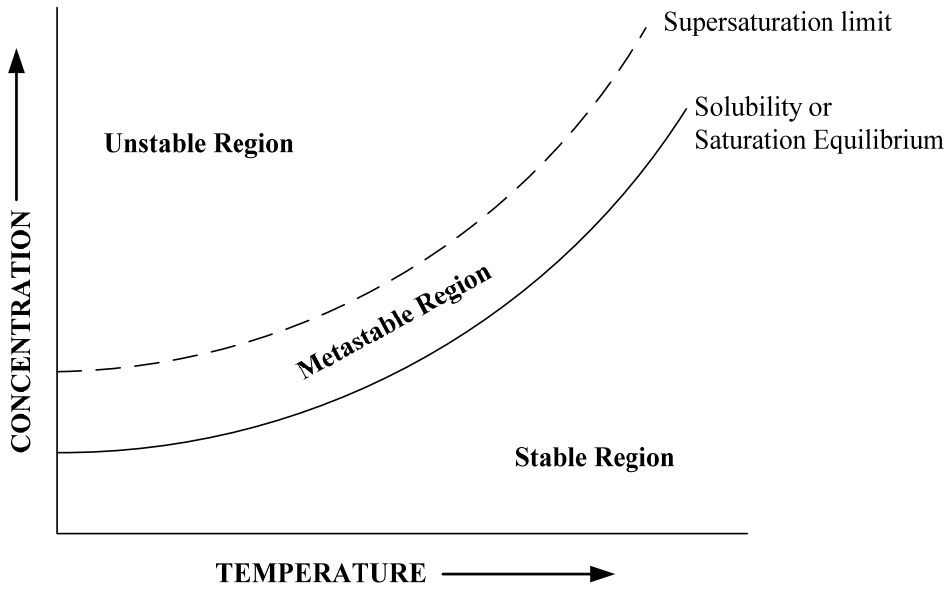

Figure 2.10 Equilibrium phase diagram for crystallization from solution.

2.3.3 Solubility of Sucrose

Since significant time and trouble are required to achieve accurate solubility data for even a single species, it is more convenient to use a published expression for solubility if one is available, and is generally accepted to be accurate. For sucrose, the solubility equation of Kelly (Kelly and Keng, 1975) is one that is known to be of high accuracy over a wide range of temperature and is commonly used. Two regressions were found to satisfy the data of Kelly, in which the sucrose

percentage concentration (w/w) is related to the temperature (in Celcius) each with a standard deviation of 0.04% between the regressions and the experimental data. The two regressions can be expressed as:

$$C = 64.53 + 0.0937T + 0.0012T^2 \left(< 50^\circ C\right) \tag{2.10}$$

$$C = 61.15 + 0.2249T + 0.0001T^2 \left(> 50^\circ C\right) \tag{2.11}$$

where C has the units of grams of sucrose per 100 grams of solution and T is the temperature in °C. Table 2.9 shows the solubility of sucrose in pure water based on the above regressions (Kelly and Keng, 1975).

Table 2.9 Solubility of sucrose in pure water (Kelly and Keng, 1975).

T °C	% Sucrose by weight of solution	g Sucrose per g H_2O	T °C	% Sucrose by weight of solution	g Sucrose per g H_2O	T °C	% Sucrose by weight of solution	g Sucrose per g H_2O	T °C	% Sucrose by weight of solution	g Sucrose per g H_2O
0	64.53	1.819	26	67.78	2.104	51	72.36	2.618	76	77.66	3.476
1	64.62	1.826	27	67.93	2.118	52	72.57	2.646	77	77.87	3.519
2	64.72	1.834	28	68.09	2.134	53	72.79	2.675	78	78.08	3.562
3	64.82	1.843	29	68.26	2.151	54	73.00	2.704	79	78.29	3.606
4	64.92	1.850	30	68.42	2.167	55	73.22	2.734	80	78.50	3.651
5	65.03	1.860	31	68.59	2.184	56	73.43	2.764	81	78.71	3.697
6	65.14	1.869	32	68.76	2.201	57	73.64	2.794	82	78.92	3.744
7	65.24	1.877	33	68.93	2.219	58	73.86	2.826	83	79.13	3.792
8	65.36	1.886	34	69.10	2.236	59	74.07	2.856	84	79.34	3.840
9	65.47	1.896	35	69.28	2.255	60	74.28	2.888	85	79.54	3.888
10	65.59	1.906	36	69.46	2.274	61	74.50	2.922	86	79.75	3.938
11	65.71	1.916	37	69.64	2.294	62	74.71	2.954	87	79.96	3.990
12	65.83	1.927	38	69.82	2.313	63	74.92	2.987	88	80.17	4.043
13	65.95	1.937	39	70.01	2.334	64	75.13	3.021	89	80.37	4.094
14	66.08	1.948	40	70.20	2.356	65	75.35	3.057	90	80.58	4.149
15	66.20	1.959	41	70.39	2.377	66	75.56	3.092	91	80.79	4.206
16	66.34	1.971	42	70.58	2.399	67	75.77	3.127	92	80.99	4.260
17	66.47	1.982	43	70.78	2.422	68	75.98	3.163	93	81.20	4.319
18	66.61	1.995	44	70.98	2.446	69	76.19	3.200	94	81.41	4.382
19	66.74	2.007	45	71.18	2.470	70	76.40	3.237	95	81.61	4.440
20	66.88	2.019	46	71.38	2.494	71	76.61	3.275	96	81.82	4.501
21	67.03	2.033	47	71.58	2.519	72	76.82	3.314	97	82.02	4.562
22	67.17	2.046	48	71.79	2.545	73	77.03	3.354	98	82.23	4.627
23	67.32	2.060	49	72.00	2.571	74	77.25	3.394	99	82.44	4.695
24	67.47	2.074	50	72.19	2.596	75	77.46	3.437	100	82.64	4.760
25	67.62	2.088									

The solubility of sucrose in water-alcohol solvent mixtures such as sucrose in water–methanol, water–ethanol, and ethanol-methanol at 25, 40, and 60°C were reported by Peres and Macedo (1997). They are shown in Tables 2.10, 2.11, and 2.12, respectively.

Table 2.10 Solid-liquid equilibrium data for sucrose-water-ethanol at 25, 40, and 60°C (Peres and Macedo, 1997).

25°C			**40°C**			**60°C**		
Water*	**%Sucrose**	**SD**	**Water***	**%Sucrose**	**SD**	**Water***	**%Sucrose**	**SD**
0.000	0.0501	-	0.000	0.0816	-	0.000	0.1874	-
9.995	0.6794	0.002	9.992	1.0418	0.001	10.056	2.0512	0.004
19.894	4.2244	0.003	20.028	6.5890	0.003	20.032	11.2242	0.005
29.896	14.4279	0.005	29.884	19.0122	0.008	30.021	28.9266	0.011
39.758	26.7090	0.007	40.010	34.3119	0.012	39.730	45.4875	0.019
50.004	38.9091	0.011	50.006	45.4830	0.019	50.067	55.8653	0.023
59.924	48.2336	0.016	59.076	53.4487	0.022	59.836	61.8534	0.029
70.025	55.6056	0.022	70.524	60.4991	0.028	79.850	69.8577	0.033
79.987	60.3325	0.029	80.112	64.4311	0.031	100.000	74.3711	0.035
100.000	67.4623	0.031	100.000	70.1888	0.034			

* indicates the water mass percentage in the sugar-free mixture.

Table 2.11 Solid-liquid equilibrium data for sucrose-water-methanol at 25, 40, and 60°C (Peres and Macedo, 1997).

25°C			40°C			60°C		
Water*	**%Sucrose**	**SD**	**Water***	**%Sucrose**	**SD**	**Water***	**%Sucrose**	**SD**
0.000	0.6627	0.002	0.000	0.9962	0.003	0.000	1.8309	0.003
9.905	2.2217	0.002	10.098	3.2821	0.003	9.997	6.7843	0.005
19.979	6.3312	0.004	19.989	9.7585	0.005	19.895	18.4980	0.009
29.944	15.7410	0.007	29.218	21.6473	0.009	29.902	36.0736	0.017
39.758	28.9476	0.010	39.732	37.9694	0.013	39.787	50.0608	0.023
49.977	41.1992	0.017	50.082	49.7914	0.022	49.762	58.7036	0.028
59.936	49.8836	0.021	59.832	56.1027	0.027	59.951	64.4322	0.032
70.032	56.8490	0.026	69.990	61.4483	0.030	80.077	70.7825	0.033
79.970	61.0928	0.029	80.005	64.9330	0.031	100.000	74.3780	0.035
100.000	67.4623	0.031	100.000	70.1888	0.034			

* indicates the water mass percentage in the sugar-free mixture.

Table 2.12 Solid-liquid equilibrium data for sucrose-ethanol-methanol at 25, 40, and 60°C (Peres and Macedo, 1997).

25°C			40°C			60°C		
EtoH*	**%Sucrose**	**SD**	**EtoH***	**%Sucrose**	**SD**	**EtoH***	**%Sucrose**	**SD**
0.000	0.6627	0.002	0.000	0.9962	0.003	0.000	1.8309	0.003
10.020	0.5300	0.003	10.085	0.8025	0.005	10.012	1.5147	0.004
19.623	0.4380	0.001	19.984	0.6436	0.005	19.971	1.2560	-
29.961	0.3475	0.003	30.056	0.5142	0.002	29.911	1.0120	0.001
40.116	0.2637	-	39.915	0.4066	0.003	39.961	0.8025	0.001
50.646	0.1980	-	49.872	0.3249	0.001	49.876	0.6445	0.005
59.989	0.1518	-	59.960	0.2443	-	60.327	0.4967	0.002
70.060	0.1157	-	70.034	0.1855	-	69.867	0.4012	0.001
80.004	0.0871	-	80.104	0.1430	-	79.848	0.3132	0.003
100.000	0.0501	-	100.000	0.0816	-	100.000	0.1874	-

* indicates the ethanol mass percentage in the sugar-free mixture.

2.3.4 Nucleation

The two main processes in crystallization from solution are nucleation and crystal growth. Although the kinetic processes of both require a driving force (supersaturation), nucleation commonly occurs in the higher supersaturation region only. Nucleation can be explained by either primary or secondary mechanisms (Randolph and Larson, 1988a). The categorization of the different mechanisms is shown in Figure 2.11.

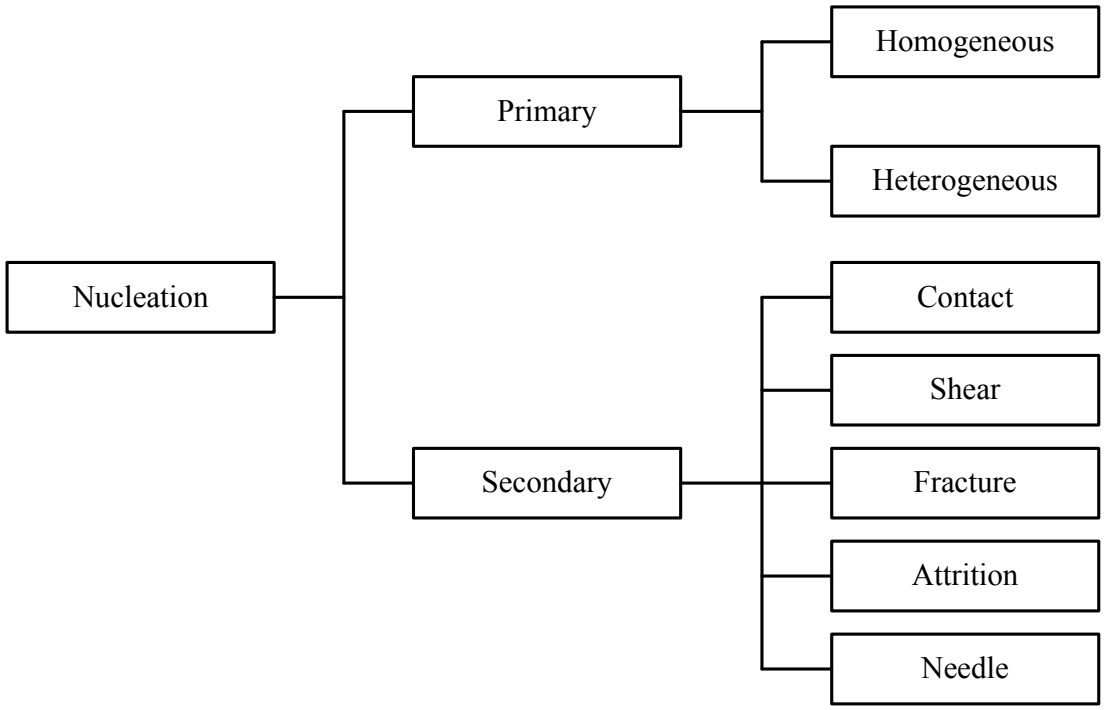

Figure 2.11 Known nucleation mechanisms (Randolph and Larson, 1988a).

The term homogeneous primary nucleation is used to describe the mechanism where nuclei are formed in solutions containing neither particles of foreign substances nor solute crystals. Heterogeneous primary nucleation is a mechanism where the formation of nuclei occurs associated with the presence of foreign particles suspended in the solution. Secondary nucleation includes mechanisms of nucleation in solutions where solute crystals are suspended, as in the well known case of seed addition. It can be used to describe the formation of nuclei due to factors such as contact, fluid shear, fracture process, attrition, and needle breeding. Figure 2.12 illustrates metastable zone widths for several types of nucleation mechanism. It can be seen that secondary nucleation generally occurs at lower supersaturations than the other mechanisms of nucleation. Additionally, there is a significant difference between the zone widths of the two primary mechanisms,

with heterogeneous nucleation occurring at significantly smaller supersaturations than are required for homogeneous nucleation. This is because the free energy required in the case of heterogeneous nucleation is lower due to the decrease in the activation energy for the process which occurs because of contact or wetting of the solid phase (Mersmann, 1995; Mullin, 2001a; Myerson and Ginde, 2002; Randolph and Larson, 1988a).

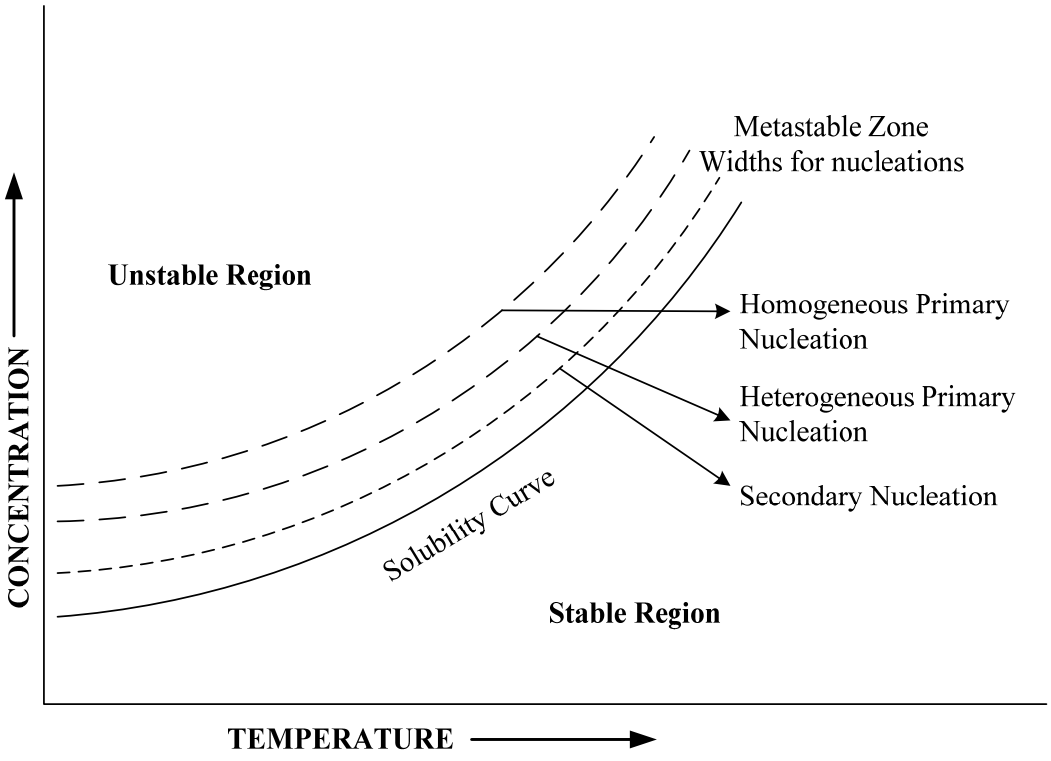

Figure 2.12 Metastable supersaturation regions for several types of nucleation mechanisms (adapted from Mersmann, 1995).

2.3.5 Crystal Growth

There are two main steps for the crystallization process. The first step is the birth of new crystals or nuclei, which is called nucleation, and the later step is growth of these nuclei to a larger size by the addition of solute molecules from the

supersaturated solution, which is known as crystal growth. The growth rate is often described by the change of a linear crystal dimension with time. A linear crystal dimension can be related to the volume or surface area of the crystal through the shape factors α_V *and* α_A. There are a number of faces apparent on any real crystal, and these faces grow at different rates. The mean growth rate is commonly used for engineering design. The crystal shape factors are often used for determination of linear growth rate if the main objective is to determine how a particular packing structure (apparent on a single face) interacts with the solution. If the crystal is a sphere (a poor assumption for almost all realistic crystals), it is easy to use the diameter as the characteristic dimension. In more realistic situations, where the crystal is another shape, the second longest dimension is usually used because it is an approximation to the size for which a crystal can pass through a screen or sieve of the specified size. An alternative way of performing a crystal growth study is measurements based on the mass increase of the crystal with time. It can be directly related to the overall linear growth rate (Myerson and Ginde, 2002).

2.3.6 Theories of Crystal Growth Kinetics

There are many models that presume that the rate of crystal growth can be modeled on a two step mechanism. It is generally proposed that the mechanism of crystal growth from solution consists of the sequential steps of mass transport of solute molecules from the bulk supersaturated solution to the crystal-solution interface followed by the incorporation of the molecules into the crystal lattice through the surface integration process. If the rate of mass transport to the crystal surface is higher than the rate of surface integration, the overall growth rate is limited by the surface integration. Alternatively, if the rate of molecular incorporation into

the crystal lattice is higher that the mass transport rate, the growth rate is controlled by mass transport, commonly mass diffusion in the boundary layer around the crystal (Randolph and Larson, 1988a; Karpinski and Wey, 2002).

1. Growth controlled by mass transport

In many crystal growth processes, especially precipitation processes, the mean free distance between growing crystals is very large compared to the diffusion distance, and therefore growth occurs in an infinite diffusion field. It is appropriate to describe these processes by diffusion-controlled growth model. Figure 2.13 shows the mass diffusion through the boundary layer.

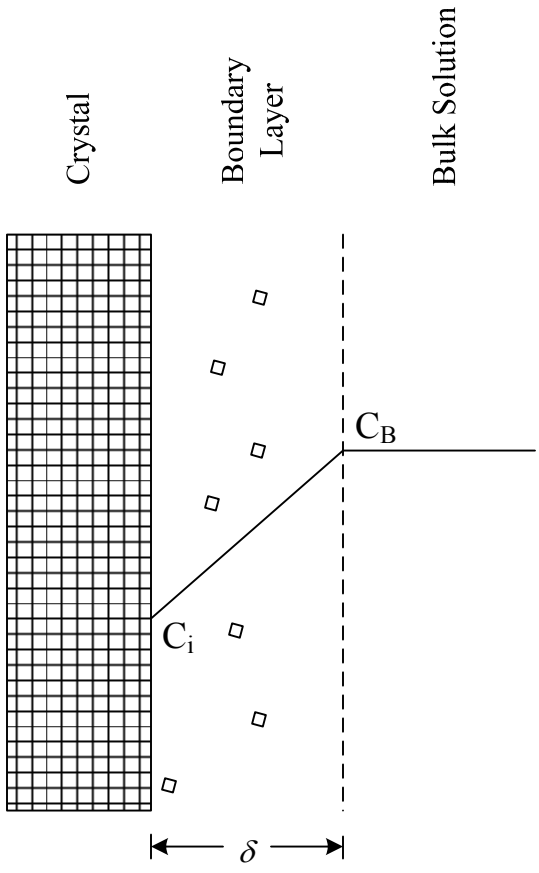

Figure 2.13 Mass diffusion in the boundary layer.

In this model, the rate of growth unit diffusion through a boundary layer of thickness δ is very low. The simplest model of mass transport is the bulk diffusion of growth units through a stagnant boundary layer near the crystal surface where the concentration profile is linear. The growth rate can be obtained by using Fick's law of diffusion which may be written as

$$\frac{dm_c}{dt} = DA_c\left(\frac{dC}{dx}\right) \tag{2.12}$$

where dm_c/dt is the crystal mass increasing with time (g/s), D is the diffusion coefficient (m^2/s), A_c is the surface area of the crystal (m^2), C is the solute concentration (g/m^3), and x is position from the crystal surface (m). The concentration relating to a position through the boundary layer can be written as

$$\frac{dC}{dx} = \frac{C_b - C_i}{\delta} \tag{2.13}$$

where C_b and C_i are the bulk and interfacial concentrations, respectively (g/m^3). The linear growth rate G can be derived for a spherical crystal by integrating Fick's law based on the assumption that there is a fictional linear concentration gradient across the boundary layer;

$$G = \frac{2D}{\rho_c \delta}\left(C_b - C_i\right) = \frac{2k_d}{\rho_c}\left(C_b - C_i\right) \tag{2.14}$$

where ρ_c is the crystal density (g/m^3), and k_d is defined as the ratio of the diffusion coefficient and the thickness of the boundary layer (m/s) (Mullin, 2001b; Myerson

and Ginde, 2002; Karpinski and Wey, 2002). If mass diffusion is the limiting mechanism, the crystal growth rate increases with a decrease in the boundary layer thickness due to stirring or high flow of the solution. If increases in mass transfer rates no longer result in increasing growth rates it can be concluded that the growth is surface integration-controlled.

2. Growth controlled by surface integration

In the case where crystal growth is controlled by the surface integration process, the overall crystal growth rate can be obtained by the rate of incorporation of growth units into the crystal lattice. Two main models are commonly used to describe the process; the two-dimensional nucleation model and the Burton-Cabrera-Frank (BCF) model.

The two–dimensional nucleation model proposes that perfectly flat surfaces on crystal faces are unfavorable for the formation of new growth layers, so two-dimensional nuclei must be generated to provide step sites for the incorporation of growth units. The nuclei formation is illustrated in Figure 2.14. Three significant variants of this model have been proposed. In the mononuclear model, the limiting step is the formation of one nucleus, which then spreads across the crystal surface at an infinite rate. The polynuclear model represents the opposite extreme, with an assumption of no spreading growth of the nuclei across the crystal surface; the facial layer is occupied only by a sufficient number of surface nuclei sized entities to complete the face. These two concepts are quite extreme cases, however a modified case known as the “birth-and-spread” model predicts that nuclei are formed and then subsequently spread at a finite rate. However, the model fails to explain the formation

of nuclei in very low supersaturation solutions where the crystal can grow (Mullin, 2001b; Myerson and Ginde, 2002; Karpinski and Wey, 2002).

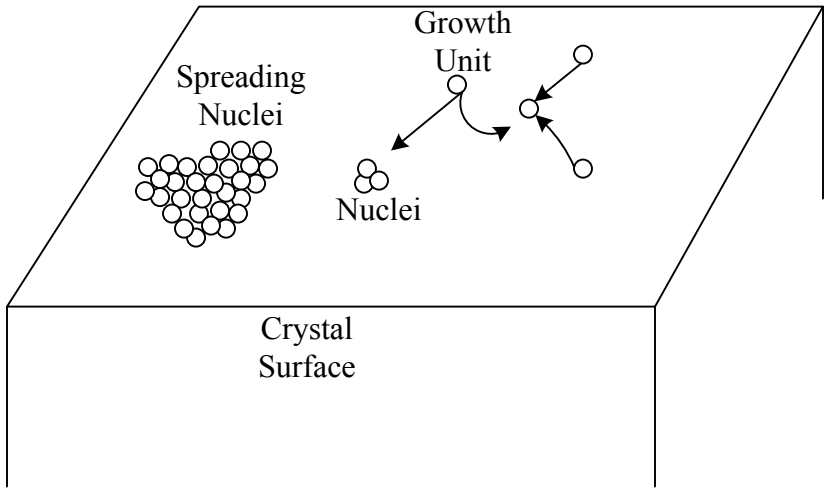

Figure 2.14 Formation of nuclei and their spreading to produce new layers.

The Burton-Cabrera-Frank (BCF) model has been proposed to describe the growth mechanism based on the idea of growth promotion by a screw dislocation. When a screw dislocation occurs on the crystal surface, it continues to produce a self-repeating spiral step throughout the crystal growth period. This type of dislocation in the crystal is a source of new steps, and provides for continuous incorporation of the growth units. A simple screw dislocation for crystal growth is illustrated schematically in Figure 2.15.

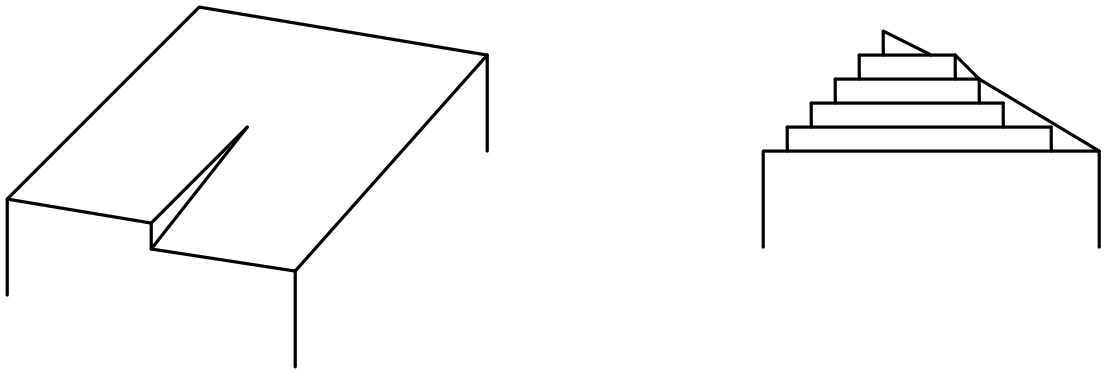

(a) (b)

Figure 2.15 (a) Screw dislocation in a crystal and (b) growth as a continuous spiral step (adapted from Myerson and Ginde, 2002).

The linear crystal growth rate based on the BCF model has been developed in the form

$$G \propto \frac{\sigma^2}{\sigma_c} \tanh\left(\frac{\sigma_c}{\sigma}\right) \tag{2.15}$$

where σ is the relative supersaturation defined by $(C - C^*)/C^*$ for the case of a very high rate of mass diffusion in the boundary layer, and σ_c is a complex temperature dependent constant which includes parameters depending on step spacing. At low supersaturation, the above equation can be approximated as the growth rate being proportional to the square of the relative supersaturation, and at high supersaturation, the growth rate is approximately proportional to the supersaturation. Since it is seen that the power component in the correlation falls between 1 and 2, a simple power-law equation for the growth rate can be written as

$$G = k_r \sigma^n \tag{2.16}$$

where the power n varies between 1 and 2, and k_r is a surface reaction rate constant. This equation is frequently used to represent the growth rate controlled by surface integration as well as used in growth rate data fitting for research since it tends to fit either experimental data or BCF theory under certain common conditions (Mullin, 2001b; Myerson and Ginde, 2002; Karpinski and Wey, 2002).

2.3.7 Classification of Crystallization Operations

In industrial crystallization processes, the crystallizer is typically operated by using the application of batch or continuous basis. The mixed-suspension, mixed-product-removal (MSMPR) is commonly used to represent a continuous crystallizer, although most real industrial crystallizers will not match the conditions necessary for the MSMPR. This type of crystallizer is an analogy to the continuous-stirred tank reactor (CSTR). In this case, a continuous stream of supersaturated solution is fed to a stirred vessel while product is simultaneously removed to maintain a constant crystallization volume. Following a transient period, the MSMPR system reaches a steady state. In the mathematical model of the MSMPR crystallizer, the assumption of complete mixing and steady state operation is often used for the system, so that the population density function for the crystals present in the system can be considered as dependent on crystal size only. In addition, continuous operation results in larger production capacity. In the case of batch crystallizers, feed solution is placed into an agitated vessel, and either seed or nuclei in the solution are allowed to grow until the batch run is completed. The assumption of steady state cannot be realized for batch systems, so the prediction of the CSD is more complex since it depends on both crystal size and time even in completely mixed systems. However, there are benefits

of batch operations, including that a batch crystallizer can produce a narrower crystal size distribution than a continuous crystallizer. Furthermore, if the crystals are growing at a slow rate, a batch crystallizer can be controlled more easily so that larger crystals are produced (Karpinski and Wey, 2002; Wey and Karpinski, 2002; Randolph and Larson, 1988b; Randolph and Larson, 1988c; and Berglund, 2002). In sugar manufacturing, the batch crystallizer is preferred for the crystallization process because of better control over the particle size distribution.

2.3.8 Growth Rate Dispersion

In fact, crystals of the same size can grow at different rates due to different environments in the crystallizer, and also due to slight differences in the internal and surface structures of the individual crystals. This is known as the phenomenon of "growth rate dispersion" (GRD). It is quite different to the concept of size-dependent growth (Martins and Rocha, 2007). Size-dependent growth means that the crystal growth rate is a function of the current crystal size of the growing crystal. However, an apparent (but not real) size-dependent growth can be a consequence of GRD. Two models have been developed to describe the phenomenon of GRD. The first model, known as the "random fluctuation" (RF) model, proposes that the growth of individual crystals can change by random fluctuations over the time peiod of the crystallization. The second model, known as the "constant crystal growth" (CCG) model, assumes that each crystal has a constant growth rate and maintains that growth rate throughout the crystallization process unless crystallization conditions change, however there is a distribution of growth rates among the crystal population. The effect of RF growth rate dispersion has been demonstrated to have an effect on the CSD in batch operation, but there is no effect on the CSD in continuous crystallizers.

Conversely, CCG growth rate dispersion affects the CSD of both batch and continuous crystallizers (Mersmann, 1995; Mullin, 2001b; Randolph and Larson, 1988b; Berglund, 2002).

2.3.9 Effect of Impurities on Growth Kinetics and Crystalline Product

It has been recognized that the presence of impurities has an effect on the crystal growth kinetics. During the growth mechanism impurities can also diffuse to the crystal surface and may be then adsorbed onto the surface or even integrated into the lattice at the surface of the crystal. The rate of impurity transport normally relates to the mobility of the impurities and their tendency to incorporate into the crystal lattice, which can be influenced by their concentration, temperature, and supersaturation. Surfaces that contain adsorbed and/or integrated impurities may have significantly retarded crystal growth since the movement of steps on the crystal surface is inhibited. The growth rate reduction can be described by two extremes of mechanisms for impurity adsorption. In the first model, impurities are assumed to be fixed at the site that they first reach at the crystal surface, and this mechanism is known as immobile adsorption. In the second model, it is assumed that adsorbed impurities can diffuse in two-dimensions on the crystal surface by mobile adsorption. In industrial crystallization, strongly adsorbing impurities are expected to have a much greater effect on the crystal growth rate and produce lower crystal product purity than that of weakly bonding impurities. In addition, the presence of impurities affects the overall crystal growth rate, and also can strongly affect the shape of the crystal. The effect on crystal shape is the consequence of the relative growth at different rates of individual faces of the crystal due to facial selective adsorption of the impurities (Mullin, 2001b; Weissbuch *et al.*, 1995; Meenan *et al.*, 2002). The

effect of impurities on crystal growth was discussed in this section, however diversely; the crystal growth rate can have an effect on the incorporation mechanism of impurities, which will be discussed in Chapter VII.

2.4 References

Andreis, H. J., Rizzuto, A. B., and Bichsel, S. E. (1990). Processing sugar from sugarcane and sugar beets. In N. L. Pennington and C. W. Baker (eds.). **Sugar: A User's Guide to Sucrose** (pp. 11-35). New York: Van Nostrand Reinhold.

Baker, R. W. (2004a). Overview of membrane science and technology. **Membrane Technology and Applications** (2nd ed., pp. 1-14). Great Britain: John Wiley and Sons.

Baker, R. W. (2004b). Ultrafiltration. **Membrane Technology and Applications** (2nd ed., pp. 237-274). Great Britain: John Wiley and Sons.

Baker, R. W. (2004c). Microfiltration. **Membrane Technology and Applications** (2nd ed., pp. 275-300). Great Britain: John Wiley and Sons.

Baker, R. W. (2004d). Membrane transport theory. **Membrane Technology and Applications** (2nd ed., pp. 15-88). Great Britain: John Wiley and Sons.

Berglund, K. A. (2002). Analysis and measurement of crystallization utilizing the population balance. In A. S. Myerson (ed.). **Handbook of Industrial Crystallization** (2nd ed., pp. 101-114). USA: Butterworth-Heinemann.

Bubnik, Z. and Kadlec, P. (1995). Sucrose solubility. In M. Mathlouthi and P. Reiser (eds.). **Sucrose Properties and Applications** (pp. 101-125). Great Britain: Blackie Academic and Professional.

Cayle, T. (1990). Sugar in the body. In N. L. Pennington and C. W. Baker (eds.). **Sugar: A User's Guide to Sucrose** (pp. 82-102). New York: Van Nostrand Reinhold.

Chen, J. C. P. (1993). Outline of raw sugar process and extraction of juice. In J. C. P. Chen and C. C. Chou (eds.). **Cane Sugar Handbook** (12th ed. pp. 48-55). New York: John Wiley and Sons.

Chen, J. C. P. and Chou, C. C. (1993). Microbiological control in sugar manufacturing and refining. In J. C. P. Chen and C. C. Chou (eds.). **Cane Sugar Handbook** (12th ed. pp. 641-658). New York: John Wiley and Sons.

Cheryan, M. (1998a). Introduction. **Ultrafiltration and Microfiltration Handbook** (pp. 1-30). Pennsylvania, USA: Technomic Publishing Company, Inc.

Cheryan, M. (1998b). Membrane chemistry, structure, and function. **Ultrafiltration and Microfiltration Handbook** (pp. 31-70). Pennsylvania, USA: Technomic Publishing Company, Inc.

Cheryan, M. (1998c). Performance and engineering models. **Ultrafiltration and Microfiltration Handbook** (pp. 113-170). Pennsylvania, USA: Technomic Publishing Company, Inc.

Cheryan, M. (1998d). Fouling and cleaning. **Ultrafiltration and Microfiltration Handbook** (pp. 237-292). Pennsylvania, USA: Technomic Publishing Company, Inc.

Chou, C. C. and Wnukowski, M. (1981). Dextran problems in sugar refining: A critical laboratory evaluation. In: **Proceedings of the 1980 Technical Session on Cane Sugar Refining Research** (pp. 1-25). LA, USA: Science and Education Administration.

Clarke, M. A. (1993). Sugars and nonsugars in sugarcane. In J. C. P. Chen and C. C. Chou (eds.). **Cane Sugar Handbook** (12th ed. pp. 21-39). New York: John Wiley and Sons.

Cuddihy, J. A., Porro, M. E., and Rauh, J. S. (2001). The presence of total polysaccharides in sugar production and methods for reducing their negative effects. **J. Amer. Soc. Sugarcane Technol**. 21: 73–91.

Flood, C. and Flood, A. E. (2006). Removal of color from the sugar manufacturing process by membrane treatment. **Suranaree J. Sci. Technol.** 13(4): 331-342.

Karpinski, P. H. and Wey, J. S. (2002). Precipitation processes. In A. S. Myerson (ed.). **Handbook of Industrial Crystallization** (2nd ed., pp. 141-160). USA: Butterworth-Heinemann.

Kelly, F. H. C. and Keng, M. F. (1975). **The Sucrose Crystal and Its Solution** (p. 6, and p. 94). Singapore University Press.

Knecht, R. L., (1990). Properties of sugar. In N. L. Pennington and C. W. Baker (eds.). **Sugar: A User's Guide to Sucrose** (pp. 46-65). New York: Van Nostrand Reinhold.

Martins, P. M. and Rocha, F. (2007). New development on size-dependent growth applied to the crystallization of sucrose. **Surface Science.** 601: 5466-5472.

Meenan, P. A., Anderson, S. R., and Klug, D. L. (2002). The influence of impurities and solvents on crystallization. In A. S. Myerson (ed.). **Handbook of Industrial Crystallization** (2nd ed., pp. 67-100). USA: Butterworth-Heinemann.

Mersmann, A. (1995). Fundamentals of crystallization. In A. Mersmann (ed.). **Crystallization Technology Handbook** (pp. 1-78). New York: Marcel Dekker.

Mullin, J. W. (2001a). Crystal growth. **Crystallization** (4th ed. pp. 181-215). Great Britain: Butterworth-Heinemann.

Mullin, J. W. (2001b). Crystal growth. **Crystallization** (4th ed. pp. 216-288). Great Britain: Butterworth-Heinemann.

Myerson, A. S. and Ginde, R. (2002). Crystals, crystal growth, and nucleation. In A. S. Myerson (ed.). **Handbook of Industrial Crystallization** (2nd ed., pp. 33-66). USA: Butterworth-Heinemann.

Peres, A. M. and Macedo, E. A. (1997). Phase equilibria of D-glucose and sucrose in mixed solvent mixtures: Comparison of UNIQUAC-based model. **Carbohyd. Res.** 303: 135-151.

Porter, M. C. (1990). Ultrafiltration. In M. C. Porter (ed.). **Handbook of Industrial Membrane Technology** (pp. 136-259). New Jersey, USA: Noyes Publications.

Randolph, A. D. and Larson, M. A. (1988a). **Theory of Particulate Processes** (2nd ed., pp. 109-134). USA: Academic Press.

Randolph, A. D. and Larson, M. A. (1988b). **Theory of Particulate Processes** (2nd ed., pp. 80-108). USA: Academic Press.

Randolph, A. D. and Larson, M. A. (1988c). **Theory of Particulate Processes** (2nd ed., pp. 135-173). USA: Academic Press.

Rauh, J. S., Cuddihy, J. A., Jr., and Falgout, R. N. (2001). Analyzing dextran in the sugar industry: A review of dextran in the factory and a new analytical technique. In **Proceedings of XXVII Conference West Indies Sugar Technology** (p. 1). Port of Spain: Sugar Association of the Caribbean.

Schwartz, A. M. and Myerson, A. S. (2002). Solutions and solution properties. In A. S. Myerson (ed.). **Handbook of Industrial Crystallization** (2nd ed., pp. 1-32). USA: Butterworth-Heinemann.

Strathmann, H. (1990). Synthetic membranes and their preparation. In M. C. Porter (Ed.). **Handbook of Industrial Membrane Technology** (pp. 1-60). New Jersey, USA: Noyes Publications.

Strickland-Constable, R. F. (1968). **Kinetics and Mechanism of Crystallization** (pp. 7-43). London: Academic Press.

Weissbuch, I., Leiserowitz, L., and Lahav, M. (1995). "Tailor-Made additives" and impurities. In A. Mersmann (ed.). **Crystallization Technology Handbook** (pp. 401-458). New York: Marcel Dekker.

Wey, J. S. and Karpinski, P. H. (2002). Batch crystallization. In A. S. Myerson (ed.). **Handbook of Industrial Crystallization** (2nd ed., pp. 231-248). USA: Butterworth-Heinemann.

Zydney, A. L. (1996a). Module design and membrane configurations. In L. J. Zeman and A. L. Zydney (eds.). **Microfiltration and Ultrafiltration Principles and Applications** (pp. 327-349). New York: Marcel Dekker.

Zydney, A. L. (1996b). Bulk mass transport. In L. J. Zeman and A. L. Zydney (eds.). **Microfiltration and Ultrafiltration Principles and Applications** (pp. 350-379). New York: Marcel Dekker.

Zydney, A. L. (1996c). Membrane fouling. In L. J. Zeman and A. L. Zydney (eds.). **Microfiltration and Ultrafiltration Principles and Applications** (pp. 397-446). New York: Marcel Dekker.

CHAPTER III

DEXTRAN ANALYSIS METHODS DEVELOPMENT

3.1 Abstract

A new method for determination of dextran content in sugar samples was developed based on ^{13}C Nuclear Magnetic Resonance (^{13}C NMR). The method development begins with a study of the effect of dextran molecular weight on the ^{13}C NMR spectrum of the compound. Low fraction dextran (60,000-90,000 Da molecular weight), high fraction dextran (approximately 250,000 Da molecular weight), and an equal weight mixture of both were tested in the study. It was found that the molecular weight does not strongly affect the chemical shift of the peak distribution in the NMR spectrum, so in further studies only one range of dextran molecular weight was used for convenience. To give results applicable over the widest range of conditions the mixture of high and low fraction dextran was considered to be most appropriate for use in the method development. The differences between the ^{13}C NMR spectrum of dextran and that of starch was analyzed to determine the most suitable reference peak for dextran in order to determine the dextran content without interference by the peaks of starch, which is a similar polysaccharide common in sugar syrups. It was seen that the C6 atoms of both materials had the largest difference in chemical shift so the intensity of this peak was used as the key measured variable in the calibration of the method. Since there is only a relatively small amount of dextran in a 57.5% Brix sucrose solution it is difficult to see the dextran peaks within the distribution of very large peaks representing sucrose. Therefore, dextran separation from the sucrose

solution by precipitation with ethanol is required. It was found that dextran completely precipitates from the solution when the volume ratio of ethanol to solution is 2:1, while sucrose does not precipitate to a large extent in these mixtures. A calibration for dextran determination using the ^{13}C NMR technique was prepared from an analysis of the peak areas of the C6 atom of dextran in various concentrations. The equation for the calibration can be expressed as % D = 0.14±0.01*I* (where *I* represents the integral of the peak) with a reproducibility of 1.2-7.7% (variation of standard error of each dextran content determination). The determination of dextran content in solution using the method is suitable for analyzing solutions that contain dextran at a concentration of at least 0.2% (detection limit).

3.2 Introduction

A new method for dextran determination in sugar solution samples using ^{13}C NMR is developed. Sugar syrups from the factory are often contaminated by various materials such as proteins, polysaccharides such dextran and starch, albumins, gums and other compounds (Chen, 1993; Roberts, 1981). Of these materials only starch could interfere with the method since the NMR spectrums of dextran and starch are similar: they are both polymers of glucose units which are likely to have approximately the same NMR peak shifts for some carbon atoms. If the method is necessary to apply to real samples where there are many types of impurities, especially having various types of polysaccharide, the differences between the spectra of dextran and starch should be the primary concern.

3.2.1 Dextran and Its Molecular Structure

Dextrans are homologous polymers of glucans containing predominantly α(1-6) linked glucans with some branches. The degree of branching is estimated as 5% (De Belder, 1990). Dextrans have a variety of types and amounts of branch linkages due to differences in the bacteria species that produce the dextran. For example, dextran with side chains attached mainly by α(1-2) linkages is formed by the bacteria of *Leuconostoc mesenteroides*; the dextran of *Leuconostoc dextranicum* appears to branch mainly with α(1-3) linkages with a smaller amount of α(1-4) linkages, and *Lactobacillus spp.* produces branches of only α(1-3) linkages (Roberts, 1981; Cuddihy *et al.*, 2001; Clarke, 1993). The chemical structures of dextrans are shown in Figure 3.1. Most native dextrans have a high molecular weight, from several thousand Da up to about two million Da.

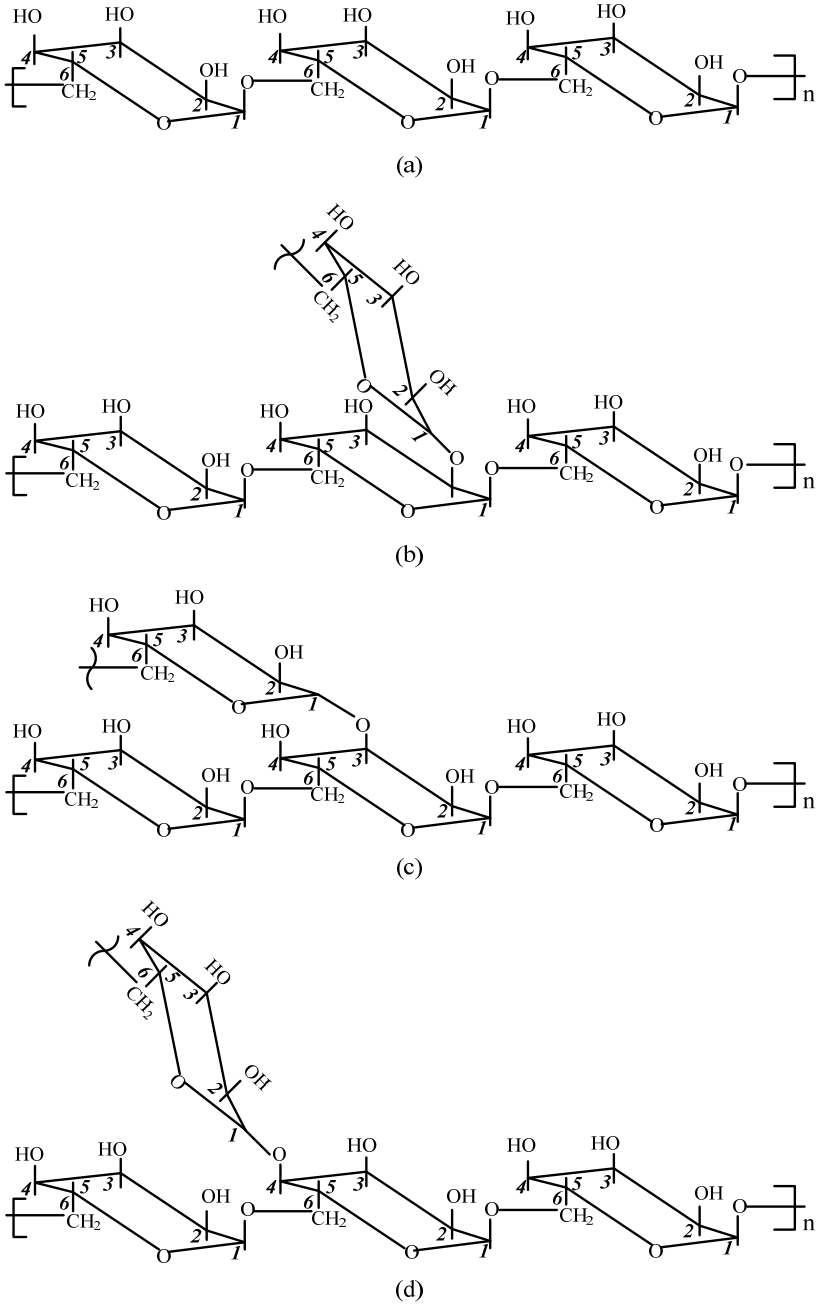

Figure 3.1 Dextrans. (a) Linear α(1-6) linked dextran; (b) Linear α(1-6) linked dextran with α(1-2) branches; (c) Linear α(1-6) linked dextran with α(1-3) branches; (c) Linear α(1-6) linked dextran with α(1-4) branches.

3.2.2 Starch and Its Molecular Structure

Most natural starch consists of two fractions, namely amylose and amylopectin, both of which are polymers of glucose units. The polymers propagate their chains by connecting between the initial chain and adding α-D-glucose by means of α(1-4) linkages. The chain length of starchs is variable with 19-28 units of glucose in amylopectins, and in excess of 2000 glucose units in amylases. Amylopectin consists of a large number of braches that are linked at (1-6) into the main chain, while amylose consists only of either a single or a few longer chains. Most starch has an amylose faction of 0.2-0.3 of the total. The granules of starch are well soluble in dimethylsulfoxide (DMSO) and this is often used as solvent for starch analysis (Cuddihy *et al.*, 2001; Bertoft, 2004). The chemical structures of starches are shown in Figure 3.2.

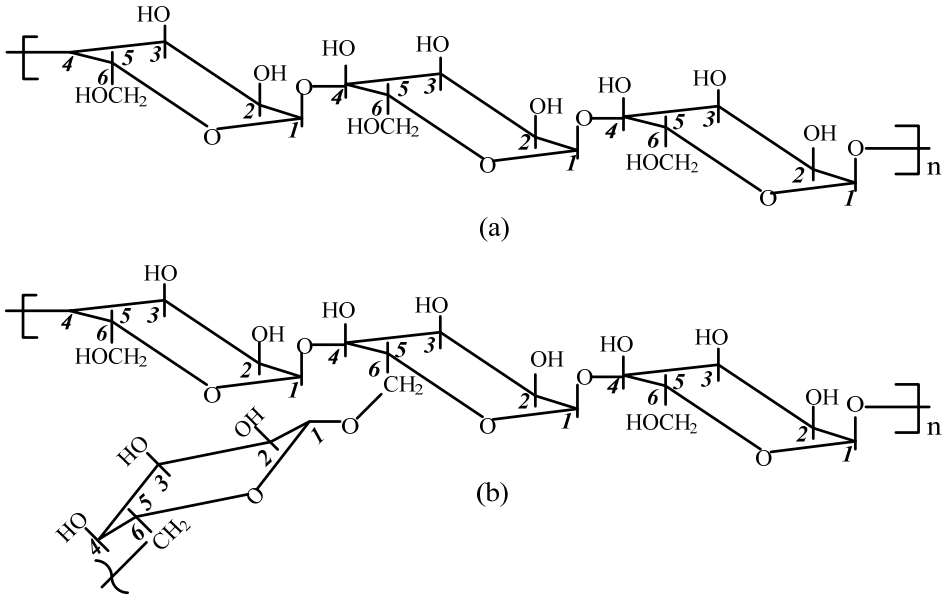

Figure 3.2 Starch (a) α(1-4) linked starch (amylase); (b) α(1-4) linked starch with many α(1-6) linked branches (amylopectin).

3.2.3 The Haze Method

The haze method was the first widely accepted procedure for dextran determination in sugar manufacture. It was first proposed by Nicholson and Horsley in 1959 (Altenburg, 1993). The method begins with steps to remove nondextran components (such as starch, protein, and inorganic salts) from the sample solution. A haze is then formed in the solution due to dextran precipitation by alcohol addition, and the method measures the haze turbidity using spectrophotometry. The method requires a standard curve to predict dextran content from the measured turbidity. The accuracy of the prediction depends on the dextran molecular weight that was used in the standardization. A modified haze method has been developed by Chou and Wnukowski (Altenburg, 1993) to avoid the question of which molecular weight should be used in the standardization; this method measures the dextran content in milliabsorbance units (MAU) that can be converted to ppm by the expression of $ppm = (MAU + 118)/0.659$ (Altenburg, 1993).

The modified haze method begins by dissolving raw sugar in distilled water from which nondextran materials are removed in many steps before the addition of absolute ethyl alcohol. For example, starch can be removed by a suitable enzyme; protein can be removed by trichloroacetic acid followed by filtration; and any inorganic salts can be removed by ion exchange resins. A filtrate that is free of non dextran components is transferred to a volumetric flask after which an equal volume of alcohol is added to form a haze. After allowing the sample to stand for 60 min, the absorbance of the sample is measured by a spectrophotometer at 720 nm (Altenburg, 1993).

3.2.4 Roberts Test

The Roberts test is a more recent method for dextran (Altenburg, 1993). It can be used for sugar products, cane juice, syrups and molasses, since it is suitable for use on dark colored materials due to dextran separation from the sample. All polysaccharides are separated from the sample by precipitation with 80% ethanol, followed by collection with filter aid on a coarse sintered glass. The precipitate is dissolved from the filter aid by washing with distilled water then filtering through a Whatman No.42 filter paper. The dextran is in the filtrate.

The dextran can be selectively separated from the filtrate by forming a dextran-copper complex with alkaline copper sulfate. The separated dextran is hydrolyzed by addition of sulfuric acid to develop color with phenol. The color is read by absorbance on a spectrophotometer at 485 nm against a blank. The absorbance value can predict the dextran content in the sample by use of a standard curve.

The Roberts test is more specific for dextran than the Haze method due to the selective precipitation with alkaline copper sulfate. It can also determine all ranges of dextran molecular weight, while the haze method cannot detect dextran with a molecular weight below 10,000 Da, and has diminished sensitivity for dextran below 100,000 Da (Altenburg, 1993).

3.2.5 Nuclear Magnetic Resonance

NMR involves the interaction between a radio wave and a spinning nucleus of the constituent atoms of a molecule. The radio wave is generated from the radiation of an electromagnetic field. The frequency of radio wave is on the order of 100 MHz. Although the quantity of radio wave energy is too small to vibrate, rotate

or electronically excite an atom or molecule, it is enough to spin the nucleus of an atom in a molecule. The spinning nuclei which absorb radio frequency energy will change the direction of their spinning axis. In analytical chemistry, the NMR technique is used in the analysis of shape and structure of molecules by the variation of nuclei spinning in atoms having different bonding and/or environment. The most common application of NMR in organic compounds concerns ^{1}H or ^{13}C isotopes. It is necessary to use ^{13}C (spin number $1/2$), although this isotope represents only 1% of the total C present, for analysis using the NMR technique since the ^{12}C isotope (zero spin number) does not respond in NMR (Robinson, 1987).

1. Chemical shifts

The constituent atoms in different types of molecules absorb at slightly different frequencies in NMR, due to the different chemical character of the atoms present changing the electronic environment of the nuclei. The energy shifts relative to other nuclei are called the chemical shifts (Robinson, 1987). In quantitative measurement using NMR, a standard material must be selected to be the reference, and this is most simple if there is only one chemical shift in the standard compound and this chemical shift is in a region very distinct from the chemical shifts of the sample.

2. Carbon-13 NMR

Carbon-13 (^{13}C) NMR was first studied in 1957, but was not used to a significant extent until the first NMR instrument had been developed in 1970. The reason for this delay is due to the sensitivity of the instrument being insufficient to detect the weak signal from the ^{13}C nucleus due to its low natural isotopic abundance. However, ^{13}C NMR can be more useful than proton NMR in organic and

biochemical structure analysis since it presents information about the backbone of the molecules rather than about the periphery. Moreover, there is less peak overlap in the ^{13}C spectra because it has a wider range of chemical shifts (up to 200 ppm) while the ^{1}H spectra is limited to about 15 ppm. Therefore structural analysis by ^{13}C NMR should result in a more accurate structure (Skoog et al., 1998).

3.2.6 Objectives of the Study

Although there are few methods that have been used in determination of dextran content in sugar streams, either they can not give a very accurate result due to the variation of dextran molecular weight, or they are complicated methods. In the current study, ^{13}C NMR will be used to develop a very accurate method for analyzing dextran content in sugar syrups and crystals. The developed method should be simpler, and not affected by the molecular weight of the sample or by the presence of starch or other polysaccharides. For the purpose of the method development, it is necessary to calibrate the function relating the dextran concentration in the sample to the response of the NMR spectrum.

3.3 Materials and Methods

3.3.1 Materials

In the study a high purity (>99.9%) commercial refined sugar was used as a source of sucrose, and high fraction dextran (specified by the company as approximately 250,000 Da molecular weight) and low fraction dextran (specified by the company approximately 60,000-90,000 Da molecular weight), both from ACROS Organics. Glycine (used as the internal standard) and required solvents such absolute ethanol and deuterium oxide were analytical grade as specified by ACS.

3.3.2 Methods

It was necessary to identify a NMR spectral peak that is fully separated from other peaks of the dextran molecule and also the peaks of other molecules likely to be present in sample mixtures. This peak can be used to determine the dextran content by integration of the peak. A peak with a resolvable peak shift in the ^{13}C NMR spectra of complex mixtures can be difficult to find since overlapping peaks are common for complex solutions.

It is necessary to determine a sufficient amount of absolute ethanol required to precipitate all dextran from sucrose solutions, while minimizing precipitation of sucrose. Calibration standards of various dextran content (from 0.2 to 3 grams dextran per mL of initial solution) in 57.5% Brix sucrose solutions were produced in quantities of 50 mL. These solutions were precipitated by ethanol in various ratios of ethanol to solution. The precipitates were separated from the solutions by filtering through a Whatman No. 42 filter paper. Long chain polymeric materials such as dextran and starch precipitate more readily than sucrose, so that sucrose did not precipitate to a large extent. Table 3.1 shows that the solubility of sucrose in a 20% ethanol in water mixture reduces only 10.6% from that in pure water. However complete precipitation of dextran in this mixture is expected. The dextran precipitates were dissolved in 10 mL of water to concentrate the dextran content of the initial solution by five times for ^{13}C NMR analysis. 400 μL of this dextran solution was mixed with D_2O (200 μL) and glycine (100 μL, 0.7 M) as an internal standard, and then analyzed by NMR.

Table 3.1 Solid-liquid equilibrium data for sucrose-water-ethanol at 25°C (adapted from the data of Peres and Macedo, 1997).

% by volume of ethanol in the sugar-free solution	% by mass of sucrose dissolved in the mixture	Relative solubility reduction (%)
0.00	67.4623	0
24.02	60.3325	10.6
35.10	55.6056	17.6
45.80	48.2336	28.5
55.81	38.9091	42.3
65.68	26.7090	60.4
74.76	14.4279	78.6
83.57	4.2244	93.7
91.92	0.6794	99.0
100.00	0.0501	99.9

A calibration for the NMR technique was prepared by determination of the peak area of the C6 carbon in the dextran molecule, which has a chemical shift of 66.1 ppm. This atom has a peak shift which gives full separation from all other carbons in the mixture (including any residual sucrose), assuming that the concentration of the other components is not extremely high. The method begins with preparation of 57.5% Brix sucrose solutions containing dextran in various known concentrations. All the dextran in 10 mL of the solutions was precipitated with 20 mL of absolute ethanol. The precipitates were separated from the solutions by filtration,

and then the NMR technique was used to analyze the dextran content in the solutions based on the peak area of the C6 carbon atom.

3.4 Results and Discussion

3.4.1 Dextran Separation from Sucrose Solution

The ^{13}C NMR spectra of three sample solutions, high fraction dextran (approximately 250,000 Da molecular weight), low fraction dextran (60,000-90,000 Da molecular weight), and the mixture of dextran factions in the ratio of 1:1 by weight, were determined using ^{13}C NMR spectroscopy. The spectra are shown in Figure 3.3a for low fraction dextran, Figure 3.3b for high fraction dextran, and Figure 3.3c for the 1:1 ratio of low fraction dextran and high fraction dextran. The NMR spectrum of dextran solution in the presence of sucrose is shown in Figure 3.4. The chemical shifts for each carbon atom of the dextran samples are shown in Table 3.2. It is seen that the chemical shifts (δ) of the six carbon atoms C1-C6 of each dextran sample are not significantly different than in the other dextran samples, and therefore that one sample can be assumed to be representative of all dextran fractions for further study. Therefore it was decided that the mixture of dextran is appropriate to use to represent a wide range of dextran molecular weight.

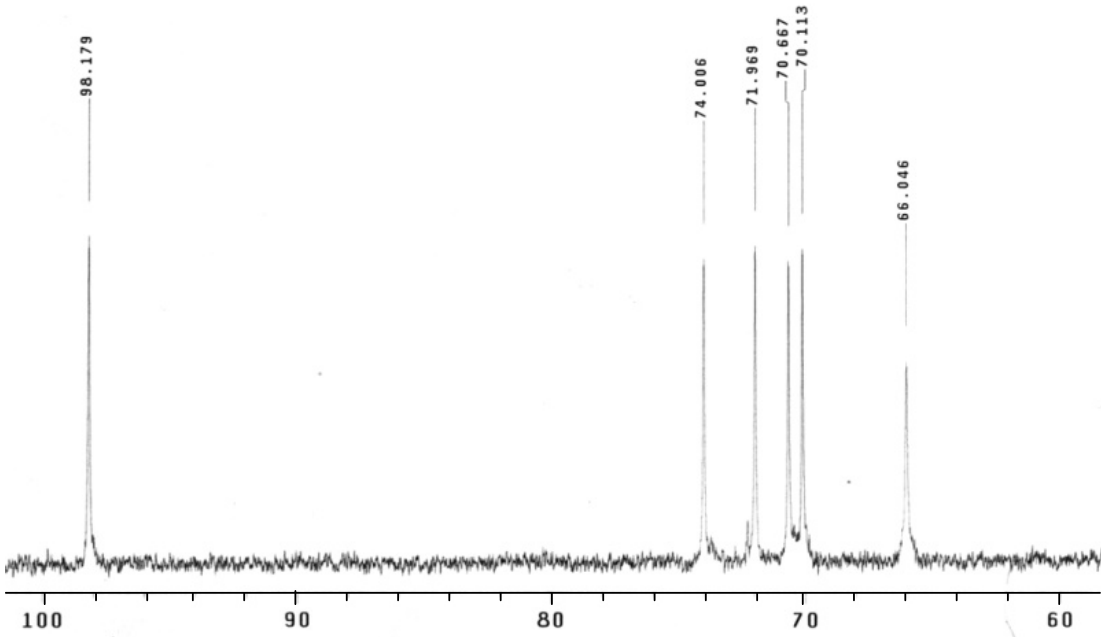

(a) The ^{13}C NMR spectrum of low fraction dextran.

Figure 3.3 The ^{13}C NMR spectra of dextran.

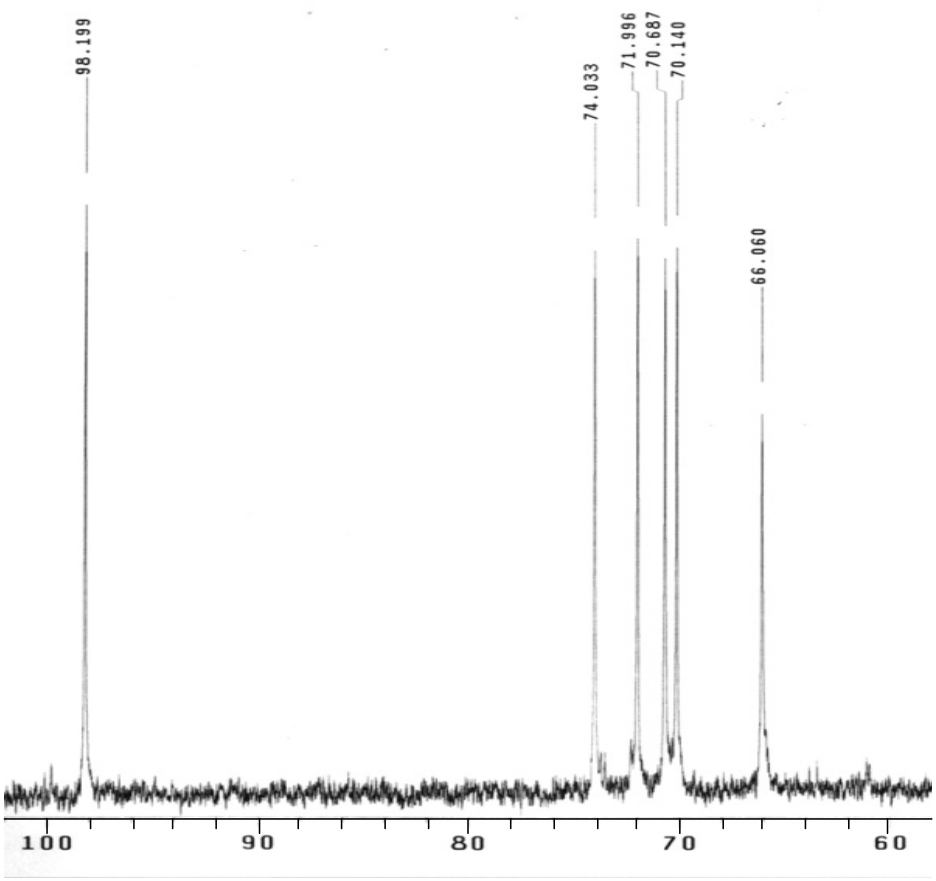

(b) The ^{13}C NMR spectrum of high fraction dextran.

Figure 3.3 The ^{13}C NMR spectra of dextran (continued).

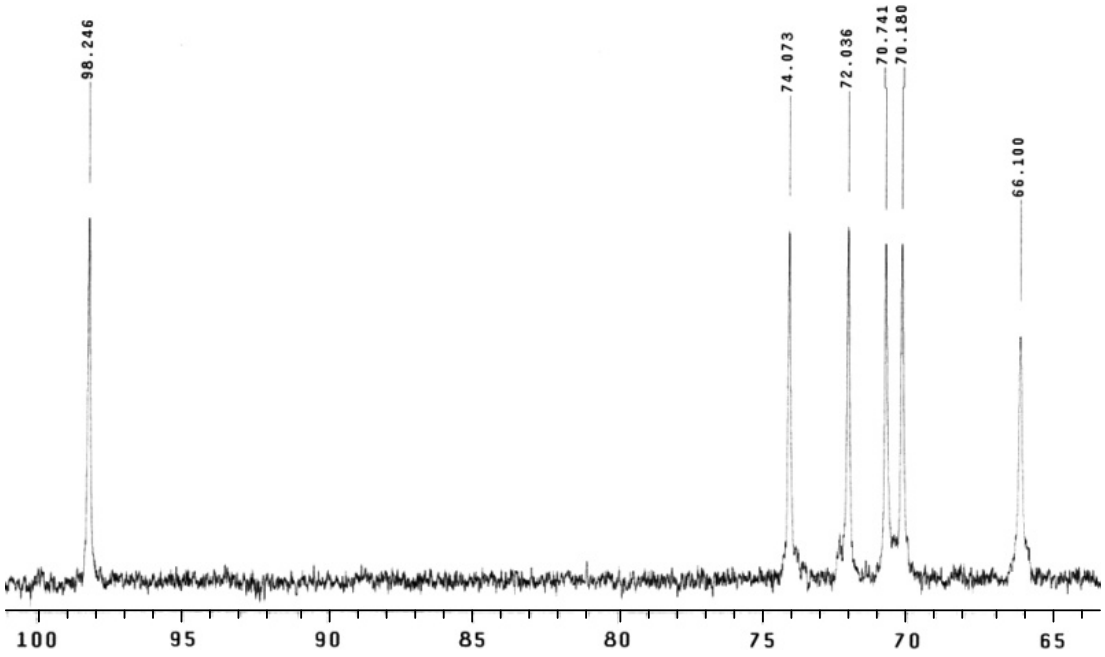

(c) The ^{13}C NMR spectrum of a 1:1 mixture of low fraction and high fraction dextrans.

Figure 3.3 The ^{13}C NMR spectra of dextran (continued).

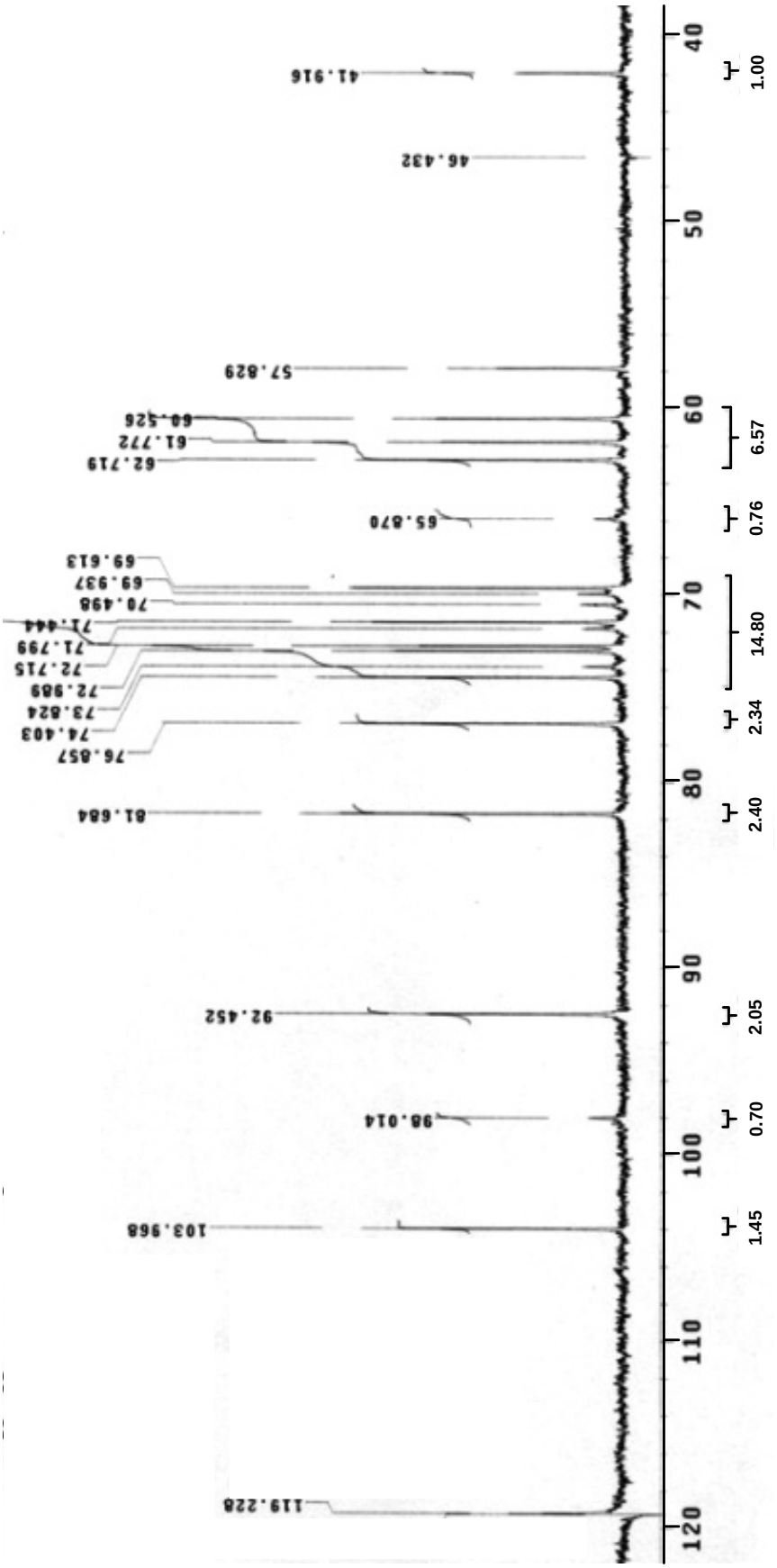

Figure 3.4 The NMR spectrum of dextran solution in the presence of sucrose.

Table 3.2 The ^{13}C NMR chemical shifts for each carbon atom of three dextran samples.

Carbon atoms	Chemical shifts of dextran		
	Low fraction dextran	**High fraction dextran**	**1:1 ratio of low and high fraction dextrans**
C1	98.179	98.199	98.246
C2	71.969	71.996	72.036
C3	74.006	74.033	74.073
C4	70.667	70.687	70.741
C5	70.113	70.140	70.180
C6	66.064	66.060	66.100

In addition, it can be assumed that differences in dextran type (based on particular branching differences between different types) has an effect on the chemical shifts of all carbon atoms, although the difference is not sufficient to distinguish the type of dextran present in the solution. The chemical shifts of the six carbon atoms (C1-C6) of each dextran type are listed in Table 3.3, which contains data from Uzochukwu and Seymour (Uzochukwu *et al.*, 2002; Seymour *et al.*, 1976).

Table 3.3 The ^{13}C NMR chemical shifts for each carbon atom of several dextran types.

Carbon atoms	Chemical shifts of each dextran			
	Linear dextran	**A(1-6) D-glucan with α(1-2) branches***	**α(1-6) D-glucan with α(1-3) branches***	**α(1-6) D-glucan with α(1-4) branches***
C1	98.67	98.71	98.93	98.70
C2	72.37	72.40	72.62	72.42
C3	74.36	74.40	74.36	74.33
C4	71.14	71.18	71.16	71.26
C5	70.52	70.54	70.62	70.44
C6	66.56	66.59	66.13	66.55

* Data from Seymour (1976)

Dextran consists of α(1-6) glucosidic linkages in the backbone of the molecule, while the backbone of the starch molecule is formed by bonding glucose units with α(1-4) linkages. Although there is a similarity between some chemical shifts of dextran and starch due to the similarity of the two molecules, it is expected that the chemical shifts of the C2, C4, and C6 carbons have a small but significant difference to distinguish dextran from starch. Previous research has shown that the chemical shifts for the C1, C4, and C6 carbons of starch are at 101.6, 80.9 and 61.2 ppm respectively, while the chemical shifts of the C2, C3, and C5 carbons vary in the range between 68.2-71.3 ppm (Stawski and Jantas, 2003). In this work the chemical shifts for dextran are reported in Table 3.3. The average values for the chemical shifts

of the C1-C6 carbons in the dextran molecule are 98.2, 72.0, 74.0, 70.7, 70.1, and 66.1 ppm, respectively. From these results, it can be seen that the chemical shifts for C4 and C5 of dextran appear in the region expected to have an overlap with starch, 68.2-71.3 ppm, so these shifts are not useful to distinguish dextran from starch. In contrast, the chemical shift for C6 of dextran would be beneficial for the study since is far away from the closest starch peak, the C6 of starch, which is at least 5 ppm different. This is sufficient for use to distinguish dextran and starch. The chemical shifts of sucrose determined in this work are also placed in Table 3.4, and it can be seen that there is no sucrose peak that should overlap the peak for the dextran C6 carbon. The chemical shift of each carbon atom in both the glucose moiety and fructose moiety of the sucrose molecule were identified by comparison with the NMR spectrum of sucrose, which has been reported (Perez, 1995). In addition, the table shows that the chemical shifts of sucrose have a high possibility for peak overlap with other sucrose peaks or by dextran peaks in the range of 70-80 ppm, and this again suggests that the peaks C2-C5 of dextran are not suitable for use as a reference peak in dextran determination using the ^{13}C NMR technique.

Table 3.4 The ^{13}C NMR chemical shifts of dextran, starch (amylose), and sucrose.

Compound	C1	C2	C3	C4	C5	C6
	Chemical shifts (ppm)					
Dextran	98.2	72.0	74.0	70.7	70.1	66.1
Starch (Gidley and Bociek, 1988)	100.9	72-73	74.6	78.6	72-73	61.9
Sucrose	Chemical shifts (ppm)					
glucose moiety	92.4	71.4	72.9	69.6	72.7	60.5
Fructose moiety	61.7	103.9	76.8	74.4	81.6	62.7

The effect of ethanol addition on the amount of dextran precipitation was investigated to determine a suitable value of the amount of ethanol required to precipitate all of the dextran in the sample. The correct ratio of ethanol addition to sample size can be observed from the relation between the ^{13}C NMR peak area of the C6 atom of dextran separated from the standard solution by precipitation with ethanol, and the ratio of ethanol added to solution sample size. Figure 3.3 shows the dextran precipitation in the solution increases with an increase in the ratio of ethanol to sample. A polysaccharide such as dextran is insoluble in ethanol so it can be separated from the sucrose rich solution by non solvent crystallization. The solubility of sucrose and dextran in the solutions decrease with an increasing amount of ethanol added, and thus the amount of precipitate can be increased up to the point of complete dextran precipitation. However during the precipitation process sucrose will also be precipitated and thus an appropriate amount of ethanol addition is necessary. Since the NMR peaks of sucrose could swamp the dextran peak if a significant amount of

sucrose was precipitated (remembering that the sucrose content of the sample is more than an order of magnitude larger than the dextran content), an appropriate amount of ethanol should precipitate all of the dextran in solution while precipitating the least possible amount of sucrose. Figure 3.5 shows that the dextran in the solution is fully precipitated at a ratio of ethanol to sample of 2:1 (volume to volume).

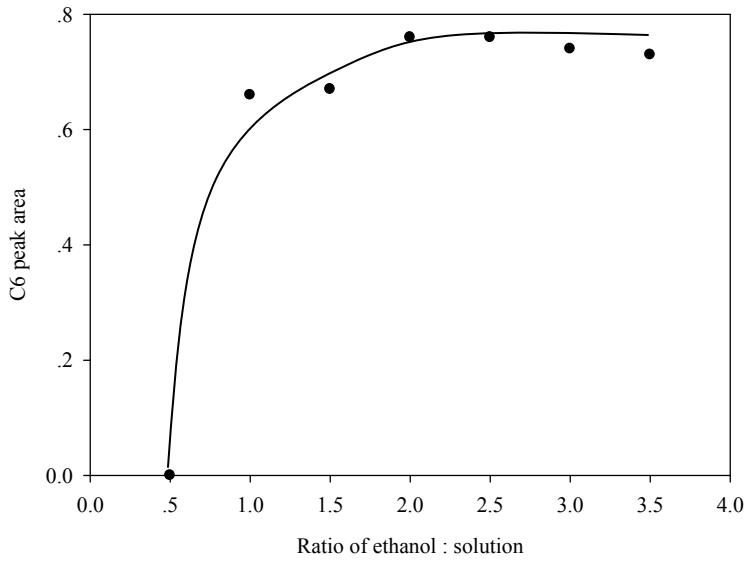

Figure 3.5 Dextran precipitations due to addition of ethanol. C6 NMR peak area relates to the amount of dextran that precipitated in the solution sample.

There is a previous study of the effect of alcohol addition on dextran precipitation (Chou and Wnukowski, 1981). Results have been reported in terms of the relation between the volume percent of alcohol in the solution and the variation of absorbance at 720 nm due to the formation of dextran haze. The results showed that an initial precipitation of dextran occurs at approximately 35% by volume ethanol, however the exact point is not clear since the amount of dextran precipitated is very small. Therefore an effectively initial precipitation commenced at 42% and the

precipitation increases with the addition of ethanol up to an almost complete precipitation at 48% ethanol. In the current work, it was found that the 2:1 volume ratio of ethanol to sucrose solution (approximately 67% ethanol) was optimum, so it is quite sure that dextran precipitation is complete at this ratio. Another study on the effect of ethanol concentration on dextran precipitation in raw sugar samples is shown in Table 3.5 (Brown and Inkerman, 1992). Dextran levels were determined by an HPLC technique. The results show increasing dextran precipitation with increasing ethanol content added into the solution samples. The authors suggested that "the results indicate that ethanol concentrations of 75% or greater were sufficient to precipitate all of the dextran present in raw sugar, i.e., the entire range of molecular weight size of dextran found in raw sugar."

Table 3.5 Effect of ethanol concentration on dextran levels in raw sugar.

Sugar	**Dextran obtained by precipitation due to the presence of each % by volume ethanol in sugar juice (ppm on solids)**				
	33.3	50.0	66.6	75.0	80.0
A	261	841	954	1038	1035
B	139	770	1000	1041	1021
C	676	656	897	900	911
D	552	616	797	847	855

3.4.2 Calibration by Relating Between Peak Area and Dextran Content

Figure 3.6 shows a calibration for the NMR technique that has been prepared to show the relationship between the dextran concentration in the prepared

standards (using the precipitation and re-dissolution technique described above) as well as aqueous samples prepared directly for this test, and the peak area of the C6 carbon in the dextran molecule, which has a chemical shift 66.1 ppm. There are two types of data plotted in Figure 3.6; one is the calibration data of dextran content in pure water, and the second is the calibration data of dextran content in 57.5% Brix sucrose solution, which has been analyzed after the ethanol precipitation process described above. It is seen that both sets of data can be correlated using one line fitting the C6 peak area of dextran; the result from both prepared standards, and samples prepared using the precipitation technique on raw sugar samples give the same result. This result supports the interpretation that there is no loss of dextran during the alcohol precipitation with a 2:1 ratio of ethanol to sample solution. The calibration is also a linear result, which enhances its ease of use. The calibration result is that the % Dextran content (D) is 0.14 times the C6 peak integral (I) with ±0.01% for 95% confidence intervals. The detection limit of the dextran content determination by using NMR method is about 0.2% based on preparation of 10 mL concentrated sample from 50 mL of initial sample. The method is quite flexible since if dextran content is low, larger samples can be used for alcohol precipitation in order to achieve more concentrated dextran samples which can be used in the NMR analysis. However there is a potential limit to the dextran content applicable, since too much alcohol or too much sample might be required if the dextran content in the sample is very low, such as at the ppm level.

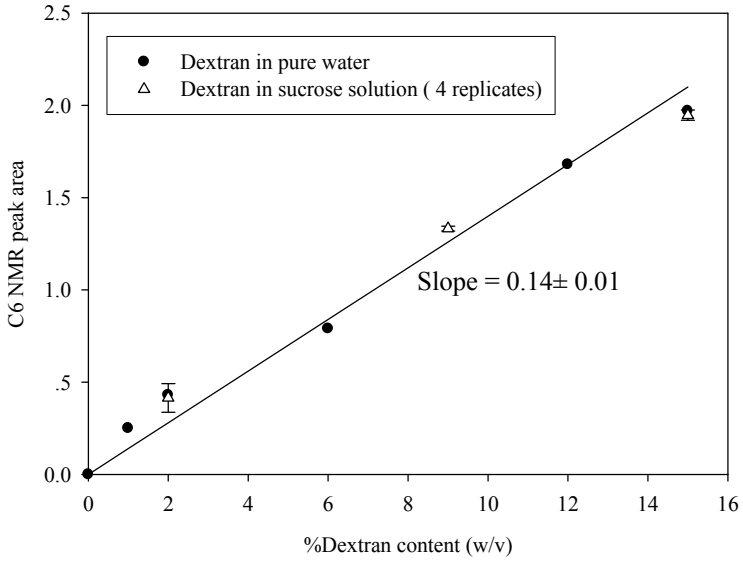

Figure 3.6 Calibration for determination of dextran content in solution samples. Unit of dexttran content is g/100 mL solution.

There are examples in the literature of quantitative analyses for some compounds based on the application of ^{13}C NMR. One example is an application for determination of cellulose concentration in tobacco by using the C1 resonance of cellulose as the analyzed peak (Hall and Wooten, 1998). The cellulose concentration was determined using a calibration of the peak integral of standard cellulose related to 4-(N-Methylpyrrolidino)bicyclo[3.2.1]octan-8-one trifilate ("d321") that is used as internal standard. It was found that there is at least 5.8±0.1% by weight cellulose content in dried tobacco lamina. The reproducibility of the method used in the research varies from ±0.1% to ±0.8% for 95% confidence intervals. A second application is the determination of mesophases composition of cubic MCM-48 and hexagonal MCM-41 (both have 17 carbon atoms in the molecule) mixtures by using integration of many NMR peaks (C5-C14 resonances) divided by the intensity of the C1 resonance (Nur *et al.*, 2004). Since this research was performed for determination

of the composition in mixtures of the two components so a purer component is often used as a key for detection so that the amount of another component can be calculated, therefore in this case the detection limit for NMR method is not a concern. The quantitative measurement of lignins is an application of ^{13}C NMR based on the comparison to internal standards such as 1,3,5-trioxane, and pentafluorobenzene (Xia *et al.*, 2001). This shows the standard errors for the NMR spectra for each interval for the range between 52.5 ppm and 154.6 ppm chemical shifts, which varies from 0.7 to 8.1%. The measurement was used for determination of the concentration at the percent level. However these examples are presented to show the application for quantitative measurement of ^{13}C NMR with an internal standard. Their detection limits and their reproducibility vary with the variation of either sample preparation or sub-technique for analyzing by NMR, so they can not be used to compare directly to the result of the current study.

3.5 Conclusions

The result of ^{13}C NMR spectrums of three dextran molecular weight fractions, low fraction, high fraction, and the mixture of 1:1 (by weight) of both, shows an identical distribution of NMR peaks. Therefore the 1:1 by mass ratio of dextran mixture was used to represent a wide representative range of dextran molecular weight in the current study. Besides the variation of molecular weight, another problem concerns polysaccharides such as starch which may have an effect on the dextran analysis using NMR, since starch is similar in structure to dextran, with some peak overlap being possible. The observation of the chemical shifts of both dextran and starch showed that the largest difference in peak shift occurs for the C6 atoms,

where the peak shift for dextran is 66.1 ppm, while the peak shift for starch is 61.2 ppm. The C6 peak for dextran also does not overlap with other peaks of starch or sucrose. Since the dextran concentration in juice or syrup in sugar process in very small, it is necessary to separate dextran from the solutions by precipitation before applying the NMR technique. The amount of ethanol addition was adjusted to determine the condition under which all of the dextran in the solution was precipitated, while minimizing the amount of sucrose precipitated. It was seen that full dextran precipitation in the solution sample begins with a 2:1 ratio by volume of ethanol to sample. A calibration for dextran determination for the NMR technique was prepared from the peak areas of the C6 atom of dextran in various concentrations. The equation for the calibration can be expressed as $\% D = 0.14 \pm 0.01I$ with a reproducibility of 1.2-7.7% (variation of standard error of each dextran content determination). In the current study, it was seen that the detection limit of the dextran content determination using NMR method is about 0.2%. However the detection limit is quite flexible and can be lowered by using a concentrated sample from a larger amount of solution. Since dextran contents for the further work involving membrane filtration or partition coefficient by crystallization are very low (at the level of ppm), the NMR method is still not realized for use in these further studies.

3.6 References

Altenburg, W. (1993). Determination of dextran and starch. In J. C. P. Chen and C. C. Chou (eds.). **Cane Sugar Handbook** (12th ed. pp. 904-921). New York: John Wiley and Sons.

Bertoft, E. (2004). Analysing starch structure. In A. C., Eliasson (ed.). **Starch in food: structure, function, and applications** (pp. 57-96).USA: Woodhead Publishing.

Brown, C. F. and Inkerman, P. A. (1992). Specific method for quantitative measurement of the total dextran content of raw sugar. **J. Agric. Food Chem**. 40: 227-233.

Chen, J. C. P. (1993). Outline of raw sugar process and extraction of juice. In J. C. P. Chen and C. C. Chou (eds.). **Cane Sugar Handbook** (12th ed. pp. 48-55). New York: John Wiley and Sons.

Chou, C. C. and Wnukowski, M. (1981). Dextran problems in sugar refining: A critical laboratory evaluation. In: **Proceedings of the 1980 Technical Session on Cane Sugar Refining Research** (pp. 1-25). LA, USA: Science and Education Administration.

Clarke, M. A. (1993). Sugars and nonsugars in sugarcane. In J. C. P. Chen and C. C. Chou (eds.). **Cane Sugar Handbook** (12th ed. pp. 21-39). New York: John Wiley and Sons.

Cuddihy, J. A., Porro, M. E., and Rauh, J. S. (2001). The presence of total polysaccharides in sugar production and methods for reducing their negative effects. **J. Amer. Soc. Sugarcane Technol**. 21: 73–91.

De Belder, A. N. (1990). **Dextran** (pp. 1-5). Sweden: Amersham Biosciences.

Gidley, M. J. and Bociek, S. M. (1988). ^{13}C CP/MAS NMR studies of amylase inclusion complexes, cyclodextrins, and the amorphous phase of starch granules: Relationships between glycosidic linkage conformation and solid-state ^{13}C chemical shifts. **J. Amer. Chem. Soc.** 110: 3820-3829.

Hall, R. A. and Wooten, J. B. (1998). Quantitative analysis of cellulose in tobacco by ^{13}C CPMAS NMR. **J. Agric. Food Chem**. 46: 1423-1427.

Nur, H., Guan, L. C., Endud, S., and Hamdan, H. (2004). Quantitative measurement of a mixture of mesophases cubic MCM-48 and hexagonal MCM-41 by ^{13}C CP/MAS NMR. **Mater. Lett.** 58: 1971-1974.

Peres, A. M. and Macedo, E. A. (1997). Phase equilibria of D-glucose and sucrose in mixed solvent mixtures: Comparison of UNIQUAC-based model. **Carbohydrate Research.** 303: 135-151.

Perez, S. (1995). The structure of sucrose in the crystal and in the solution. In M. Mathlouthi and P. Reiser (eds.). **Sucrose Properties and Applications** (pp. 11-32). Great Britain: Blackie Academic and Professional.

Roberts, E. J. (1981). Dextran analysis: Methods and problems. In: **Proceedings of the 1980 Technical Session on Cane Sugar Refining Research** (pp. 128-133). LA, USA: Science and Education Administration.

Robinson, J. W. (1987). Nuclear magnetic resonance. **Undergraduate Instrumental Analysis** (4^{th} ed, pp. 85-120). New York: Marcel Dekker.

Seymour, F. R., Knapp, R. D., and Bishop, S. H. (1976). Determination of the structure of dextran by ^{13}C nuclear magnetic resonance spectroscopy. **Carbohydrate Research.** 51: 171-194.

Skoog, D. A., Holler, F. J., and Nieman, T. A. (1998). Nuclear magnetic resonance spectroscopy. **Principles of Instrumental Analysis** (5^{th} ed, pp. 479-480). USA: Brook/Cole.

Stawski, D. and Jantas, R. (2003). Preparation and characterisation of (meth)acryloyloxystarch. **Autex Res. J.** 3(2): 85-89.

Uzochukwu, S., Balogh, E., Loefler, R. T., and Ngoddy, P. O. (2002). Structural analysis by ^{13}C-nuclear magnetic resonance spectroscopy of glucans elaborated by gum-producing bacteria isolated from palm wine. **Food Chem.** 73(3): 287-291.

Xia, Z., Akim, L. G., and Argyropoulos, D. S. (2001). Quantitative ^{13}C NMR analysis of lignins with internal standards. **J. Agric. Food Chem.** 49: 3573-3578.

CHAPTER IV

DEXTRAN SEPARATION BY ULTRAFILTRATION

4.1 Abstract

Dextran separation from a synthetic clarified juice stream that contained a total dissolved solid of 15% Brix (mostly sucrose) was performed on a stirred-cell ultrafiltration (UF) unit operated in a dead-end configuration. Transmembrane pressure and magnetic stirrer speed were varied to study their influence on the permeate flux and the percent rejection of the process. Commercial membranes of two materials with a variety of pore sizes (RC MWCO 5,000, 10,000, and 30,000, and PES MWCO 5,000) were used in the study. In a comparison of the performance of the membranes, it was found that the RC membrane with a 5,000 MWCO has a larger percent rejection than that of the other membranes, while its flux is suitable. Furthermore, it was seen that the flux in the membrane separation of the synthetic solutions can be improved both by operating at high speed agitation and increasing transmembrane pressure as much as possible without causing damage to the membrane. The percent rejection can be improved only by increasing the stirring speed, which reduces the concentration polarization effect.

4.2 Introduction

4.2.1 Ultrafiltration

UF is a separation technique based on selective passage of molecules or other species through a microporous membrane. It is a widely used technique to separate larger molecules from smaller molecules that are dissolved in solvents (most commonly water). The average pore size of the UF membrane is in the range of 10-1000 Å. However, commercial UF membranes are typically specified by the molecular weight cut-off (MWCO). The term MWCO came into being for UF membranes, and is defined as the size of a globular protein that would have a rejection of at least 90% for a particular membrane (Baker, 2004a; Cheryan, 1998a; Porter, 1990).

4.2.2 Permeate Flux

In membrane processes, the permeation flux is proportional to the driving force. The driving force for ultrafiltration is the transmembrane pressure and thus the relationship between the flux (J) and the transmembrane pressure (ΔP) is usually considered to be proportional. The equation modeling this is Darcy's law

$$J = \frac{\Delta P}{\mu R_m} \tag{4.1}$$

where R_m is the membrane resistance and μ is the viscosity of the permeate (Cheryan, 1998b). The flux is commonly measured in units of *volume/area·time*. Alternatively, the flux can be expressed as

$$J = \frac{\Delta P \varepsilon}{32 \mu \ell} \cdot d^2 \tag{4.2}$$

where ε, ℓ, and d are porosity, the pore length, and the pore diameter, respectively (Baker, 2004b; Cheryan, 1998b).

The above equations are restricted to membrane flux without fouling or concentration polarization since they only account for the resistance of the membrane. Inclusion of resistance due to fouling, R_f, and resistance due to concentration polarization, R_{cp}, gives (Cheryan, 1998b),

$$J = \frac{\Delta P}{\mu\left(R_m + R_f + R_{cp}\right)} \tag{4.3}$$

In some instances, the osmotic pressure ($\Delta\pi$) due to the accumulation of rejected solute at the membrane surface is significant (Cheryan, 1998b). In this case, Darcy's equation can be written as

$$J = \frac{\Delta P - \Delta\pi}{\mu R_m} \tag{4.4}$$

4.2.3 Membrane Rejection

During the UF process, molecules that have a molecular size approximately equal to or larger than the membrane pore size may be rejected by the membrane. The term "rejection" is widely used to characterize the membrane ability for the separation. The percent rejection can be defined as

$$\text{Rejection (\%)} = \frac{\left(C_f - C_p\right)}{C_f} \times 100 \tag{4.5}$$

where C_f and C_p represent the concentration of the feed solution and that of the permeate, respectively (Yoon *et al.*, 2006). There are several factors which affect permeation through the membrane such as the interaction between molecules and the membrane, and the size of molecules, which is generally specified by the molecular weight. However, besides the molecular weight, the shape of the molecule is also an important factor that has an effect on the membrane rejection. For example, Figure 4.1 shows a comparison between linear molecules and globular molecules attempting to pass through a porous membrane. It can be seen that when the molecular weight of both molecules are the same, a linear shaped molecule with a molecular weight larger than the MWCO may snake through the pores, while a globular or spherical shaped molecule of the same size may be retained by the membrane (Baker, 2004b; Cheryan, 1998c; Porter, 1990).

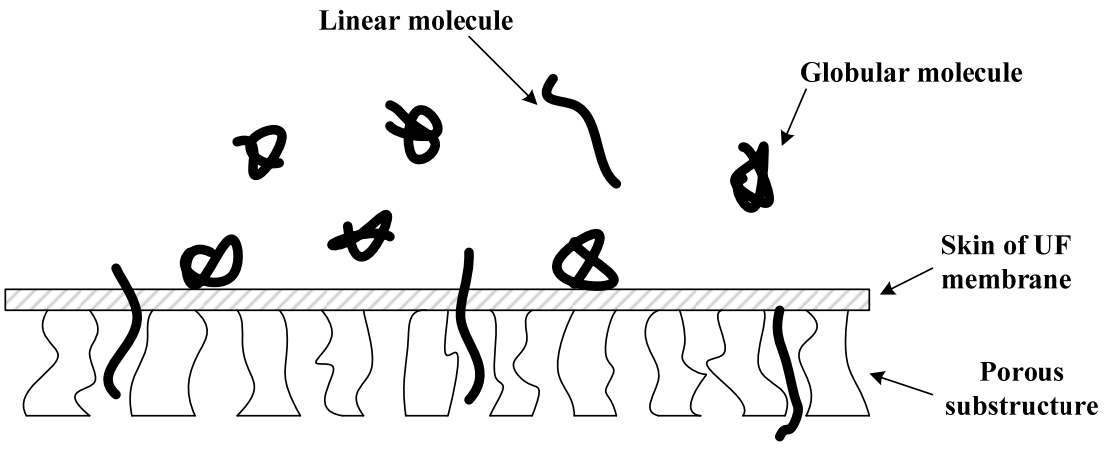

Figure 4.1 Retention of spherical and linear molecules (adapted from Baker, 2004b; Cheryan, 1998; Porter, 1990).

4.2.4 Concentration Polarization

Concentration polarization is a phenomenon where there is an increasing concentration of the rejected molecules at the membrane interface since the material passing through the membrane is necessarily depleted of these molecules. Further increases in pressure will increase the permeate flux as well as increase the accumulation of the rejected molecules. In practice, the accumulation can be reduced by increasing the tangential velocity of the feed across the membrane so that the rejected molecules can flow back to the bulk solution more rapidly (Cheryan, 1998c; Porter, 1990).

4.2.5 Flux Reduction

Flux decline is a common tendency for a filtration process. It might be a result of concentration polarization, membrane fouling, and membrane adsorption of some solutes which changes the membrane properties, or a combination of these factors. The relative flux reduction (*RFR*) can be defined as

$$RFR = \frac{J_0 - J_a}{J_0} \times 100\% \tag{4.6}$$

where J_0 and J_a are the initial flux and the flux after long-term fouling, respectively (Susanto and Ulbricht, 2005).

4.2.6 Objectives of the Study

UF is a possible technique that can be used to reduce the dextran content of streams in sugar production processes. However, the performance of the membrane might be low if the feed solution is very viscous, therefore it would be optimum if the technique is applied on the clarified juice which has already passed

one separation operation removing molecules (the clarification step) and also has a relatively low sugar concentration, which should result in a low viscosity. The purpose of this work focuses on determination of a reasonable membrane to separate dextran from a synthetic solution that is similar to the classified juice. The flux and rejection ability of the membrane are considered as criteria for the determination.

4.3 Materials and Methods

4.3.1 Materials

In this work, a high purity commercial refined sugar was used as a source of sucrose, and a high fraction dextran (approximately 250,000 Da molecular weight) and a low fraction dextran (approximately 60,000-90,000 Da molecular weight) from ACROS Organics were used as the key solute components in the filtration. Chemicals required for the dextran determination in the Roberts test were ACS grade, as specified in the industrial standard test (Altenburg, 1993) such as absolute ethyl alcohol, sodium hydroxide, copper sulfate, sodium citrate, sodium sulfate, celite filter aid, phenol, trichloroacetic acid, and sulfuric acid.

Commercial membranes of two materials with various pore sizes (regenerated cellulose MWCO 5,000, 10,000, and 30,000, and polyethersulfone MWCO 5,000) were purchased from Millipore Corporation (USA). Chemical structures of regenerated cellulose and polyethersulfone are shown in Figure 2.6.

4.3.2 Apparatus

A dead-end membrane configuration is used in this experiment. The separation operates on a 76 mm diameter membrane placed in a 400 mL Amicon model 8400 (Millipore Co., USA) filtration unit. The filtration process requires a feed

pressure that can be produced by pumping compressed gas into the stirred cell. Oxygen was used to generate the pressure in the current study. The equipment used in the study is shown in Figure 4.2.

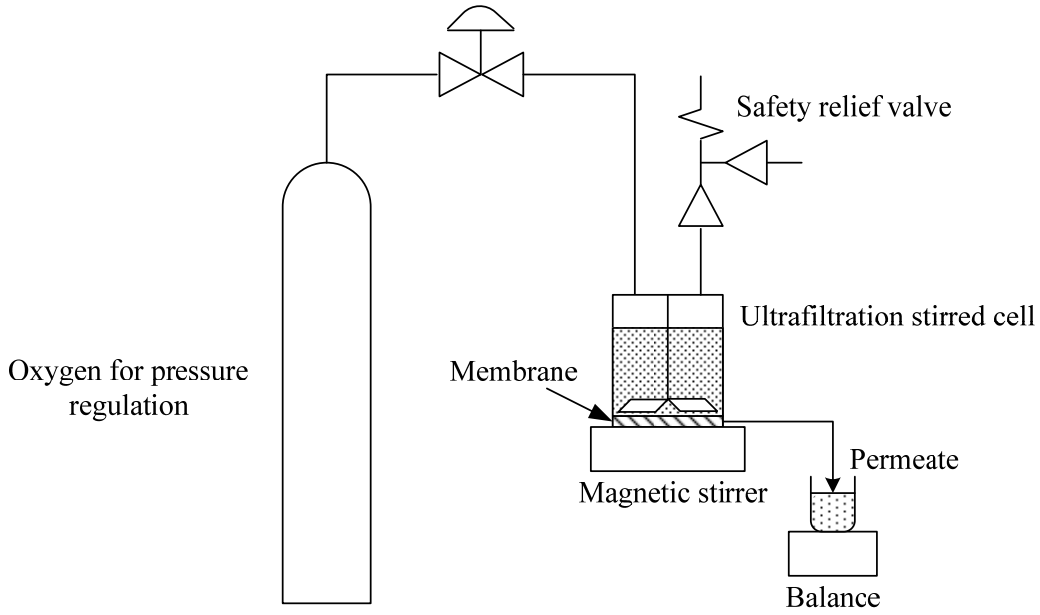

Figure 4.2 Schematic diagram of the stirred cell ultrafiltration unit used in the study.

4.3.3 Process Variables and Methods

Before the dextran separation, the molecular weight distributions of the dextran in the juice should be known so that suitable membranes can be used in the experiment. Molecular weight distributions of both dextrans that have been used in the current study have been determined using GPC.

The feed solution was prepared with a dextran content of 5,000 ppm/Brix (higher than the average value commonly found in raw sugar production process although typical of processes having feeds with a significant problem with dextran) of an equal weight mixture of the high fraction dextran and low fraction dextran in a 15% Brix sucrose solution. This synthetic solution is analogous to the

clarified juice stream in the process of raw sugar production. The membranes used had a variety of pore sizes and materials. The transmembrane pressure and stirrer speed were varied from 1 bar to 3 bar, and 100 rpm and 200 rpm, respectively.

Long-term fouling times for flux measurement of each case are varied from 1 hour to 9 hours since flux reduction rate of either each membrane material or each condition is different. When the flux seems to be time independent, it would be considered to be a flux at long-term fouling for analyzing in the study.

In the study on membrane pore distribution, the membrane was freezed by dipping into liquid nitrogen then it was cracked in the cross section direction. The membrane support was removed from the membrane. A gold coated membrane was analyzed using SEM for observation of the membrane pore.

4.3.4 Dextran Determination (Roberts Test)

The dextran concentrations in the permeate and feed solutions were determined using the Roberts test (Altenburg, 1993). While the full procedure is given by Altenburg, it is useful to give a brief procedure here. All polysaccharides are precipitated in the juice sample by addition of 80% ethanol, followed by collection of the precipitate with filter aid on a coarse sintered glass. The precipitated materials are separated from the filter aid by washing with distilled water then filtered through a Whatman No.42 filter paper. The filtrate contains dissolved polysaccharides, especially dextran.

The dextran can be selectively separated from the other polysaccharides that are present in the filtrate by forming a dextran-copper complex with alkaline copper sulfate. The separated dextran is hydrolyzed by sulfuric acid addition to develop color using phenol. The color is determined using absorbance at

485 nm on a spectrophotometer in comparison with a blank. The absorbance value can predict the dextran content in the sample by using a calibration curve. The calibrations were prepared from using both low and high fraction dextrans but they are not significantly different. Therefore the calibration of low fraction can be used to represent any dextran. The calibration is written as

$$F = 0.1025a - 0.00056 \tag{4.7}$$

where a is the absorbance.

The dextran content can be determined from the following formula (Altenburg, 1993).

$$dextran(ppm) = F \times E \times \frac{C}{D} \times \frac{1}{B} \times \frac{100}{A} \times 1{,}000 \tag{4.8}$$

where A = weight of sample solids diluted to 100 mL (g)

B = aliquot taken for alcohol precipitation (mL)

C = volume of solution containing the precipitate (mL)

D = aliquot taken for copper precipitation (mL)

E = volume of final solution of copper-dextran complex (mL)

F = dextran content (from the calibration) (ppm)

4.4 Results and Discussion

The average molecular weight of dextran sample is reported based on analysis by the National Metal and Material Technology Center (MTEC) as shown in Table 4.1. The full dextran distributions determined by GPC are shown in Appendix C. The result of the average molecular weight is a little different from the dextran molecular

weight specified by the company (in the range of 60,000-90,000 Da for low fraction dextran and 250,000 Da for high frction dextran). The difference may due to the influence of the molecular weight distribution.

Table 4.1 The average molecular weight of dextran distribution.

Sample description	**Weight average molecular weight (Da)**	**Polydispersity****
Low fraction dextran	7.0×10^4	1.9
High fraction dextran	2.3×10^5	6.2
1:1 mixture of low and high fraction dextrans	1.4×10^5	3.5
Dextran in clarified juice*	4.4×10^4	1.8
Dextran in raw syrup*	5.1×10^4	1.5

* Samples collected from Ratchasima Sugar Factory

** Polydispersity is a measure of the distribution of molecular weights of polymer sample, which is described in Appendix C.

The permeate flux after long time fouling and the percent rejection on the dextran separation by using ultrafiltration processes are shown in Table 4.2. Note that the feed solution is composed of 5,000 ppm/Brix dextran and 15% Brix sucrose.

Table 4.2 Membrane separation of dextran in 15 percent dissolved solid of sucrose by regenerated cellulose (RC) and polyethersulfone (PES) membranes.

Membrane material	**MWCO (kDa)**	**Operating condition**	**Initial flux (m/s)**	**Flux after long-term fouling* (m/s)**	**Percent rejection**
RC	30	1 bar, 200 rpm	2.80×10^{-5}	9.34×10^{-6}	27.8
RC	10	1 bar, 200 rpm	9.34×10^{-6}	8.48×10^{-6}	86.5
RC	5	1 bar, 200 rpm	2.43×10^{-6}	2.32×10^{-6}	100
RC	5	2 bar, 200 rpm	4.42×10^{-6}	4.30×10^{-6}	100
RC	5	3 bar, 200 rpm	6.18×10^{-6}	5.95×10^{-6}	98.3
PES	5	1 bar, 200 rpm	5.80×10^{-6}	5.54×10^{-6}	98.3
PES	5	2 bar, 200 rpm	1.03×10^{-5}	9.77×10^{-6}	94.5
PES	5	3 bar, 200 rpm	1.40×10^{-5}	1.26×10^{-5}	90.2
PES	5	1 bar, 100 rpm	4.79×10^{-6}	4.38×10^{-6}	97.6
PES	5	2 bar, 100 rpm	7.86×10^{-6}	6.40×10^{-6}	91.9
PES	5	3 bar, 100 rpm	1.13×10^{-5}	8.20×10^{-6}	80.9

* Long-term fouling indicates a steady value of the flux

From the results, it is seen that both the initial flux and the permeate flux after long-term fouling of the PES membranes is higher than that of the RC membranes under the same operating conditions. If the difference of the dextran cake resistance or the resistance due to blocking of dextran molecules between both membrane materials can be neglected, the membrane resistance (discussed in the next chapter

which shows that the resistance of the polyethersulfone membrane is lower than that of the regenerated cellulose membrane) is sufficient to explain this result.

In view of the ability of the membrane to reject dextran, the rejection determined for the 30 and 10 kDa RC membranes are smaller than the rejection that would be expected based on their MWCO. This can be explained both by the effect of molecular shape and the width of the molecular weight distribution of the solute. Although the MWCO of the membranes is smaller than the average MW of dextran, they do allow some dextran permeation since dextran is a linear polymer with some braches that can snake through the pores. Additionally, due to the wide molecular weight distribution of dextran there are some smaller molecules of dextran that can pass through the pores.

The effect of size and shape of dextran on the membrane rejection is shown in Table 4.3. Each membrane rejects those molecules located above the line but passes those below the line. This is reviewed by Porter (1990). It is mentioned that since the molecular weight cut-off of a membrane is defined based on 90% rejection of globular proteins, the rejection of branched polysaccharides and linear flexible proteins is usaully lower than the MWCO specification for the membrane.

Table 4.3 Effect of size and shape of molecules on UF rejection (adapted from Porter, 1990).

Membrane	**Solute material**		
	Globular proteins	**Branched polysaccharides**	**Linear, Flexible polymers**
	γ-Globulin (160 kDa) Albumin (69 kDa)		
Diaflo XM50 kDa	Pepsin (35 kDa)	Dextran 250 (236 kDa)	
Diaflo PM30 kDa	Cytochrome C (13 kDa) Insulin (5.7 kDa)	Dextran 110 (100 kDa)	Polyacrylic acid (pH 10; 50kDa) Polyacrylic acid (pH 7; 50 kDa)
Diaflo PM10 kDa	Bacitracin (1.4 kDa)	Dextran 40 (40 kDa) Dextran 10 (10 kDa)	
Diaflo UM10 kDa			

In the percent rejection comparison, Table 4.2 shows that the percent dextran rejection of the regenerated cellulose (RC) membrane is higher than that of the polyethersulfone (PES) membrane of the same pore size. Moreover the transmembrane pressure and the stirrer speed also influence the percent rejection. Particularly, the lower stirrer speed has a smaller value of the percent rejection because of the concentration polarization effect. Since the agitation increases a shear force to disperse accumulated dextran from the membrane surface to the bulk, the operation at high stirring speed can reduce the concentration polarization and thus reduce dextran concentration at the membrane surface. Therefore the probability of dextran passing through the membrane can be reduced by increasing agitation rate. In addition the rejection depends on the transmembrane pressure. In common with the explanation for stirring speed effect, low pressure filtration can achieve a lower concentration polarization since the back diffusion of dextran rejected by the membrane is more rapid. The dextran rejection is high for low pressure filtration, and high recovery of sugar can be also achieved (Bhattachaya et al., 2001).

There is a study on dextran rejection by a specific membrane in the research of Zaidi and Kumar (2004). The membrane contained 25% polysulfone and 21% polyvinylpyrrolidone in N-metyl-2-pyrrolidinone with 6 kDa MWCO. The result is shown in Table 4.4.

Table 4.4 Steady-state rejection (%) of dextran T-40 (39 kDa) at different applied pressure and bulk dextan concentration (Zaidi and Kumar, 2004).

Applied pressure (bar)	**Bulk dextran concentration**		
	0.2 kg/m^3	1 kg/m^3	5 kg/m^3
1.35	97.0	95.9	95.1
2.70	94.3	93.4	91.2
4.05	92.1	90.9	90.1

The result in Table 4.2 quite agrees qualitatively with the result in this research although the materials used in the two experiments are different. There is a similar tendency between Zaidi's work and the current study in view of dextran rejection decline by increasing the pressure. In addition, Zaidi (2004) has suggested that the rejection is inverse to the flux which agrees with this work since the flux directly relates to transmembrane pressure. Previous results of membrane rejection of dextran by dead-end ultrafiltration were given in the study of Molina et al. (2006). This study involves the separation 36-44 kDa dextran through a 30 kDa MWCO cellulose membrane. The results are shown in Figure 4.3. This supports that dextran rejection decreases with incresing transmembrane pressure. A similar tendency of tranmembrane pressure effect on dextran rejection has reported (Porter, 1990; Porter, 1997).

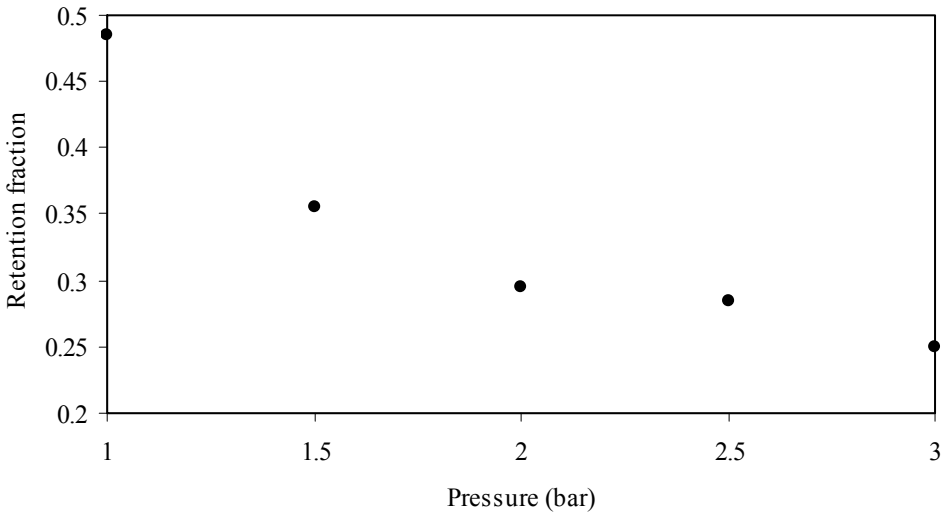

Figure 4.3 36,000-44,000 Da dextran retention by a cellulose membrane with a 30 kDa MWCO (re-drawn from the plot of Molina *et al*., 2006)

The relative flux reduction (RFR) was determined for the study on membrane separation performance without allowance of dextran adsorption or blocking on the membrane due to the interaction between dextran and membrane. The result is shown in Table 4.5. A result of Susanto concerning the RFR for dextran separation using both cellulose and polyethersulfone is also shown in the table, and this can be used in qualitative comparison to this study (Susanto and Ulbricht, 2005; Susanto and Ulbricht, 2006a; Susanto and Ulbricht, 2006b).

Table 4.5 Relative flux reduction of RC and PES membranes for various transmembrane pressures.

Transmembrane pressure (TMP)	**RFR (%) for using RC membrane**	**RFR (%) for using PES membrane**
1 bar	4.53	4.48
2bar	2.71	5.15
3bar	3.72	10.0
RFR data for 3bar by Susanto (2005)	-1.4 ± 0.2	4.0 ± 1.2

The results in Table 4.5 have a qualitative agreement with Susanto's results in that the RFR of PES membrane is higher than that of RC membrane. In addition, transmembrane pressure has an influence on the flux reduction: i.e. operation at a higher transmembrane pressure can give a higher flux reduction (Lee and Clark, 1998; Lin *et al.*, 2009; Vela *et al.*, 2006). Since there are number of differences between Susanto's work and the current study, the values in the table for the comparison do not match exactly. For example, 10 g/L dextran (MW 4,000 Daltons) concentration and both membranes having the MWCO 10 kDa were used in Susanto's work, which are significantly different to these variables in the current study. The effect of feed concentration on flux reduction is investigated (Susanto *et al.*, 2009; Lee and Clark, 1998).The negative value of Susanto's result does not make sense since it shows the flux increases with filtration time, which is not feasible.

In addition, there is evidence for the permeate flux and the flux reduction by the contact angle value of the polyethersulfone and cellulose membranes. The contact

angles for both membranes were determined by Susanto based on the captive air bubble technique in water (the angle of an air bubble in contact with an inverted membrane surface in pure water is measured by an optical contact angle (OCA) instrument system. The result is shown in Table 4.6.

Table 4.6 Static contact angle of fresh membranes and membranes that are fouled with dextran T-10 (10,000 Da), (Susanto and Ulbricht, 2005).

Membrane	**Contact angle of fresh membrane (°)**	**Contact angle of fouled membrane (°)**
RC	57.9 ± 3.8	55.9 ± 3.6
PES	61.7 ± 2.4	55.9 ± 2.9

The contact angle result shows the hydrophilicity of each membrane that influences the membrane flux and fouling. It can be seen that the cellulose membrane has more hydrophilicity than that polyethersulfone, so it should have higher initial flux (Jonsson, C. and Jonsson, A. S., 1995). The result of the initial flux in Table 4.2 has the opposite result since besides the hydrophilicity, the flux has a strong dependence on either the porosity of the membrane or the bulk porosity of the membrane support (Lohokare *et al.*, 2006). The porosity of membranes can be seen in Figure 4.4. It can be seen that polyethersulfone membrane has a higher flux because its porosity is higher. Consideration in the contact angle after fouling with dextran shows that the properties of polyethersulfone membrane surface change due to dextran adsorption much more than that of the cellulose acetate membrane so the flux reduction of the polyethersulfone membrane is larger.

The observation on the pores of RC and PES membranes both with a MWCO of 5,000 Da were investigated. The membrane pore distributions can be seen by analyzing the surface of each membrane as in Figure 4.4 (b) for the RC membrane and in Figure 4.4 (d) for the PES membrane. The pore size cannot be measured perfectly by analyzing the cross section of each membrane since the thickness of the membranes are very low approximately 10 μm for the RC membrane (Figure 4.4 (a)) and approximately 100 μm for the PES membrane (Figure 4.4 (c)).

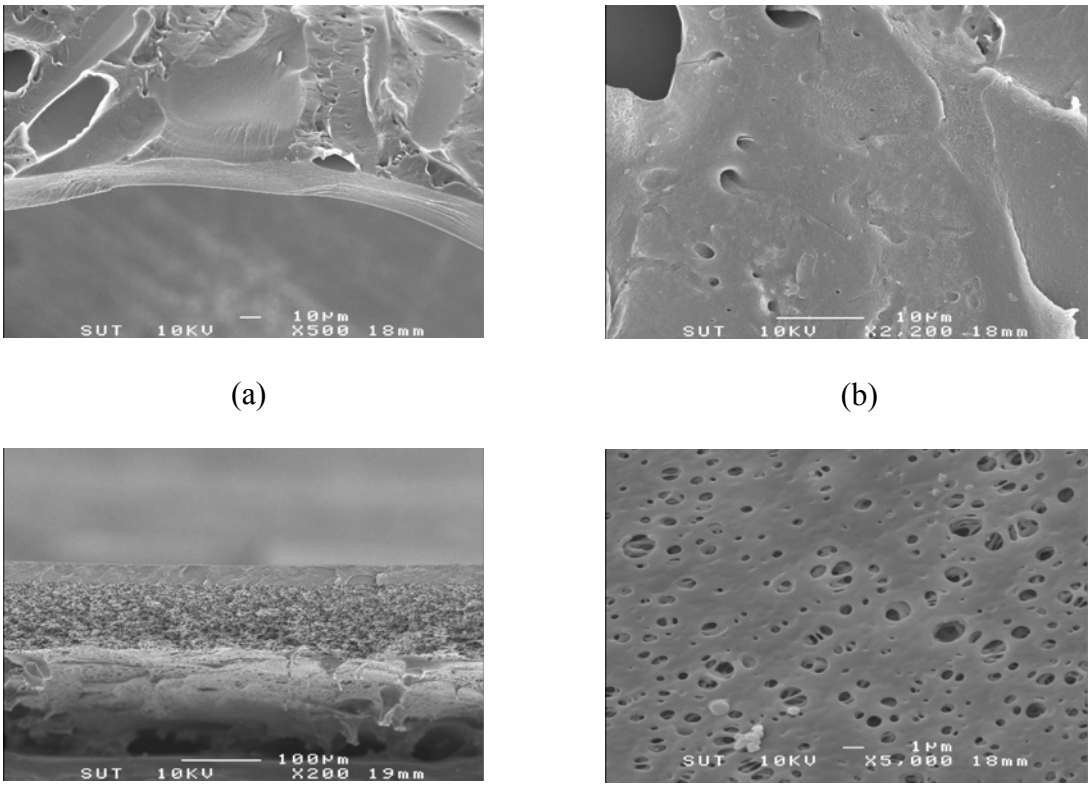

(a) (b)

(c) (d)

Figure 4.4 Membrane pore distributions. (RC 5,000 Da (a) cross section and (b) surface; PES 5,000 Da (c) cross section and (d) surface)

The effect of transmembrane pressure and the rate of agitation on the permeate flux are investigated by the plot between the flux after long time fouling and the tramsmembrane pressure for various agitation rates as shown in Figure 4.5. The flux after long time fouling was used for the study since it can be considered to be a limiting flux rather than the initial flux. It is found that the permeate flux for both RC and PES membranes do not quite linearly relate to the transmembrane pressure. The result is not surprising since it agrees with the pore flow model of Darcy's law, accounting for the term of resistance due to the concentration polarization that change with the agitation rate.

Furthermore it can be suggested that a higher shear rate operating in the membrane separation gives a higher flux than a lower shear rate. This is obviously seen by the comparison between the filtration with 100 rpm and 200 rpm agitation rate. This result can be used to show that enhancing shear rate has a direct effect on removal of a rejected solute so that the permeate can easily pass through the membrane surface. There are previous studies on the effect of share rate generated by cross-flow velocity on the flux reduction (Zhang and Song, 2000; Lee and Clark, 1998; Song, 1998; Wang and Song, 1999). They show the flux reduction can be retarded by operating at high cross-flow velocity. Although the flux is observed on cross-flow filtration, the main idea of concentration polarization reduction by considering the cross-flow velocity is the same as the stirring rate in dead-end filtration.

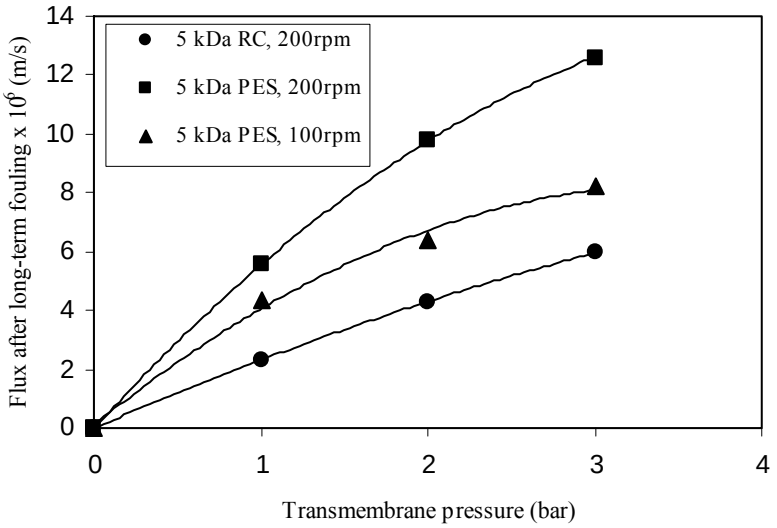

Figure 4.5 The effects of transmembrane pressure and stirring speed on flux.

Previous research of Zaidi involving dextran separation shows the flux variation due to transmembrane pressure. It was found that the flux increases with increased applied pressure, then it becomes pressure independent when the applied pressure is high enough; approximately, 2.7 bar for all dextran levels used (0.2-5 kg/m^3 dextran) (Zaidi and Kumar, 2004; De and Bhattacharya, 1996). It was suggested that this is a result of higher osmotic pressure build up due to the concentration polarization effect at higher pressure. However, in the current study, the pressure independent flux does not occur at the transmembrane pressure used in the study. It is possible that the osmotic pressure effect is not strong in the systems that contain lower amount of dextran.

4.5 Conclusions

The performance of the regenerated cellulose with a MWCO of 5000 Da for separation of dextran from synthetic solution containing 15% Brix of sucrose was

suitable for dextran removal, as it was able to achieve a high percent rejection and a suitably high flux. In addition it was found that the percent rejection and the permeate flux can be improved by raising magnetic stirrer speed. Although the permeate flux of 5000 Da MWCO polyethersulfone is higher than that of regenerated cellulose, its percent rejection is smaller. In comparison among the regenerated cellulose membranes with variation of MWCOs, it was found that regenerated cellulose with 5000 Da MWCO prevails for high rejection achievement so it is considered to use in further study on membrane fouling. However, the polyethersulfone membrane with 5000 Da MWCO will also be used in the next chapter to study the effect of membrane material on fouling.

4.6 References

Altenburg, W. (1993). Determination of dextran and starch. In J. C. P. Chen and C. C. Chou (eds.). **Cane Sugar Handbook** (12th ed. pp. 904-921). New York: John Wiley and Sons.

Baker, R. W. (2004a). Overview of membrane science and technology. **Membrane Technology and Applications** (2nd ed., pp. 1-14). Great Britain: John Wiley and Sons.

Baker, R. W. (2004b). Ultrafitration. **Membrane Technology and Applications** (2nd ed., pp. 237-274). Great Britain: John Wiley and Sons.

Bhattachaya, P. K., Agarwal, S., De, S., and Gopal, U. V. S. (2001). Ultrafiltration of sugar cane juice for recovery of sugar analysis of flux and retention. **Separation and Purification Technology.** 21: 247-259.

Cheryan, M. (1998a). Membrane properties. **Ultrafiltration and Microfiltration Handbook** (pp. 71-112). Pennsylvania, USA: A Technomic Publishing Company.

Cheryan, M. (1998b). Performance and engineering models. **Ultrafiltration and Microfiltration Handbook** (pp. 113-170). Pennsylvania, USA: A Technomic Publishing Company.

Cheryan, M. (1998c). Fouling and cleaning. **Ultrafiltration and Microfiltration Handbook** (pp. 237-292). Pennsylvania, USA: A Technomic Publishing Company.

De, S. and Bhattacharya, P. K. (1996). Flux prediction of black liquor in cross flow untrafiltration using low and high rejecting membranes. **Journal of Membrane Science.** 109: 109-123.

Jonsson, C. and Jonsson, A. S., (1995). Influence of the membrane material on the adsorptive fouling of untrafiltration membranes. **Journal of Membrane Science.** 108: 79-87.

Lee, Y. and Clark, M. M. (1998). Modeling of flux decline during crossflow ultrafiltration of colloidal suspensions. **Journal of Membrane Science.** 149: 181-202.

Lin, C. F., Lin, A. Y. C., Chandana, P. S., and Tsai, C. Y. (2009). Efeects of mass retention of dissolved organic matter and membrane pore size on membrane fouling and flux decline. **Water Research.** 43: 389-394.

Lohokare, H. R., Bhole, Y. S., and Kharul, U. K. (2006). Effect of support material on ultrafiltration membrane performance. **Journal of Applied Polymer Science.** 99: 3389-3395.

Molina, V. G., Esplugas, S., Wintgens, Th., and Melin, Th. (2006). Ultrafiltration of aqueous solutions containing dextran. **Desalination.** 188: 217-227.

Porter, M. C. (1990). Ultrafiltration. In M. C. Porter (ed.). **Handbook of Industrial Membrane Technology** (pp. 136-259). New Jersey, USA: Noyes Publications.

Porter, M. C. (1997). Membrane filtration. In P. A. Schweitzer (ed.). **Handbook of Separation Techniques for Chemical Engineers** (3rd ed. pp. 2-3 to 2-103). New York: McGraw-Hill.

Song, L. (1998). Flux decline in crossflow microfiltration and ultrafiltration: mechanisms and modeling of membrane fouling. **Journal of Membrane Science.** 139: 183-200.

Susanto, H., Feng, Y., and Ulbricht, M. (2009). Fouling behavior of aqueous solutions of polyphenolic compounds during ultrafiltration. **Journal of Food Engineering**. 91: 333-340.

Susanto, H. and Ulbricht, M. (2005). Influence of ultrafiltration membrane characteristics on adsorptive fouling with dextrans. **Journal of Membrane Science**. 266: 132-142.

Susanto, H. and Ulbricht, M. (2006a). Insights into polysaccharide fouling of ultrafiltration membranes. **Desalination**. 200: 181-182.

Susanto, H. and Ulbricht, M. (2006b). Performance of surface modified polyethersulfone membranes for ultrafiltration of aquatic humic substances. **Desalination.** 199: 348-386.

Vela, M. C. V., Blanco, S. A., Garcia, J. L., and Rodriguez, E. B. (2006). Prediction of flux decline in the ultrafiltration of macromolecules. **Desalination.** 192: 323-329.

Wang, L. and Song, L. (1999). Flux decline in crossflow microfiltration and ultrafiltration: experimental verification of fouling dynamics. **Journal of Membrane Science.** 160: 41-50.

Yoon, K., Kim, K., Wang, X., Fang, D., Hsiao, B. S., and Chu, B. (2006). High flux ultrafiltration membranes based on electrospun nanofibrous PAN scaffolds and chitosan coating. **Polymer.** 47: 2434-2441.

Zaidi, S. K. and Kumar, A. (2004). Experimental studies in the dead-end ultrafiltration of dextran analysis of concentration polarization. **Separation and Purification Technology**. 36: 115-130.

Zhang, M. and Song, L. (2000). Mechanisms and parameters affecting flux decline in cross-flow microfiltration and ultrafiltration of colloids. **Environmental Science Technology.** 34: 3767-3773.

CHAPTER V

MEMBRANE FOULING

5.1 Abstract

The results of a study of membrane fouling of synthetic clarified juice solutions containing dextran are described in this chapter. The study was performed by observing the flux decay in a dead-end filtration configuration. Synthetic sucrose solutions (15% Brix) containing 5,000 ppm dextran/Brix were used as feed solutions. Commercial membranes of two materials, RC and PES, with MWCO of 5,000 Da were used in the study. For each membrane type, the transmembrane pressure was varied from 1 bar to 4 bar and stirring was performed using a magnetic stirrer at 0 (no agitation), 100, and 200 rpm. The permeate was collected in a receiver on a digital balance and hence the permeate volume and flux can be calculated from the increase in the weight. The permeate flux decay for various transmembrane pressures in both unstirred and stirred filtration were fitted with fouling models to examine the mechanism of membrane fouling. The program Sigma Plot 9.0 (SYSTAT Software, Inc., CA) was used to fit models to the experimental data. It was seen that a dextran cake layer is formed in unstirred dead-end filtration, with a cake compressibility in the range of 0.52-0.54, while the complete pore blocking model can be used to describe the fouling mechanism in 100 rpm stirred filtration. The fouling for the filtration with 200 rpm stirring did not display sufficeient levels to distinguish a suitable fouling mechanism by using the fitted parameters. The initial flux of the

experiment can be used with the membrane resistance determination using Darcy's Law to give the result that the resistances of the PES membrane and the RC membrane are equal to $1.80\times10^{13}\,\mathrm{m}^{-1}$ and $3.36\times10^{13}\,\mathrm{m}^{-1}$, respectively. The membrane resistance of PES is a little higher than in previous research (results varying between $1.30\times10^{13}\,\mathrm{m}^{-1}$ and $1.41\times10^{13}\,\mathrm{m}^{-1}$) (Acero *et al.*, 2009). The membrane permeability (inverse to the membrane resistance) of RC (2.22×10^{-11} m/Pa·s) is lower than the previous determination with pure water permeate (3.47×10^{-11} m/Pa·s) (Kwon *et al.*, 2006). The accuracy of the predicted initial fluxes from the best fit model for the two types of membrane are within 1% and 3% respectively of the experimental values.

5.2 Introduction

For this chapter it is necessary to review membrane fouling, membrane resistance, and the compressibility of the cake layer. Membrane fouling is generally attributed to solute molecule accumulation on the membrane surface, and adsorption and precipitation of small solutes in the membrane pores. Several mathematical models have been proposed to predict the membrane flux over time based on a description of the mechanism of fouling. The membrane resistance is an inherent property of the membrane that inhibits permeation through the pores. The value of the membrane resistance commonly does not change during the filtration process unless the size of membrane pores is permanently reduced by means of internal blocking, while the resistance of cake layer built up on the membrane surface can increase due to the compressibility of the cake.

5.2.1 Membrane Fouling

Membrane fouling is a quite different process for the configurations of dead-end and cross-flow filtration. The solute molecules deposited on the membrane surface in cross-flow filtration are normally removed by the cross-flow velocity, however some molecules may be sufficiently strongly adsorbed as to not be removed, and hence the cross-flow velocity can affect the degree of membrane fouling. In this study we have used stirred cell ultrafiltration equipment with a stirring blade placed immediately adjacent to the membrane surface (and sweeping the entire surface during half a revolution) to remove solute molecules from the surface of the membrane. However fouling in this operation is still fundamentally different to a cross-flow system, which operates at a steady state: since the stirred cell still has varying solute concentration above the membrane surface, even when there is no fouling, and this is likely in most applications to display a significantly time-dependent effect on the viscosity of the liquid passing through the membrane. In the specific case of the current study, although there is the accumulation of rejected dextran by the membrane surface, the viscosity of the retentate does not change significantly during the filtration since the viscosity is more due to the very high content of sucrose (15% Brix) compared to the small concentration of dextran (5000 ppm/Brix).

The relative size between the membrane pore and the solute in the feed is an important factor affecting membrane fouling. Although initially a relatively larger pore has a higher flux than a relatively smaller pore, sometimes the flux of the larger pore reduces to become less than that of the smaller pore because its permeation is easily obstructed with adsorbed solute molecules. A comparison in the

blocking mechanism between a membrane with large pores and a membrane with small pores is illustrated in Figure 5.1. If the size of the rejected molecules is of the same order of magnitude as the range of pore sizes some of the smaller molecules could lodge in the pores without going through them, resulting in pore blocking. Alternatively, if the pores are much smaller than the molecules rejected, the molecules can not block the pores but will instead be removed from the membrane surface under the shear forces generated by the flow (Cheryan, 1998a; Baker, 2004).

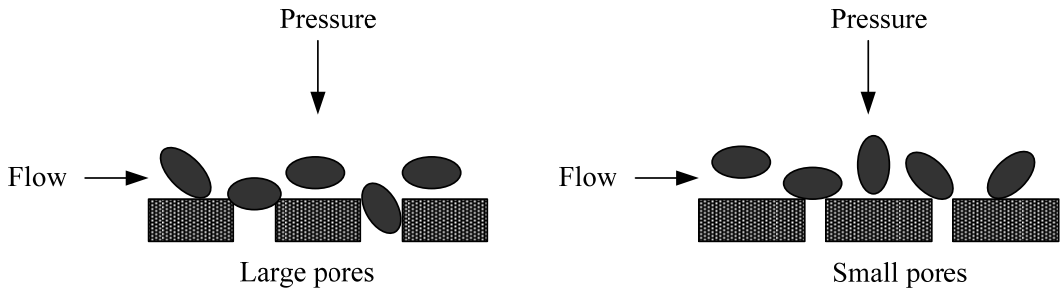

Figure 5.1 The effect of pore size on fouling mechanism (adapted from Cheryan, 1998).

Since this experiment uses two membrane materials with the same MWCO (5,000 Da), the effect of pore size on fouling can be neglected by the fact that the difference in the effective pore size of the two membranes is very small.

5.2.2 Mathematical Models of Membrane Fouling

In the experiments presented here the main determinant of the viscosity of the solution on the retentate side of the membrane is the concentration of sucrose, since this component is at 15% Brix, which is very much larger than the dextran content (at 5,000 ppm/Brix). Since sucrose is a small molecule (342 Da) relative to the pore sizes of the membranes, the concentration of sucrose on the

retentate side will not change during the ultrafiltration, and therefore the viscosity of this solution and the rate of removal of molecules from the membrane surface by the stirrer blade will be approximately constant.

In this study, many models were examined in the effort to explain the phenomena of membrane fouling observed during the filtration. Both pore blocking models and the cake filtration model have been investigated. There are several modes of fouling mechanism depending on the solute molecular size and shape in relation to the membrane pore size distribution, and the chemical interactions between the solute and the membrane material (Field *et al.*, 1996):

Complete pore blocking: Complete pore blocking occurs when the solute molecule reaches an open pore at the surface of the membrane and blocks the pore entrance, sealing the pore closed.

Partial pore blocking: Partial pore blocking occurs when the solute molecule occupies a fraction of the pore entrance causing a reduction in the permeate flux without totally sealing the pore.

Cake filtration: Cake filtration occurs when an accumulation of solute molecules occurs over the entire surface of the membrane, increasing the resistance to flow through the membrane.

Internal pore blocking: Internal pore blocking occurs when a solute molecule that can not be rejected by the pore entrance is adsorbed or trapped on the pore wall, thus reducing the flux through the pore, and encouraging further pore blocking. This form of fouling can not be mitigated by flow across the surface of the membrane (or stirring at the surface as in this study) as the blocking mechanism is internal to the membrane.

In the case of unstirred dead-end filtration, the classical constant pressure dead-end filtration equation (Hermia, 1982) has been presented in a general form through the set of differential equations defined by Field *et al.* (1995):

$$-\frac{dJ}{dt}\left(J^{n-2}\right)=kJ \tag{5.1}$$

where the exponent n and the physical meaning of the constant k depend on the mechanism of fouling.

However, the permeate flux decline in a dilute solution of a retained solute in a stirred cell filtration unit can be described by the cross-flow filtration model that is based on classical constant pressure dead-end filtration equation (Hermia, 1982) and has been proposed earlier (Field *et al.*, 1995). The assumption in the dilute solution system is that the removal rate of the fouling molecules, *B,* may be considered to be constant (and related to the membrane porosity and rate of removal of particles on the membrane surface), the rate of erosion of cake, and the back flux factor, which have been presented earlier (Field *et al.*, 1995), and is not a function of time.

$$-\frac{dJ}{dt}\left(J^{n-2}\right)=k\left(J-J^{*}\right) \tag{5.2}$$

where J^{*} is a critical flux which should not be exceeded if fouling is to be avoided. In this study J^{*} was considered the limiting flux ($J_{\lim}$) for large time periods; the constant k and index n taking different values depending upon the fouling mechanism.

1) Complete pore blocking ($n = 2$)

When particles are larger than the pore size, the membrane surface fraction of the filtration area reached by the particles is reduced by means of pore sealing (De Barros *et al.*, 2003). In the case of filtration of a dilute solution in a stirred cell, the equation can be expressed as using the same model as cross-flow filtration since the fouling removal flux will be constant. The solution to the fouling model is

$$J = J_{\lim} + (J_0 - J_{\lim})e^{-k_2 t} \tag{5.3}$$

where J is the permeate flux, J_0 is the initial permeate flux ($t = 0$), while in unstirred filtration the limiting flux ($J_{\lim}$) can be considered to be zero, since there is no fouling removal, resulting in

$$J = J_0 e^{-k_2 t} \tag{5.4}$$

2) Partial pore blocking ($n = 1$)

As in the previous section, an open pore of the membrane can be sealed by fouling by solute molecules; however each molecule does not necessarily block a pore completely. In the stirred filtration case, the solution to the fouling model (with $n = 1$) is

$$k_1 t = \frac{1}{J_{\lim}}\left[\ln\left(\frac{J_0 - J_{\lim}}{J_0} \cdot \frac{J}{J - J_{\lim}}\right)\right] \tag{5.5}$$

For the case of unstirred filtration, the resulting equation is

$$J = \frac{J_0}{J_0 k_1 t + 1} \tag{5.6}$$

3) Cake filtration ($n = 0$)

The cake filtration model is used when macromolecules, that do not enter the pores, have accumulated on the membrane surface. During the cake formation the overall resistance is composed of a cake resistance and a membrane resistance (De Barros *et al.*, 2003). The cake resistance is normally dependent on the cake material via the compressibility of the cake. The equation for stirred filtration can be written as

$$k_0 t = \frac{1}{J_{\lim}^2}\left[\ln\left(\frac{J}{J_0}\cdot\frac{J_0 - J_{\lim}}{J - J_{\lim}}\right) - J_{\lim}\left(\frac{1}{J} - \frac{1}{J_0}\right)\right] \tag{5.7}$$

And, the solution of the unstirred filtration case is given as

$$J = \frac{J_0}{\sqrt{J_0^2 k_0 t + 1}} \tag{5.8}$$

4) Internal pore blocking ($n = 1.5$)

In this model, the pore volume decreases due to either molecular deposits or adsorption on the pore wall. The membrane resistance increases as a consequence of pore size reduction. If internal pore blocking occurs the fouling mechanism becomes independent of the cross-flow velocity and there is no limiting value of the flux (De Barros *et al.*, 2003). For this reason, the solution of both the stirred and unstirred filtration models can be expressed by the same equation

$$\frac{1}{J^{0.5}} = \frac{1}{J_0^{0.5}} + k_{1.5}t \tag{5.9}$$

However in this study, all of the stirred cell results (with stirring) have non zero limiting flux so that the internal pore blocking mechanism is not evident.

5.2.3 Membrane Resistance, Cake Compressibility, and k Constant in Model Fitting

The constant k of the fouling models described in the previous section could be used to study the mechanism of fouling. If cake formation occurred, the compressibility of the cake will be considered as a factor of the permeate flux decline during the filtration process. The classical empirical equation for flow through a dead-end filter is derived from Darcy's Law (Eq. (10)). The permeate flux J is determined by combining the membrane resistance R_m, the cake resistance R_c and fouling R_f in terms of the transmembrane pressure ΔP (which includes the pressure drop across the fouling layer) and the viscosity of the permeate, μ (Lodge *et al.*, 2004; Cheryan, 1998b).

$$J = \frac{\Delta P}{\mu\left(R_m + R_c + R_f\right)} \tag{5.10}$$

The membrane resistance can be obtained by consideration of the initial flux which has not been affected by fouling or cake resistance. The initial flux can be written as

$$J_0 = \frac{\Delta P}{\mu R_m} \tag{5.11}$$

The term $1/\mu R_m$ can be called the membrane permeability.

R_c increases in proportional to the dry cake mass accumulation on the membrane surface m_{dc} (g/m^2), (Field et al., 1995):

$$R_c = \alpha \cdot m_{dc} \tag{5.12}$$

α is defined as the specific cake resistance per unit mass (m/g), that increases as a power law function with the transmembrane pressure as given by

$$\alpha = \alpha_0 \cdot \Delta P^s \tag{5.13}$$

where s is the cake compressibility

The constant k for each blocking model has been proposed (Hermia, 1982) and simplified (Field *et al.*, 1995). It is seen that the constant k_2 in the complete pore blocking model is a linear function of the transmembrane pressure ΔP following the equation

$$k_2 = \frac{A_b J_0}{\varepsilon_0} = \frac{A_b \Delta P}{\mu \varepsilon_0 R_m} \tag{5.14}$$

A_b and ε_0 are defined as the blocked area per unit volume of filtrate (m^{-1}) and the clean membrane porosity, respectively. The constant k_1 in the partial pore blocking model does depend on the pressure driving force, and is given by

$$k_1 = A_b \tag{5.15}$$

If a cake is formed during the filtration process, the constant k_0 will become a power law function with pressure in terms of the cake compressibility *s*. The relation can be expressed as

$$k_0 = \frac{\alpha k_c}{J_0 R_m} = \alpha_0 \mu k_c \Delta P^{s-1} \tag{5.16}$$

where k_c is the cake filtration constant

5.2.4 Objectives of the Study

It was seen in the results of the previous chapter that both the 5,000 MWCO RC membrane and the 5,000 MWCO PES membrane can be used to significantly reduce the dextran contamination in a 15% Brix sucrose solution which is similar to the clarified juice in a mill. Further study on membrane fouling due to dextran accumulation on the membrane surface is described in this chapter. In this study, the mechanisms of dextran blocking of the membrane are determined by using the constant k determined from fitting the experimental flux decline to the blocking models, and the resistance of both membranes are also determined based on an analysis of the initial flux data. In addition, if the mechanism of fouling is dominated by cake layer formation, the cake compressibility of dextran material could be obtained.

5.3 Materials and Methods

5.3.1 Materials

In this work, a high purity of commercial refined sugar (approximately 99.9%) was used as sucrose, and a high fraction dextran (approximately 250,000 Da

molecular weight) and a low fraction dextran (approximately 60,000-90,000 Da molecular weight) from ACROS Organics were used as the key solute components in the filtration. Two commercial membranes (Millipore Co., USA) used in the experiment: RC MWCO 5,000; and PES MWCO 5,000. Chemical structures of regenerated cellulose and polyethersulfone are shown in Figure 2.6.

5.3.2 Apparatus

Membrane fouling, membrane resistance and cake compressibility were investigated in a stirred cell filtration unit with 76 mm diameter membranes. The stirred cell (Amicon model 8400, Millipore Co., USA) has a feed capacity of 400 mL. The transmembrane pressure can be produced by pumping compressed gas into the feed side of the stirred cell. In this experiment, oxygen was used to generate the pressure.

5.3.3 Process Variables and Methods

To fit the fouling models, the permeate flux decline was measured in a constant pressure dead-end ultrafiltration mode using both 5,000 MWCO RC membranes and 5,000 MWCO PES membranes. The dextran content in 15% Brix sucrose feed solution is 5,000 ppm/Brix. The 1:1 mass ratio of low fraction and high fraction dextrans was used. For each membrane type, the transmembrane pressure was varied from 1 bar to 4 bar and the magnetic stirrer was operated in both stirred mode (at 100 and 200 rpm) and unstirred mode. The permeate was collected in a receiver on a digital balance throughout the process, and the volume flux was calculated from the rate of weight increase. The equipment is illustrated in Figure 4.2. Fouling models were fitted by the program SigmaPlot 9.0 (SYSTAT Software, Inc., CA) and the constant k of each model was determined from the best fit of the

experimental data. The membrane resistance was determined by using the plot between the initial flux and the transmembrane pressure. Moreover, if the fouling was controlled by the cake filtration mechanism, the constant k was used to determine the cake compressibility at the relevant experimental condition.

5.4 Results and Discussion

5.4.1 Model Fitting

In this section, permeate flux decline under various conditions was measured and fitted to the various fouling models using SigmaPlot 9.0. For PES and RC unstirred dead-end filtrations, where fouling results in the flux eventually decaying to zero, two parameter models were used since there was only need for a rate constant (k) and an initial flux (J_0): the experimental results and the curves of best fit are shown in Figure 5.2 for the PES membranes, and Figure 5.3 for the RC membranes. For PES and RC stirred cell filtrations at 100 rpm, where a finite limiting flux was achieved due to the removal of the fouling layer, three-parameter models were required due to the need for a rate constant (k), an initial flux (J_0), and a limiting flux $(J_{\lim})$. The experimental results and model fitting for these experiments are shown in Figure 5.4 for the PES membranes and Figure 5.5 for the RC membranes.

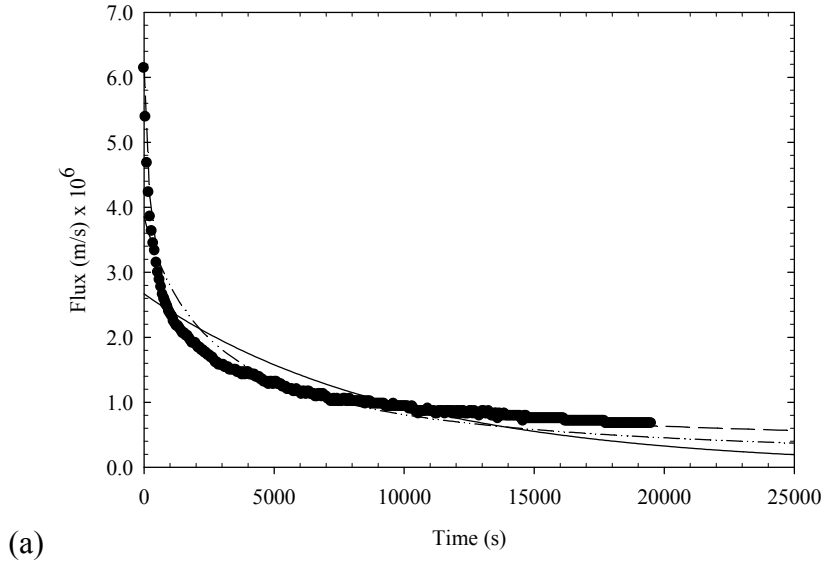

(a)

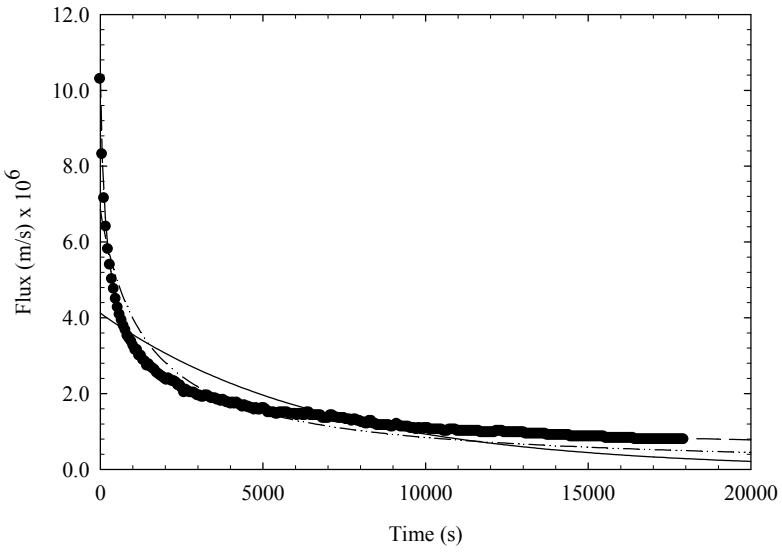

(b)

Figure 5.2 Flux decay and fouling behaviour at different transmembrane pressure for unstirred PES membrane filtration (a) 1 bar; (b) 2 bar ((•) experimental, (—) complete pore blocking, (—··—··) partial pore blocking, (－－－) cake filtration).

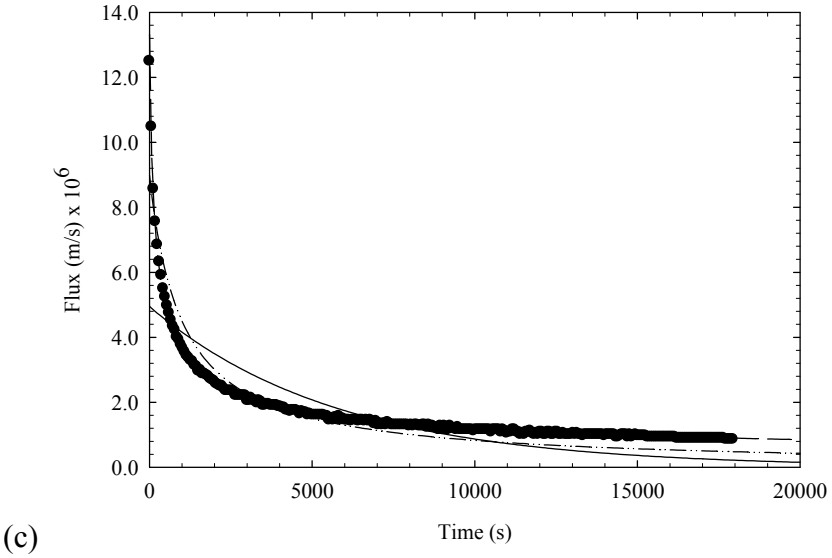

(c)

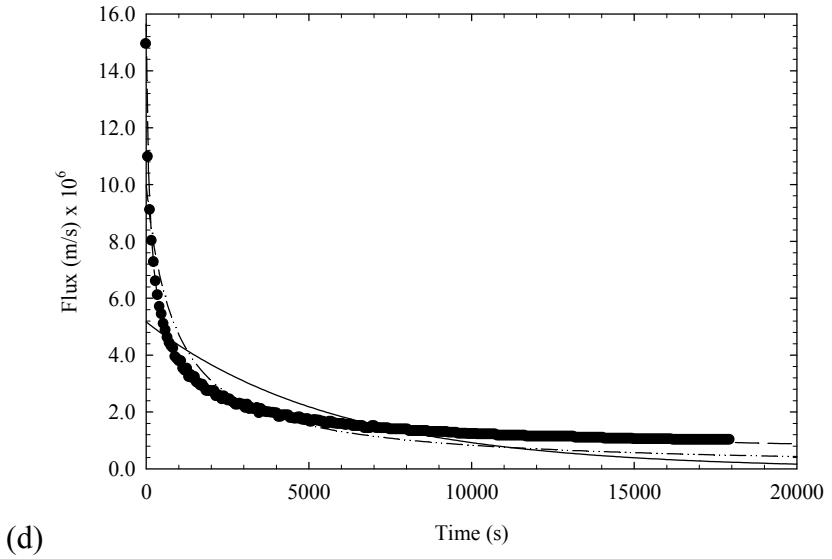

(d)

Figure 5.2 Flux decay and fouling behaviour at different transmembrane pressure for unstirred PES membrane filtration (continued). (c) 3 bar; (d) 4 bar ((•) experimental, (—) complete pore blocking, (— ·· — ··) partial pore blocking, (— — —) cake filtration).

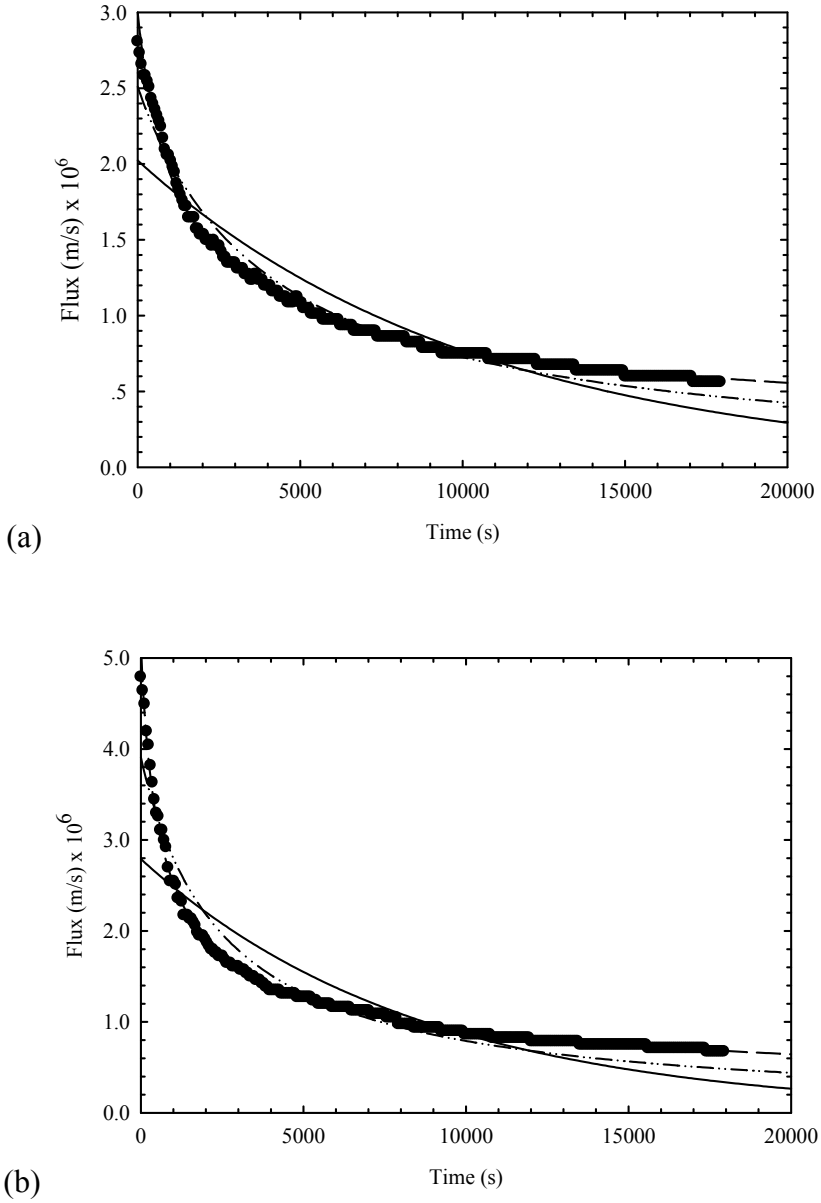

Figure 5.3 Flux decay and fouling behavior at different transmembrane pressure for unstirred RC membrane filtration (a) 1 bar; (b) 2 bar ((•) experimental, (—) complete pore blocking, (—··—··) partial pore blocking, (－－－) cake filtration).

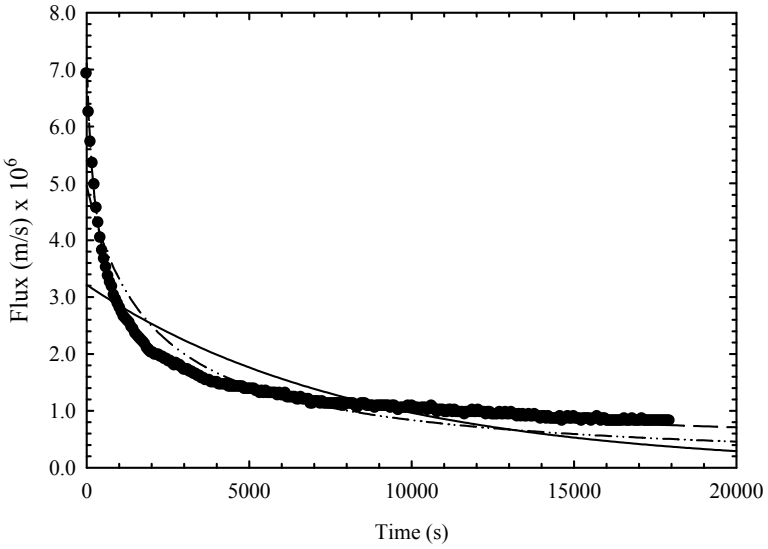

(c)

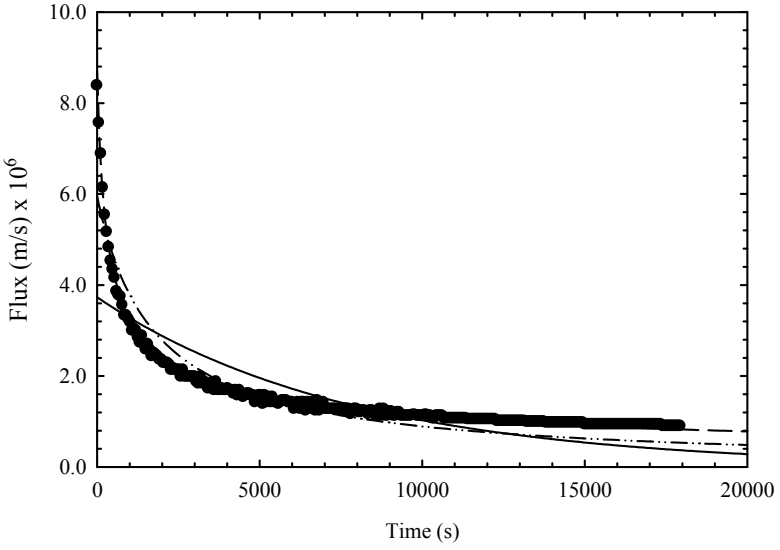

(d)

Figure 5.3 Flux decay and fouling behavior at different transmembrane pressure for unstirred RC membrane filtration (continued). (c) 3 bar; (d) 4 bar ((•) experimental, (—) complete pore blocking, (— ·· — ··) partial pore blocking, (— — —) cake filtration).

As shown in Figure 5.2 for the PES membranes and Figure 5.3 for the RC membranes, the cake filtration model adequately represents the overall fouling mechanism in unstirred dead-end filtration using both polyethersulfone and regenerated cellulose membranes. This is a result of the dextran molecules rejected by the membranes accumulating on the membrane surface without dispersion by agitation.

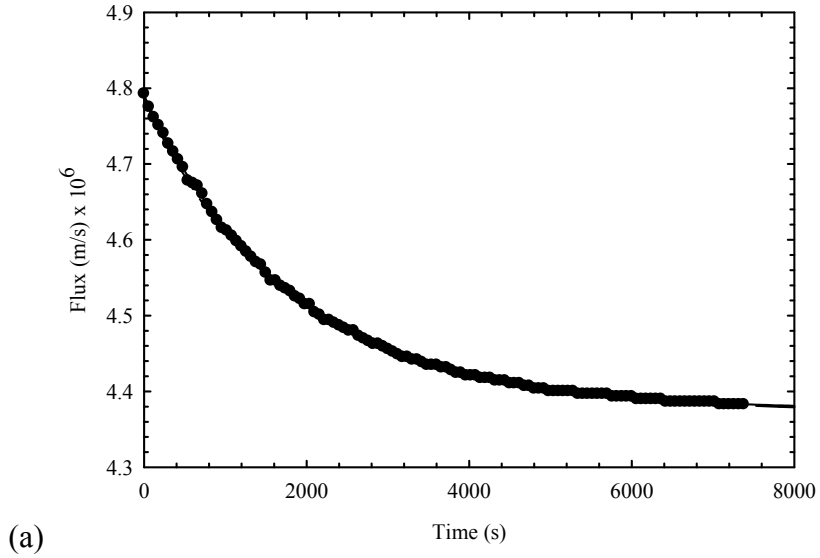

(a)

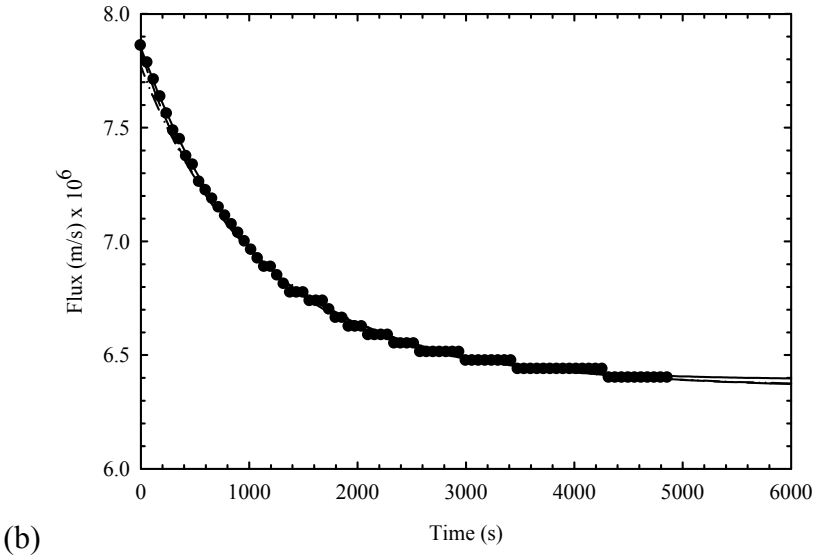

(b)

Figure 5.4 Flux decay and fouling behavior at different transmembrane pressure for 100 rpm stirred PES membrane filtration (a) 1 bar; (b) 2 bar ((•) experimental, (—) complete pore blocking, (—··—··) partial pore blocking, (－－－) cake filtration).

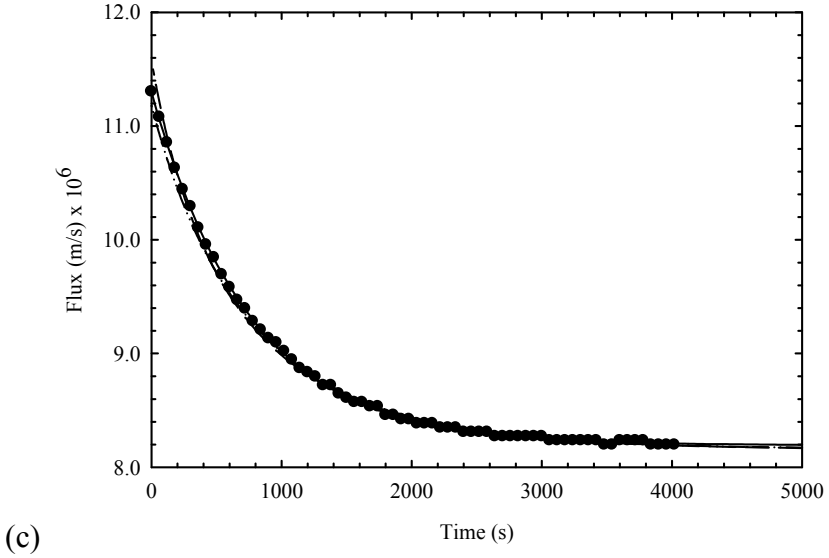

(c)

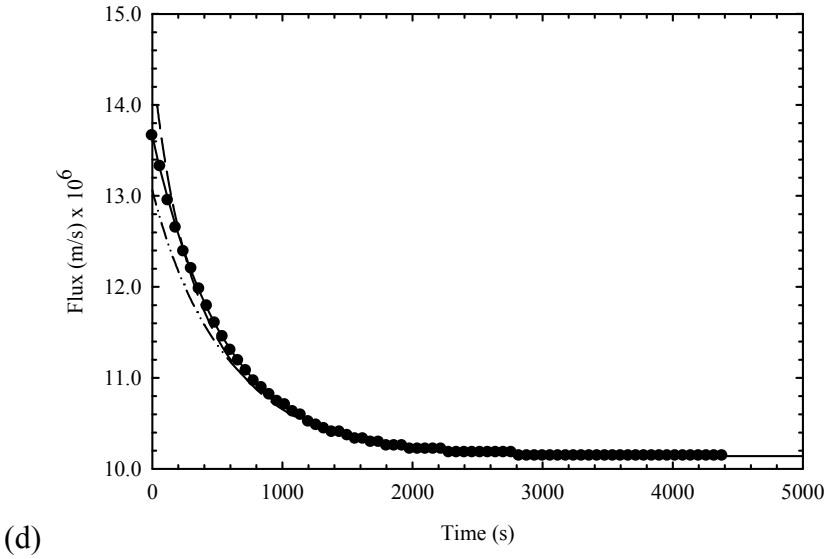

(d)

Figure 5.4 Flux decay and fouling behavior at different transmembrane pressure for 100 rpm stirred PES membrane filtration (continued). (c) 3 bar; (d) 4 bar ((•) experimental, (—) complete pore blocking, (—··—··) partial pore blocking, (－－－) cake filtration).

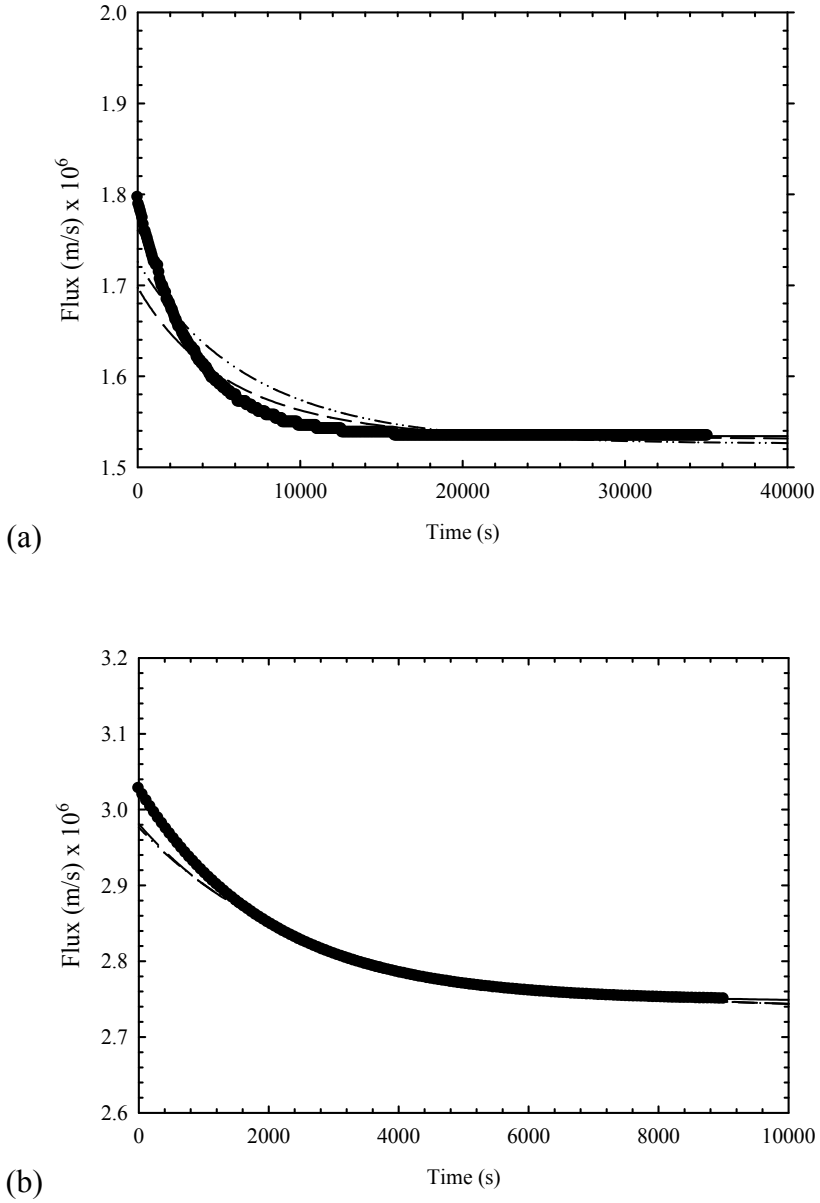

Figure 5.5 Flux decay and fouling behavior at different transmembrane pressure for 100 rpm stirred RC membrane filtration (a) 1 bar; (b) 2 bar ((•) experimental, (—) complete pore blocking, (— ·· — ··) partial pore blocking, (— — —) cake filtration).

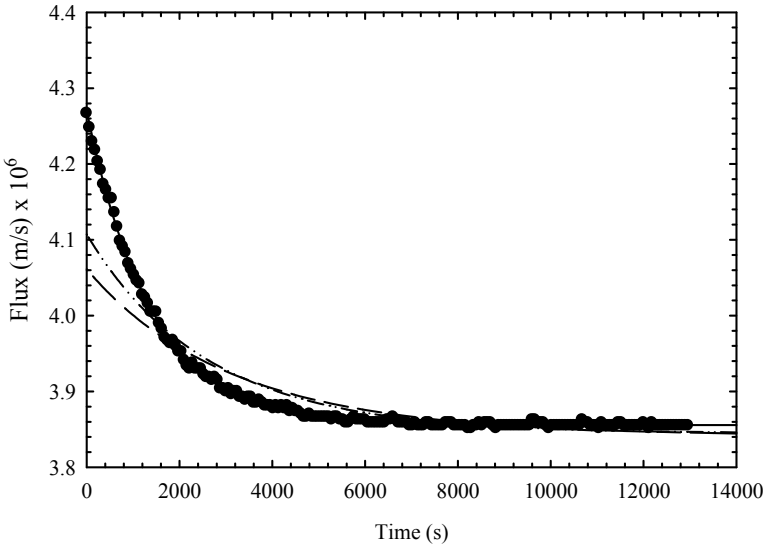

(c)

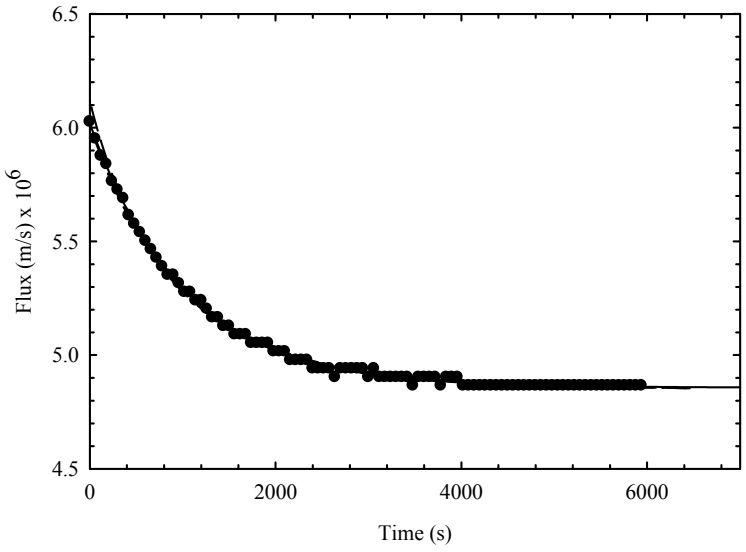

(d)

Figure 5.5 Flux decay and fouling behavior at different transmembrane pressure for 100 rpm stirred RC membrane filtration (continued). (c) 3 bar; (d) 4 bar ((•) experimental, (—) complete pore blocking, (—··—··) partial pore blocking, (－－－) cake filtration).

In the filtration with stirring at 100 rpm, the fouling behavior is controlled by the complete pore blocking model for both membrane materials, as shown by the model fitting in Figure 5.4 for the PES membranes, and Figure 5.5 for the RC membranes. However the model fitting in the two figures do not distinguish between the two fouling mechanisms (cake filtration and complete pore blocking) very well based on the flux decrease alone, so the fouling mechanism will be reconsidered in a later section based on an analysis of more complete mathematical descriptions of the behavior. The behavior of the same membrane filtrations at 200 rpm (Figure 5.6 for the PES membranes, and Figure 5.7 for the RC membranes) showed similar results, however the magnitude of the flux reduction due to fouling was smaller and the rate of fouling was also lower. This demonstrates the effect of tangential flow velocity on fouling. Since the rejected dextran dispersion is proportional to shear force generated by flow velocity, a higher rate of agitation such as 200 rpm can achieve higher dextran dispersion, and this reduces the rate of fouling. The results for the RC membranes at 200 rpm and transmembrane pressures of 1 and 2 bar did not display sufficient levels of fouling to enable models to be fitted to a suitable level of significance in the fitted parameters.

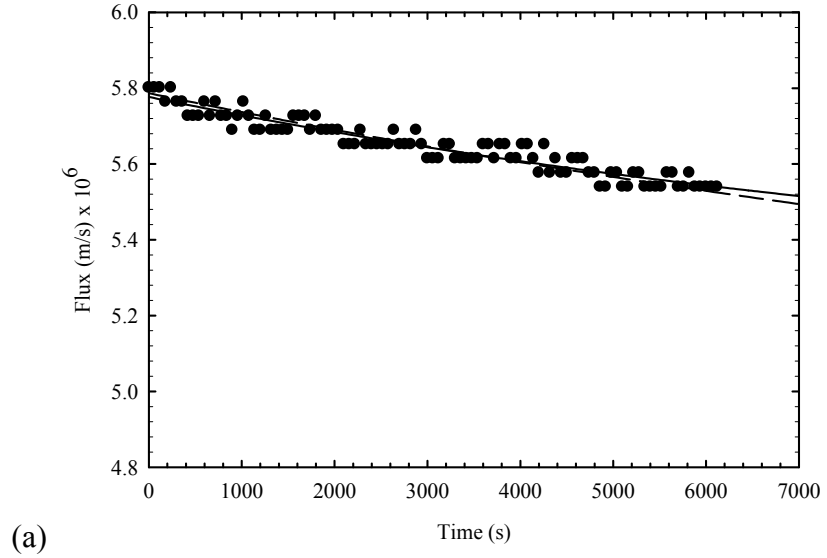

(a)

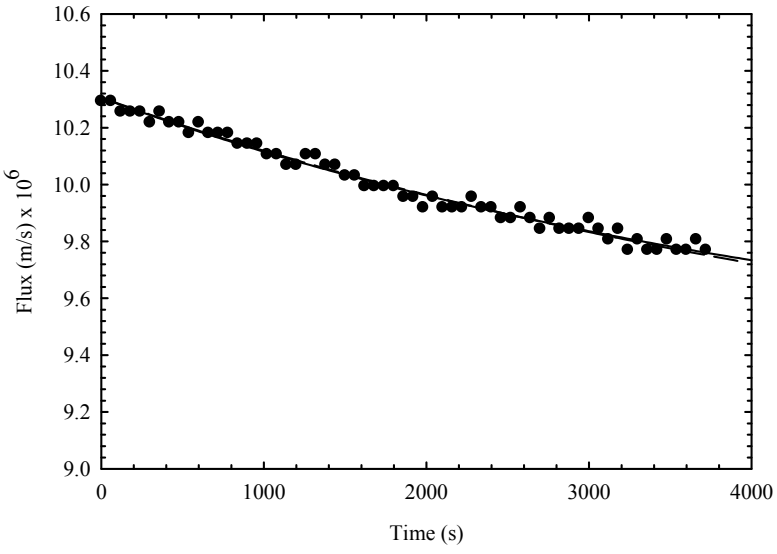

(b)

Figure 5.6 Flux decay and fouling behavior at different transmembrane pressure for 200 rpm stirred PES membrane filtration (a) 1 bar; (b) 2 bar ((•) experimental, (—) complete pore blocking, (－－－) cake filtration).

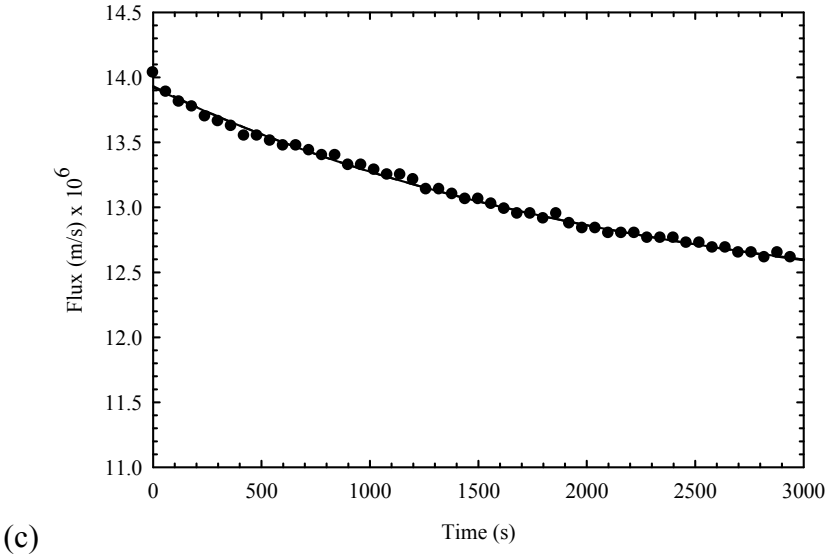

(c)

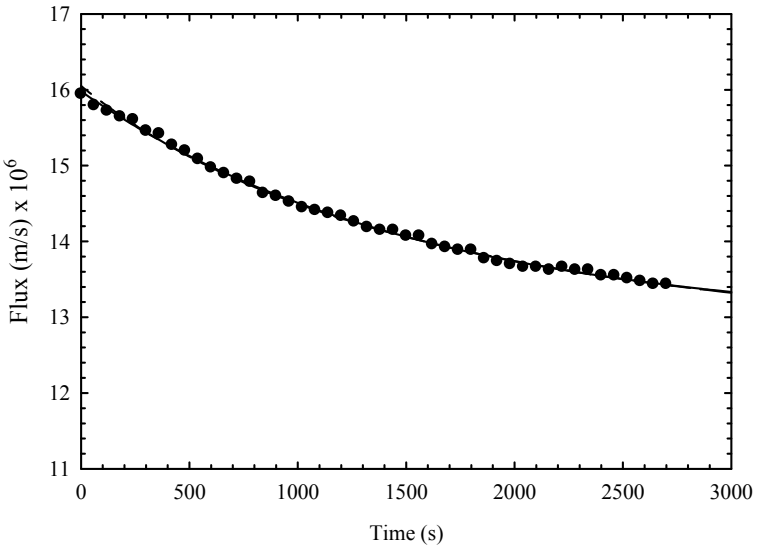

(d)

Figure 5.6 Flux decay and fouling behavior at different transmembrane pressure for 200 rpm stirred PES membrane filtration (continued). (c) 3 bar; (d) 4 bar ((•) experimental, (—) complete pore blocking, (－－－) cake filtration).

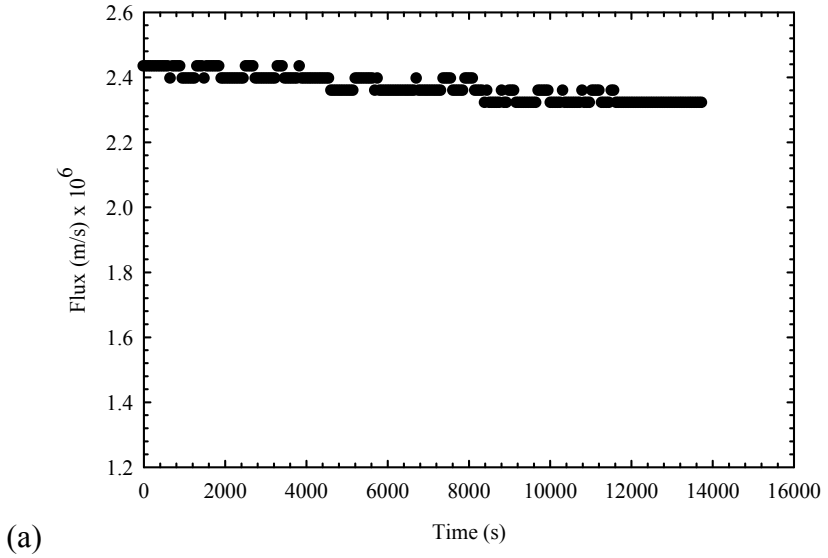

(a)

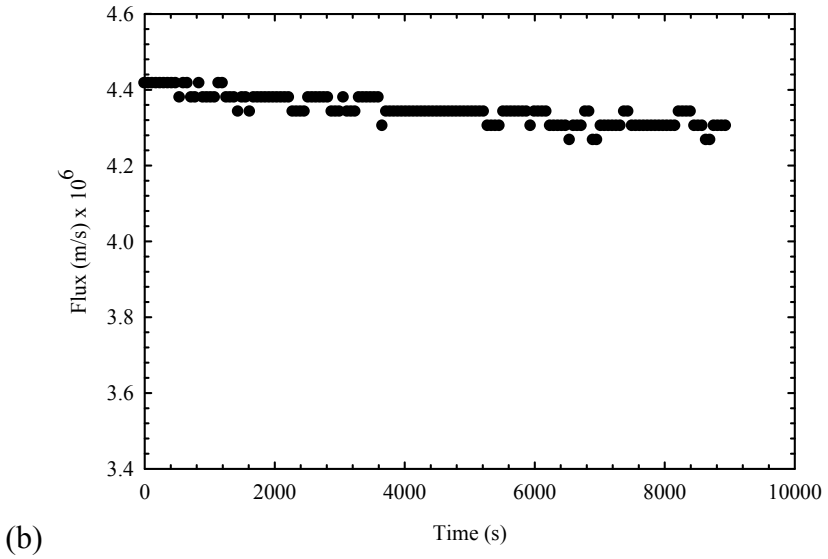

(b)

Figure 5.7 Flux decay and fouling behavior at different transmembrane pressure for 200 rpm stirred RC membrane filtration (a) 1 bar; (b) 2 bar ((•) experimental, (—) complete pore blocking, (－－－) cake filtration).

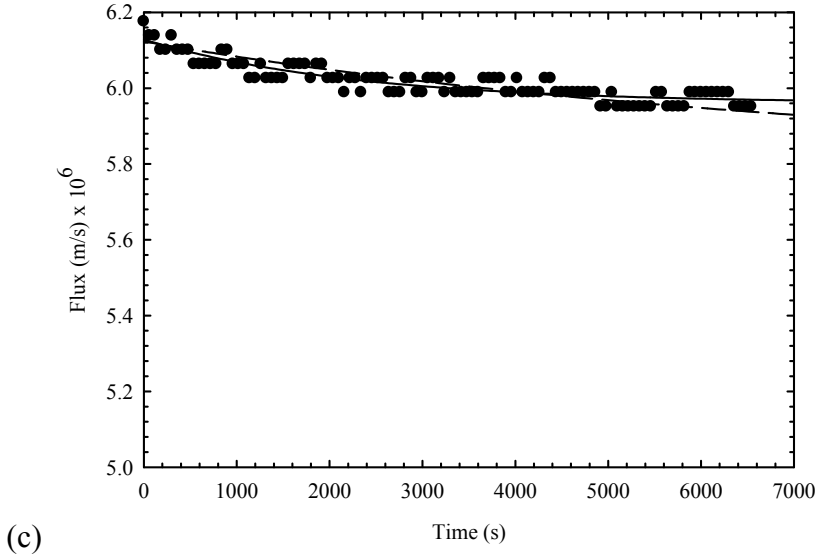

(c)

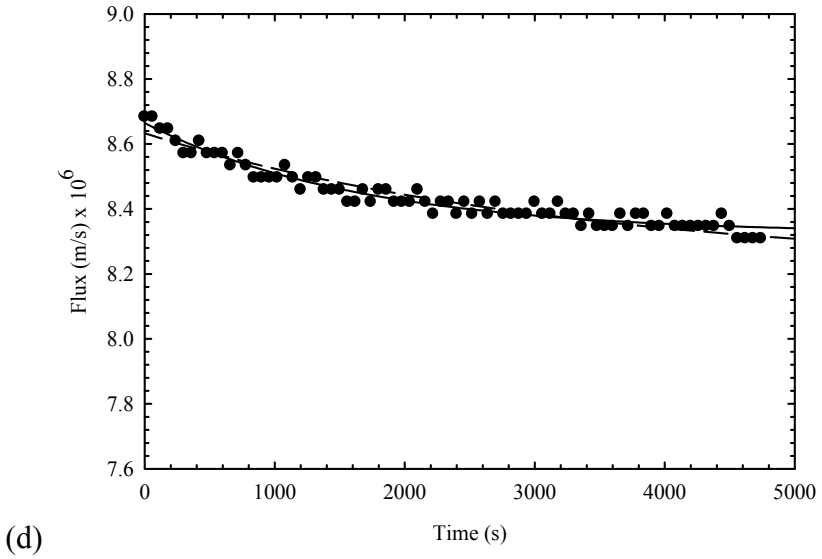

(d)

Figure 5.7 Flux decay and fouling behavior at different transmembrane pressure for 200 rpm stirred RC membrane filtration (continued). (c) 3 bar; (d) 4 bar ((•) experimental, (—) complete pore blocking, (－－－) cake filtration).

5.4.2 Membrane Resistance Determination by Darcy's Law

The initial flux through both the PES and RC membranes was plotted against the transmembrane pressure to determine the membrane resistances as shown in Figure 5.8. A comparison between the models based on the membrane resistance and the measured values of the initial flux are also shown in Figure 5.8. The accuracy of the predicted initial flux from the best fitted model of the PES membrane and the RC membrane as a fraction is 0.99 and 0.97, respectively. The comparison between the experimental results and the fitted model is very good. In addition the accuracy of predicted initial flux by the best fitted model of both membranes is shown in Figure 5.9.

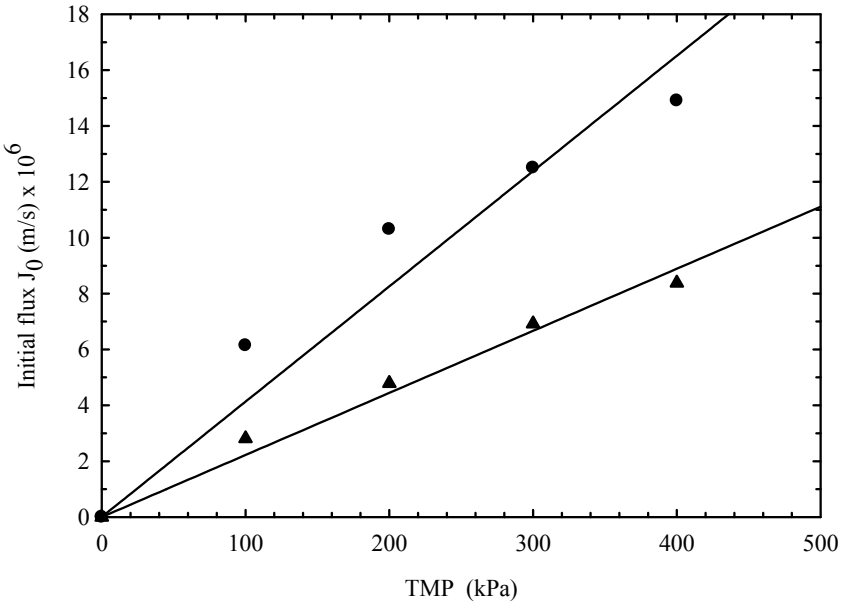

Figure 5.8 The relationship between initial flux and transmembrane pressure. (5,000 MWCO PES (●) and 5,000 MWCO RC (▲) membranes)

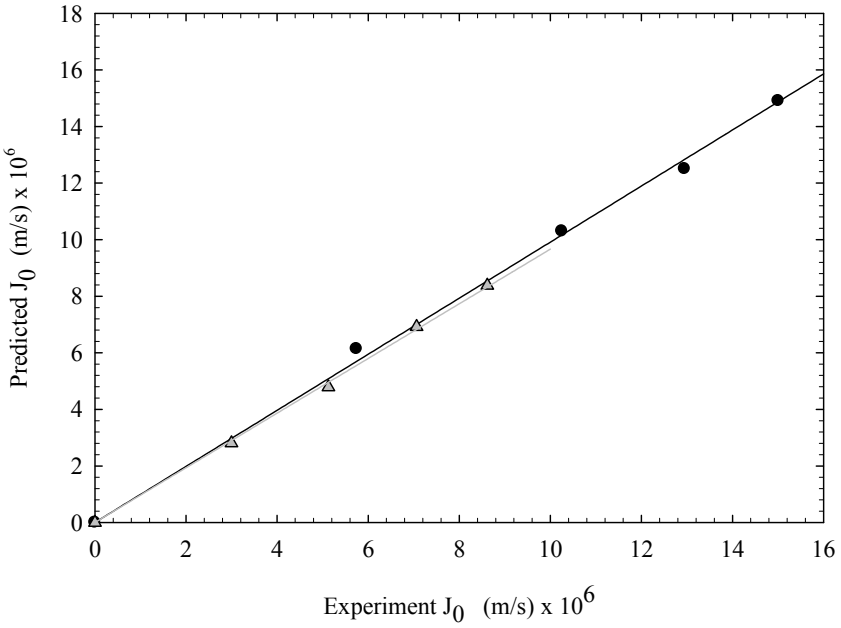

Figure 5.9 The accuracy of predicted initial flux from the best fitted model of 5,000 MWCO PES (●): fitted line (—) and 5,000 MWCO RC (▲) membranes: fitted line (—).

The membrane resistance can be calculated from Darcy's law in the absence of the cake resistance term by using the viscosity of the permeate and the slope of the plots in Figure 5.8. The permeate viscosity measured at room temperature for the experiment is 0.134 cp. The resistances of the polyethersulfone membrane and the regenerated cellulose membrane are equal to $1.80\times10^{13}\,\mathrm{m}^{-1}$ and $3.36\times10^{13}\,\mathrm{m}^{-1}$, respectively. The lower resistance is the reason for the higher flux through the polyethersulfone membrane in the experiment of dextran separation that was discussed in Chapter IV. A previous determination of the 5 kDa polyethersulfone membrane resistance was investigated on cross-flow filtration of mineral water. The result of the membrane resistance varies between $1.30\times10^{13}\,\mathrm{m}^{-1}$ and $1.41\times10^{13}\,\mathrm{m}^{-1}$ (Acero *et al.*, 2009). This is not a serious difference from the value

determined in the current study. However the difference of the membrane resistance determination could be due to the resistance of the support in the filtration system. The comparison in the membrane permeability to Kwon's result is shown in Table 5.1. Kwon (2006) determined the membrane permeability of both PES (5 kDa) and RC (5 kDa) by observing the initial flux of natural water containing organic nanocolloids.

Table 5.1 Permeability of 5 kDa PES and 5 kDa RC membranes.

Membrane	**Permeability of 15% Brix sucrose solution (This work), (m/(Pa·s))**	**Permeability of pure water (Kwon *et al.*, 2006), (m/(Pa·s))**
PES (5 kDa)	4.15×10^{-11}	1.57×10^{-10}
RC (5 kDa)	2.22×10^{-11}	3.47×10^{-11}

Although the membrane permeability for both membranes determined by Kwon is different from the result of this research, it can demonstrate by qualitative comparison that the polyethersulfone membrane has higher resistance than that of the regenerated cellulose membrane, as shown by the slope in Figure 5.8.

5.4.3 Fouling Mechanism Prediction from the Constant k in the Fitted Fouling Model

Since the limiting values of all flux declines in the experiment on stirred mode are not zero, it is evident that internal pore blocking does not control the fouling process. The values of the constant k_1 in both Table 5.2 for the unstirred filtration, and Table 5.3 for the filtration with 100 rpm stirring, obviously vary with the transmembrane pressure, and therefore it can be concluded that the partial pore

blocking mechanism is not dominant in the fouling mechanism for the process either. Consequently, there are only two models, complete pore blocking and cake filtration, that could possibly describe the mechanism of fouling.

Table 5.2 Constant k of each fouling model predicted in the unstirred experiment.

TMP (bar)	**RC membrane**			**PES membrane**		
	Complete pore blocking (k_2)	Partial pore blocking (k_1)	Cake filtration (k_0)	Complete pore blocking (k_2)	Partial pore blocking (k_1)	Cake filtration (k_0)
1	9.66×10^{-5}	97.9	1.56×10^{8}	1.05×10^{-4}	97.8	1.25×10^{8}
2	1.18×10^{-4}	101	1.19×10^{8}	1.49×10^{-4}	104	8.24×10^{7}
3	1.20×10^{-4}	99.5	9.87×10^{7}	1.74×10^{-4}	110	6.92×10^{7}
4	1.29×10^{-4}	95.5	8.15×10^{7}	1.72×10^{-4}	111	6.48×10^{7}

Table 5.3 Constant k of each fouling model predicted in the 100 rpm stirred experiment.

TMP (bar)	**RC membrane**			**PES membrane**		
	Complete pore blocking (k_2)	Partial pore blocking (k_1)	Cake filtration (k_0)	Complete pore blocking (k_2)	Partial pore blocking (k_1)	Cake filtration (k_0)
1	2.99×10^{-4}	86.9	6.41×10^{7}	5.50×10^{-4}	112	2.51×10^{7}
2	5.00×10^{-4}	129	4.58×10^{7}	9.20×10^{-4}	114	1.66×10^{7}
3	7.19×10^{-4}	95.0	1.99×10^{7}	1.33×10^{-3}	129	1.44×10^{7}
4	9.85×10^{-4}	176	3.45×10^{7}	1.83×10^{-3}	144	1.53×10^{7}

According to this the constant k of both the complete pore blocking model and cake filtration model were plotted in relation to the transmembrane pressure to predict the mechanism of membrane fouling. The fouling mechanism prediction of unstirred filtration is shown in Figure 5.10.

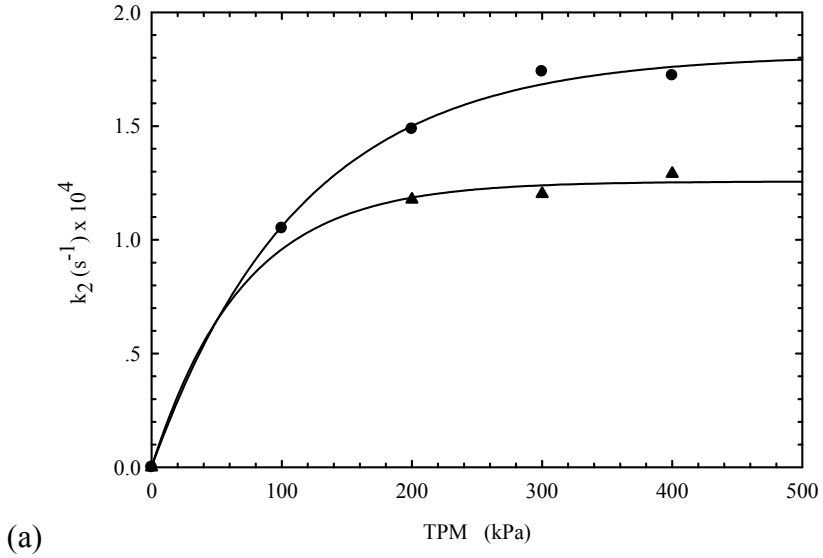

(a)

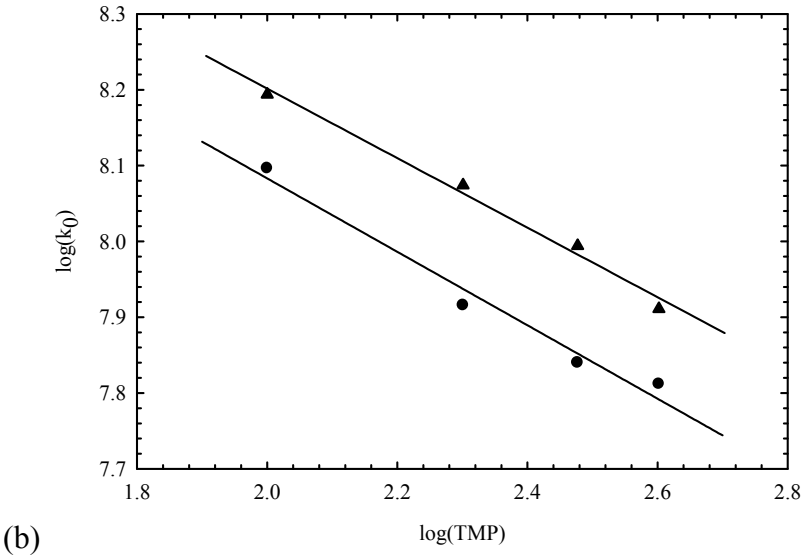

(b)

Figure 5.10 The relationship between the constant *k* of (a) complete pore blocking model; (b) cake filtration model, and the transmembrane pressure for unstirred dead-end filtration. (PES (●) and RC (▲)).

As shown in Figure 5.10, it is seen that the complete pore blocking is not correct in this instance because the constant k_2 is not a linear function of the transmembrane pressure, as it would be if this model was correct. The constant k_0 is a power law relation to the pressure (Figure 5.10(b)) so it is clear that the fouling mechanism is cake filtration. Moreover, the compressibility (s) of dextran cake layer and the constant coefficient ($\alpha_0 \mu k_c$) can be calculated from the slope and the intercept of the plot of k_0 respectively. The cake compressibility of dextran for the filtration using both membrane materials is not significantly different because this constant depends only on the characteristic of the dextran molecules fouling on the membrane. In result, the cake compressibility is between 0.52-0.54 and the constant coefficient is equal to 3.16×10^{10}.

This result agrees with previous research for the cake compressibility of different materials such as silica colloids, that "the cake compressibility is independent of the membrane, and is controlled by the colloid properties and water chemistry" (Singh and Song, 2006). Singh's work shows the compressibility coefficient for the silica colloid based on the use of zirconia and titania membranes are 0.812±0.04 and 0.826±0.02, respectively. Moreover the cake compressibility of dextran determined from the current study is in the possible range, in which zero is the extreme case of incompressible material, and one is the extreme case of zero volume of the compressed cake layer. Table 5.4 shows the cake compressibility of various materials that have been collected from many sources. It is seen that although the researchers worked on the same material, the results are different since there is work performed using different procedures. In addition, there is an effect of feed

concentration on the cake compressibility, which is evidenced by Hamachi's results in the table.

Table 5.4 The cake compressibility for various types of solute.

Material	Cake compressibility (s)
Bovine serum albumin (Ho and Zydney, 2000)	0.82
Latex particle (Antelmi *et al.*, 2001)	0.50
$CaCO_3$ (Tien et al., 2001; Teoh *et al.*, 2006)	0.44
Kaolin clay (Tien *et al.*, 2001; Teoh *et al.*, 2006)	0.85
0.1μm Fluorescent polystyrene latex beads (Park *et al.*, 2007)	0.26-0.50 (varies for 7 run numbers)
0.25 g/L of bentonite clay (Hamachi and Peuchot, 1999)	0.54
0.375 g/L of bentonite clay (Hamachi and Peuchot, 1999)	0.73
Bentonite clay (Murase *et al.*, 1995)	0.96
Kaolin clay (Murase *et al.*, 1995)	0.46

The comparison between the dextran cake compressibility for the current study and that for previous results was investigated. The cake compressibility for the previous result was determined based on the power law of cake resistance by using approximate values of the specific cake resistances form Cheng's work (Cheng

and Huang, 2002). It is found that the result for the current study is quite similar to the previous result for dextran T-70. The cake compressibility can be determined from the slope in Figure 5.11, to obtian 0.50 and 0.69 for dextran T-70 (69 kDa) and dextran T-500 (473 kDa) respectively (Cheng and Huang, 2002).

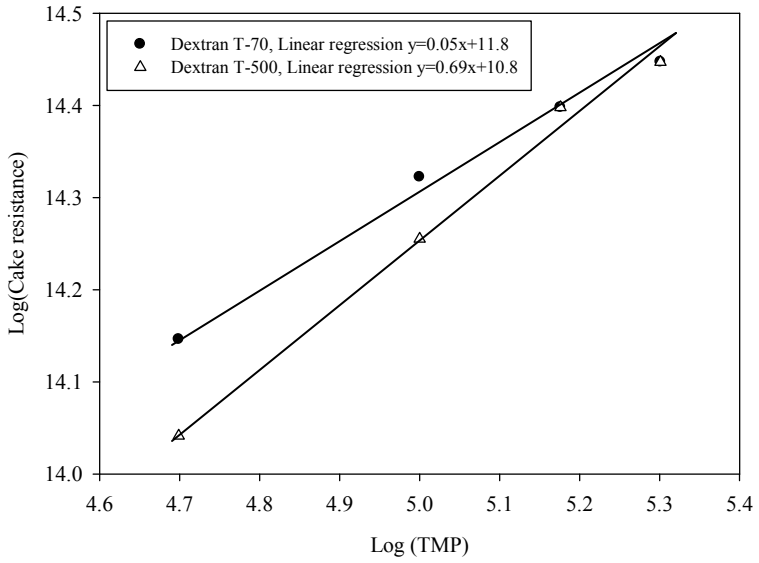

Figure 5.11 The cake compressibility for dextran T-70 and dextran T-500.

The effect of tramsmembrane pressure on the specific cake resistance of polymethyl methacrylate (PMMA) and the k parameter of the cake filtration model can be seen in Figure 15.12. This shows that either the cake resistance or the k parameter can be used to determine the cake compressibility by the plot against transmembrane pressure on a log-log scale.

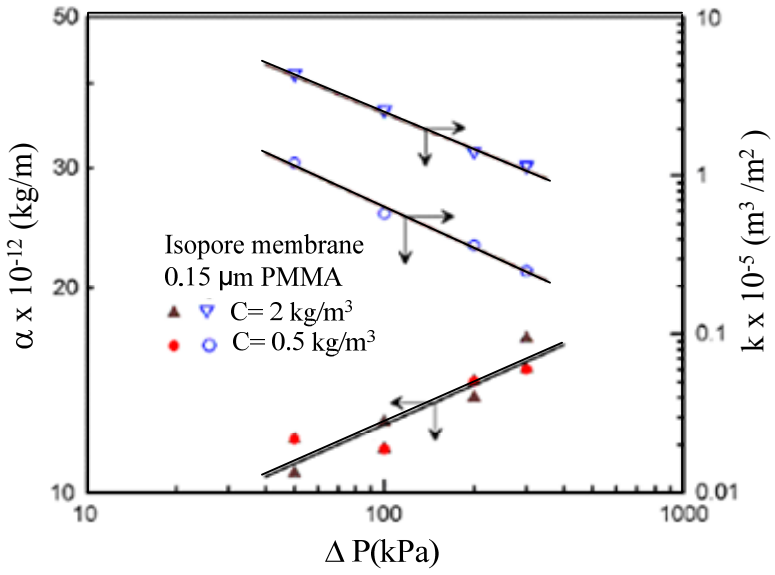

Figure 5.12 Effect of filtration pressure on the cake resistance α and the k parameter of cake filtration mechanism (Hwang *et al.*, 2007).

However if the filtration was performed with magnetic stirring at a speed of 100 rpm, the fouling mechanism becomes complete pore blocking as exhibited in Figure 5.13. Moreover the qualitative comparison in terms of the fouling of both membranes can be deduced, suggesting that fouling of the polyethersulfone membrane is faster than that of the regenerated cellulose membrane, as shown by the exponential coefficient constant (k_2).

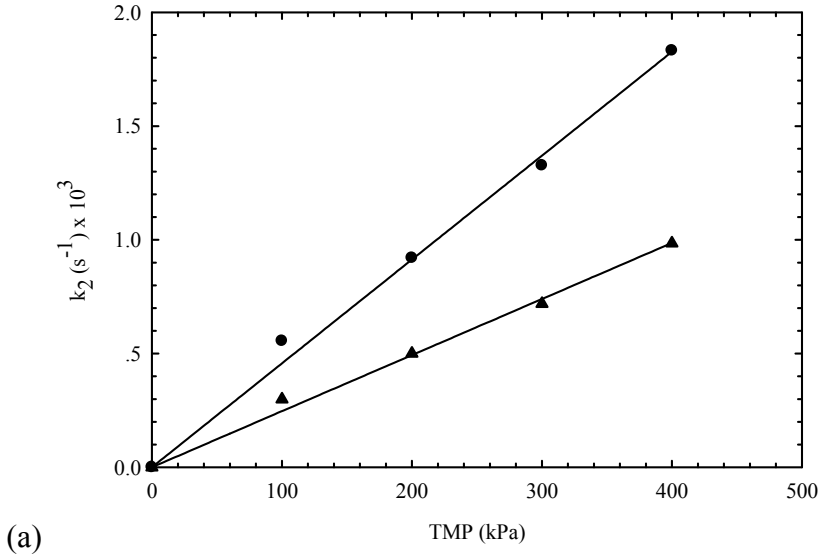

(a)

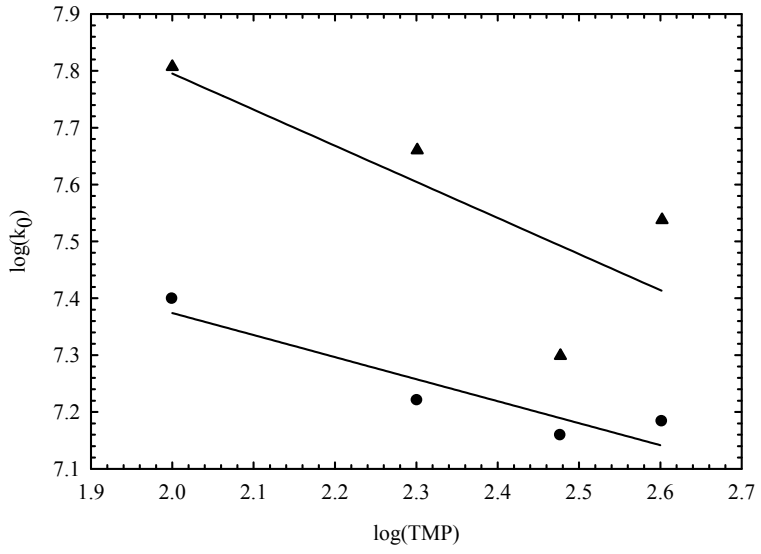

(b)

Figure 5.13 The relationship between the constant *k* of (a) complete pore blocking model; (b) cake filtration model, and the transmembrane pressure for stirred dead-end filtration at speed of 100 rpm. (PES (●) and RC (▲)).

Results of dextran (T-70 and 2,000 which indicates the molecular weight of 70,000 and 2,000,000 Daltons) fouling on cross-flow ultrafiltration of the Carbosep membrane (MWCO 50 kDa) have shown that the fouling was due to both internal pore blocking and cake filtration (De Bruijn *et al.*, 2005). Although a monolayer blocking usually occurs before the cake formation (Song, 1998; Ho and Zydney, 2000; De Bruijn *et al.*, 2002; Hwang *et al.*, 2007), complete pore blocking prevails for the results in the current study since dextran tends to adsorb on the PES membrane with a monolayer rather than with cake formation (Susanto and Ulbricht, 2005; Susanto *et al.*, 2007). This is due to the stronger interaction between dextran and the PES membrane than the dextran-dextran interaction. In common with the PES membrane, the monolayer can block the RC membrane although the interaction between the RC membrane and dextran is weaker than that between the PES membrane and dextran. For unstirred dead-end filtration, the cake layer can be formed since the rejected dextran by the membrane surface is not dispersed by any shear force.

Complete pore blocking was used to describe the fouling mechanism in this research rather than the internal pore blocking since the results have shown there is a finite limiting flux for the filtration with stirring (Figure 5.5, Figure 5.6, Figure 5.7, and Figure 5.8) and the limiting flux depends on the stirring speed (Figure 4.4), which is not possible based on the theoretical concept of the internal pore blocking model (De Barros *et al.*, 2003).

5.5 Conclusions

The resistances of the polyethersulfone membrane and of the regenerated cellulose membrane are equal to $1.80\times10^{13}\,m^{-1}$ and $3.36\times10^{13}\,m^{-1}$ respectively. Moreover, the accuracy of the predicted initial flux from the best fitted model of polyethersulfone membrane and of regenerated cellulose membrane as a fraction are 0.99 and 0.97, respectively.

In this study it was found that the fouling due to dextran (mean molecular weight 53,000 Da) in an unstirred dead-end ultrafiltration is due to the cake filtration mechanism. The compressibility of the dextran cake layer is between 0.52-0.54. When the filtration was performed with agitation by a magnetic stirrer at a speed of 100 rpm, the fouling mechanism becomes complete pore blocking. The flux decline of the filtration with 200 rpm stirring did not display sufficient levels to fit to a suitable fouling mechanism by using the fitted parameters of each fouling model.

5.6 References

Acero, J. L., Benitez, F. J., Real, F. J., and Garcia, C. (2009). Removal of phenylurea herbicides in natural waters by UF membrane: Permeate flux, analysis of resistances and rejection coefficients. **Separation and Purification Technology.** 65: 322-330.

Antelmi, D., Cabane, B., Meirales, M., and Aimar, P. (2001). Cake collapse in pressure filtration. **Langmuir.** 17: 7137-7144.

Baker, R. W. (2004). Ultrafiltration. **Membrane Technology and Applications** (2nd ed., pp. 237-274). Great Britain: John Wiley and Sons.

Cheng, T. W. and Huang, C. Y. (2002). Filtration characteristics of the rejected-solute layer in dead-end ultrafiltration. **Journal of Membrane Science.** 209: 485-492.

Cheryan, M. (1998a). Fouling and cleaning. **Ultrafiltration and Microfiltration Handbook** (pp. 237-292). Pennsylvania, USA: A Technomic Publishing Company.

Cheryan, M. (1998b). Performance and engineering models. **Ultrafiltration and Microfiltration Handbook** (pp. 113-170). Pennsylvania, USA: A Technomic Publishing Company.

De Barros, S. T. D., Andrade, C. M. G., Mendes, E. S., and Peres, L. (2003). Study of fouling mechanism in pineapple juice clarification by ultrafiltration. **J. Membr. Sci.** 215: 213-224.

De Bruijn, J. P. F., Venegas, A., and Borquez, R. (2002). Influence of crossflow ultrafiltration on membrane fouling and apple juice quality. **Desalination.** 148: 131-136.

De Bruijn, J. P. F., Venegas, A., Martinez, J. A., and Borquez, R. (2003). Ultrafiltration performance of Cabosep membranes for the clarification of apple juice. **Lebensm.-Wiss. U.-Technol.** 36: 397-406.

De Bruijn, J. P. F., Salazar, F. N., and Borquez, R. (2005). Membrane blocking in ultrafiltration a new approach to fouling. **Trans. Inst. Chem. Eng.** 83(C3): 211-219.

Field, R. W., Wu, D., Howell, J. A., and Gupta, B. B. (1995). Critical flux concept for microfiltration fouling. **J. Membr. Sci.** 100: 250-272.

Field, R. W., Wu, D., Howell, J. A., and Gupta, B. B. (1996). Mass transport and the design of membrane systems. In K. Scott and R. Hughes (eds.), **Industrial Membrane Separation Technology** (pp. 67-113). London: Chapman & Hall.

Hamachi, M. and Peuchot, M. M. (1999). Experimental investigations of cake characteristics in crossflow microfiltration. **Chemical Engineering Science.** 54: 4023-4030.

Hermia, J. (1982). Constant pressure blocking filtration laws. Application to power law non-Newtonian fluids. **Trans. Inst. Chem. Eng.** 60: 183-187.

Ho, C. C. and Zydney, A. L. (2000). A combined pore blocking and cake filtration model for protein fouling during microfiltration. **Journal of Colloid and Interface Science.** 232: 389-399.

Hwang, K. J., Liao, C. Y., and Tung, K. L. (2007). Analysis of particle fouling during microfiltration by use of blocking models. **Journal of Membrane Science.** 287: 287-293.

Kwon, B., Cho, J., Park, N., and Pellegrino, J. (2006). Organic nanocolloid fouling in UF membranes. **Journal of Membrane Science.** 279: 209-219.

Lodge, B., Judd, S. J., and Smith, A. J. (2004). Characterisation of dead-end ultrafiltration of biotreated domestic wastewater. **J. Membr. Sci.** 231: 91-98.

Murase, T., Ohn, T., and Kimata, K. (1995). Filtration flux in crossflow microfiltration of dilute suspension forming a highly compressed fouling cake layer. **Journal of Membrane Science.** 108: 121-128.

Park, P. K., Lee, C. H., and Lee, S. (2007). Determination of cake porosity using image analysis in a coagulation-microfiltration system. **Journal of Membrane Science.** 293: 66-72.

Singh, G. and Song, L. (2006). Cake compressibility of silica colloids in membrane filtration processes. **Ind. Eng. Chem. Res.** 45(22): 7633-7638.

Song, L. (1998). Flux decline in crossflow microfiltration and ultrafiltration: mechanisms and modeling of membrane fouling. **Journal of Membrane Science.** 139: 183-200.

Susanto, H., Franzka, S., and Ulbricht, M. (2007). Dextran fouling of polyethersulfone ultrafiltration membranes - Causes, extent and consequences. **Journal of Membrane Science**. 296: 147-155.

Susanto, H. and Ulbricht, M. (2005). Influence of ultrafiltration membrane characteristics on adsorptive fouling with dextrans. **Journal of Membrane Science**. 266: 132-142.

Teoh, S. K., Tan, R. B. H., and Tien, C. (2002). Correlation of C-P cell and filtration test data using a new test cell. **Separation and Purification Technology.** 29: 131-139.

Teoh, S. K., Tan, R. B. H., and Tien, C. (2006). A new procedure for determining specific filter cake resistance from filtration data. **Chemical Engineering Science.** 61: 4957-4965.

Tien, C., Teoh, S. K., and Tan, R. B. H. (2001). Cake filtration analysis-the effect of the relationship between the pore liquid pressure and the cake compressive stress. **Chemical Engineering Science.** 56: 5361-5369.

CHAPTER VI

DEXTRAN PARTITION COEFFICIENT AND GROWTH RATE IN SUCROSE CRYSTALLIZATION

6.1 Abstract

The dextran partition coefficient between the impure syrup and the sucrose crystal was correlated to the crystal growth rate to find the suitable growth condition for production of sucrose crystal with low dextran content and to understand the mechanism of dextran incorporation into the crystal. The crystallization experiments were performed in a stirred batch crystallizer with agitation at 1,000 rpm. The rate of crystal growth was studied under several operating conditions. The crystallizer was operated isothermally at temperatures of 30°C, 40°C, and 50°C, at constant relative supersaturations of 0.05, 0.07, and 0.09, and with mother liquor dextran concentrations of 1,000 ppm/Brix and 2,000 ppm/Brix. The dextran content in the crystal product was determined by using the CSR method. A 1:1 mass ratio of high fraction dextran (approximately 250,000 Da) and low fraction dextran (60,000 - 90,000 Da) was used to represent as wide a range of dextran as possible in mill syrups. It was seen that the amount of dextran incorporating into the crystalline phase during the crystallization increases with either increasing supersaturation or increasing crystallization temperature. However it appears that these are secondary effects, with

the partition coefficient correlating almost perfectly with the crystal growth rate alone, despite the regressed data having large variations for temperature, mother liquor dextran content, and supersaturation. The relation between the dextran partition coefficient and the crystal growth rate can be presented by the empirical equation $K_{eff}[\%] = (9.8 \pm 1.0) \times \left(1 - \exp^{(-1.7 \pm 0.4)G}\right)$. The dextran concentration in the solution affects the absolute value of the dextran content in the crystal, but does not strongly affect the dextran partition coefficient.

6.2 Introduction

6.2.1 Dextran Contamination in Sugar Crystal

Raw sugar quality has long been a serious concern, largely due to it being the raw material used in sugar refineries. One of the main criteria used to assess the quality of raw sugar crystal is its dextran content. The dextran content in a raw sugar product typically varies from 100 to 1,000 ppm or more (Priester, 1981; Vane, 1991). The false grain growth, or needle-shaped elongation is one consequence of dextran, and is a commonly found abnormal crystal habit. The crystal elongation is a result of unrestricted growth along the *c* axis of the sugar crystal, while the growth along the *a* and *b* axes of the crystal are retarded by dextran. The threshold of the crystal elongation has been reported at 600 ppm dextran contamination in raw sugar product (Chou and Wnukowski, 1981). The variation of dextran content in raw sugar crystals commonly depends on the dextran concentration in the syrup from which they grew. At lower dextran concentrations (less than 4,000 ppm/Brix), it has been proposed that the crystal product would be contaminated at a level of approximately 10% of the dextran content of the syrup (Rauh *et al.*, 2001: Cuddihy *et al.*, 1999).

This value was observed in a sugar mill, where the growth rates of the crystals should be significantly larger than those apparent in the current study.

6.2.2 Partition Coefficient

In many industrial crystallization processes, the amount of impurities incorporated in the crystalline phase is larger than that predicted by a simple thermodynamic equilibrium between the liquid phase and the solid phase. The excess impurity incorporation has been suggested to be due to the influence of nonequilibrium incorporation or due to the accumulation of rejected impurities in the boundary layer during the growth process, the actual amount of impurity incorporation is larger than the predicted value (Meenan *et al.*, 2002). For these reasons, the effective partition coefficient of impurities between the two phases has been the subject of many studies. However there are only a few models of impurity incorporation into growing crystals. The most well known is that of Burton who proposed the model (Burton *et al.*, 1953)

$$K_{eff} = \frac{K}{K + (1 - K)\exp\left(\frac{-G\delta}{D}\right)} \tag{6.1}$$

where K is the equilibrium thermodynamic partition coefficient between the crystal and the solution for the impurity, K_{eff} is the effective partition coefficient, G is the crystal growth rate, D is the diffusion coefficient of the impurity species, and δ is the boundary layer thickness (beyond which it may be assumed that the solution concentration is maintained constant through flow). The model is based upon the concept that partial rejection of impurities at the crystal surface due to growth leads to an increased concentration of the impurity molecules in the boundary layer around the

growing crystal. The model predicts a finite effective distribution coefficient at zero growth rate (which will then be the equilibrium distribution coefficient), however this is unlikely in most industrial crystallizations from solution where very slow growth is likely to lead in most cases to extremely high purity (in essence 100% purity) crystals (Mersmann, 2001; Dowling, 1990).

Dextran in sugar syrups from the milling process is usually measured using units of ppm/Brix which indicate *x* mg dextran/kg solution of dextran per kg total solid (largely sugar) in the solution. In the quantitative study on dextran incorporation into the crystal, the partition coefficient between the liquid phase and the solid phase $\left(K_{eff}\right)$ can be defined as the ratio of ppm of dextran in the crystal product and ppm/Brix of dextran in solution, which is dimensionless since the crystal is 100% solids and therefore equivalent to 1 Brix.

6.2.3 Growth Rates

The experiments discussed in the current work involve determination of the growth rates under various conditions of temperature, sucrose concentration, and dextran impurity levels, as well as the partition coefficients for dextran in sugar crystallization. The most common variable used to characterize the driving force for crystallization of molecular species is the relative supersaturation, which can be defined as

$$\sigma = \frac{C - C^*}{C^*} \tag{6.2}$$

where σ is the relative supersaturation, C is the sucrose concentration as a mass fraction, and C^* is the sucrose solubility at the experimental temperature. The most

common method of characterizing the level of impurity is to determine the mass impurity to water ratio (I/W), (White, 2000; Smythe, 1967a), although direct impurity concentrations (i.e. ppm) may also be used.

Under the assumption of a seeded batch crystallization with no nucleation, breakage or agglomeration, the growth rate can be calculated using the weight of crystal produced, the weight of the seed, and the crystal sphericity of sucrose of 0.87 (Kelly and Keng, 1975). The most significant of these mechanisms for batch crystallization of sucrose is the mechanism of secondary nucleation. A review on sugar crystallization in mills (White, 2000) gives a correlation of the secondary nucleation thresholds (SNT) for crystallization of sucrose based on work by Broadfoot (1972), quoted in White (2000).

$$\sigma_{SNT} = 0.11 + 3.6\left[\frac{I}{(S+I)}\right]^3 \tag{6.3}$$

In the current experiments, the impurity levels in the solutions are not over 2,000 ppm/Brix so the SNT of sucrose crystallization is about a relative supersaturation of 0.11. Since the supersaturation was maintained below the secondary nucleation limit, nucleation was not expected to occur. The validity of the assumptions of zero nucleation, agglomeration, and breakage was verified by visual inspection of suspension samples under a microscope in order to detect these mechanisms through the appearance of crystals smaller than the seed crystal size, aggregated crystals, or crystals with rounded edges. Nucleation, agglomeration, and breakage were not noted in any of the experiments.

The relation between the weight of the crystal in a sample and the mean size of the crystal product can therefore be defined by

$$W = 0.87 \times 10^{-12} \frac{\pi}{6} \rho N \bar{L}^3 \tag{6.4}$$

where W is weight of crystal product (g), ρ is the density of the sucrose crystal (1.588 g/cm^3) (Reiser, *et al.*, 1995) , N is the number of seed crystals, and $\bar{L}$ is mean size of product crystal (μm). This relationship may be used to calculate the average size of the product crystals, and if the average size of the seed is known then the average crystal growth rate may also be calculated. Analysis of sucrose crystal growth under industrial conditions, including in the presence of impurities has been studied by many groups, with large amounts of information in works by Smythe (1967a; 1967b) and Martins and co-workers (Martins and Rocha, 2006; Martins *et al.*, 2005; Martins *et al.*, 2006).

In the sugar crystallization process either surface integration or creation of surface nuclei usually controls the growth mechanism. Based on the results of fundamental growth models the power law is often used to model the surface integration step for all ranges of supersaturations (Myerson and Ginde, 2002; Shiau, 2003).

$$G = k_r \sigma^n \tag{6.5}$$

where the exponent n varies between 1 and 2, and k_r is a surface reaction rate constant.

The rate constant is typically strongly temperature-dependent, however this dependence can usually be expressed accurately via the Arrhenius equation. Thus, the mean growth rate becomes

$$G = k_r \exp\left(\frac{-E_A}{RT}\right)\sigma^n \tag{6.6}$$

where E_A is the activation energy (kJ/mol), R is the ideal gas constant (8.314 kJ·K/mol) and T is temperatutre (K).

6.2.4 Objectives of the Study

Since the raw sugar is the raw material in the refinery, many troubles due to the presence of dextran are introduced into sugar refining if the raw sugar product is not clean. The current study is undertaken to investigate methods to reduce the dextran contamination in the raw sugar product, particularly attempts to reduce the rate of dextran incorporation into crystals that are growing in syrup having relatively low dextran content. Several factors which affect the growth kinetics of sucrose crystals will be adjusted to observe the relation between these factors and the dextran partitioning. These factors include temperature, supersaturation and dextran content. It is expected that suitable growth conditions for production of sucrose crystals with lower amounts of dextran contamination can be established.

6.3 Materials and Methods

6.3.1 Materials

High purity (>99.9%) commercial refined sugar was used as a source of sucrose, and high fraction dextran (approximately 250,000 Da molecular weight)

and low fraction dextran (approximately 60,000-90,000 Da molecular weight), both from ACROS Organics were used as an impurity in the ratio of 1:1, except where otherwise specified.

Since synthetic solutions containing dextran as the only polysaccharide were used rather than sugar syrup sourced from the factory, in this case, total polysaccharide is equivalent to total dextran. Thus, CSR method (Roberts, 1981) should be more accurate and more reproducible than the Roberts test (Altenburg, 1993) since it has fewer steps in which random error can be introduced to the method. Chemicals such as absolute methanol, absolute ethanol, isopropyl alcohol, celite filter aid, phenol, and sulfuric acid required for the dextran determination in the CSR method were analytical grade as specified by ACS.

6.3.2 Apparatus

A 2 liter glass crystallizer agitated by a 45° pitched-blade impeller driven by an overhead stirrer at 1000 rpm was used for the sucrose crystallization process as shown in Figure 6.1. Temperature control was provided by a thermostat through a cooling coil. The total dissolved solid (% Brix) in the solution was measured using a PAL-α model digital pocket refractometer (Atago Co., Japan). Zylon membrane, 47 mm in diameter and with a pore size of 5 μm, was used for filtration in the CSR method.

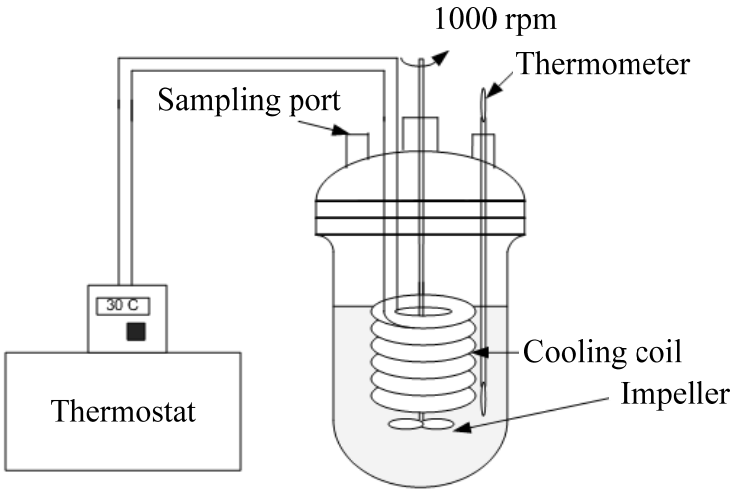

Figure 6.1 The thermostated glass crystallizer used in the experiments.

6.3.3 Crystallization Conditions

Growth conditions were varied by adjusting conditions such as temperature (30°C-50°C), relative supersaturation (0.05-0.09), and dextran content (1,000 and 2,000 ppm/Brix) in synthetic solutions, to study the variation of the effective partition coefficient with each of these variables. It can be assumed that the supersaturation level for the study is effectively constant since the amount of seed crystal (about 0.5 g) was very small compared with the supersaturation and total volume of the crystallizer. The seed crystals were prepared by sieving commercial refined sugar through 150-250 μm mesh sizes. The particle size distribution for the seed crystal, shown in Figure 6.2, was determined by measuring the size of suspended seed in sucrose saturated ethanol using a Malvern Mastersizer.

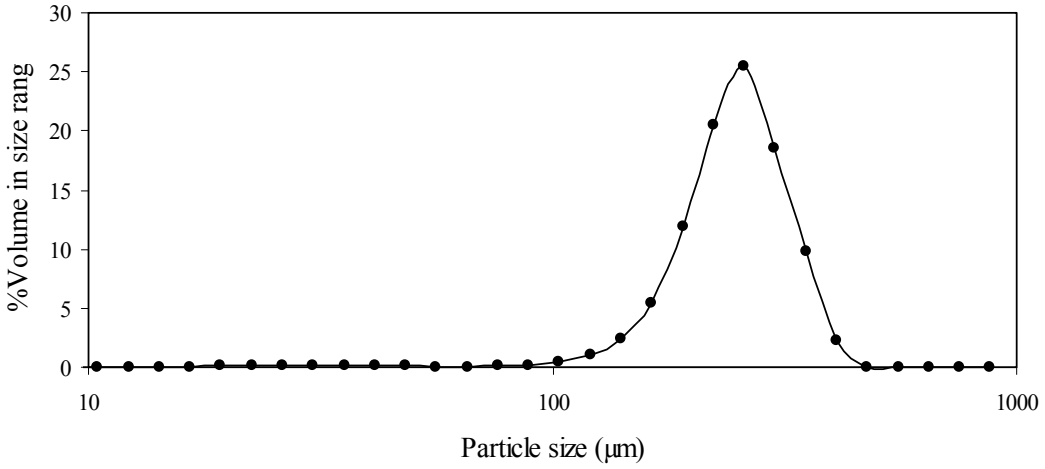

Figure 6.2 Particle size distribution of seed crystal used in the experiment.

Since the dextran content in the solutions is very small (not over 2,000 ppm/Brix), the effect of dextran on the sucrose solubility can be neglected. Therefore the following equation (Kelly and Keng, 1975) can be used to predict the sucrose solubility in the experiment.

$$C = 64.53 + 0.0937T + 0.0012T^2 \left(< 50^\circ C\right) \tag{6.7}$$

where C is % sucrose by weight of solution and T is temperature in °C.

6.3.4 Crystal Product Separation

When the crystallization was complete, the majority of the mother liquor was decanted after settling of the product crystals. A large amount of aqueous saturated solution of sucrose was added into the massecuite so that the viscosity of the massecuite is reduced and the dextran content in the liquid phase is diluted approximately 25 times from the initial level. A 47 mm diameter vacuum filter holder (Thermo Scientific Nalgene) with a 51 μm stainless steel mesh was used to separate

the crystal product from the mother liquor. This was sufficient to separate crystals from the mother liquor quickly, but did not result in any loss of crystal product since there was no nucleation or breakage occurring in the crystallizer, and since the seed crystals were significantly larger than this size. The crystal product was cleaned by addition of sucrose saturated methanol, and after all of the methanol passed through the filter, sucrose saturated ethanol was added, followed by isopropyl alcohol, in order to clean the crystals of all remaining mother liquor attached to the surface of the crystal. The final step was to dry the crystals at room temperature to remove any remaining alcohol.

6.3.5 CSR Method

The dextran content of the initial mother liquors and the sugar crystal products were determined using the CSR method. A brief recap of this procedure follows; all polysaccharides are precipitated in the juice sample by addition of 80% ethanol, followed by collection the precipitate with filter aid on a Zylon membrane. The polysaccharides are dissolved out of the filter aid and the filter paper by boiling in 1% V/V sulfuric acid. The solution containing the polysaccharides is separated by filtering through a Whatman No.42 filter paper. For the current study all dissolved polysaccharide in the filtrate is dextran.

The dextran in the filtrate is hydrolyzed by sulfuric acid addition to develop color with phenol. The absorbance of the developed color is read by a spectrophotometer at 485 nm against a blank prepared in the same way as the sample. The absorbance value can be used to predict the dextran content in the sample by using a calibration (Roberts, 1981). The calibration for the CSR method is the same as for the Roberts test that is shown in Chapter IV.

6.4 Results and Discussion

During the growth process of sucrose, impurities (dextran in the current study) in the solution phase incorporate into the crystalline phase. The degree of dextran incorporation can be indicated by the partition coefficient $\left(K_{eff}\right)$ between the two phases. The first experiments in the current study focused on determination of the effect of the molecular weight of the dextran used on the partition coefficients. Sucrose crystallizations were performed at 40.0°C and supersaturations of 0.07, with dextran as an impurity at 2000 ppm/Brix. Three experiments were performed at these conditions; using 60,000-90,000 Da (low fraction dextran), 250,000 Da (high fraction dextran), and a 1:1 mass ratio of low and high fraction dextran: the results are shown in Table 6.1.

Table 6.1 The dextran partition coefficient for various dextran compositions.

Compositions	**%K_{eff}**
100 percent low fraction dextran	7.0
100 percent high fraction dextran	7.5
1:1 mass ratio of low and high fraction dextrans	7.4

Note: the dextran partition during the crystallization at 40°C, 0.07 relative supersaturation, and a dextran concentration of 2000 ppm/Brix.

The results in Table 6.1 demonstrate that the molecular weight ranges of the dextran used do not have a significant effect on the partition coefficient between the syrup and the sugar crystals during the growth process. A possible explanation is that the molecular weight of the dextran does not significantly alter the effect the dextran

has on the growth kinetics (which should be related to the partition of dextran between the liquid and crystal phases) at low supersaturation (Abdel-Rahman *et al.*, 2008). The next result will show the dextran concentration in solution does not significantly affect the growth rate at low supersaturation (less than 0.09), which agrees with Abdel-Rahman's work (Abdel-Rahman *et al.*, 2008). This suggests that the influence of the dextran molecular weight on the rate of dextran incorporation should be weaker than the influence of the dextran concentration. According to this result, the 1:1 ratio of low fraction dextran and high fraction dextran was considered to be representative of all ranges of dextran molecular weight, and this dextran mixture was used in all other experiments in the study.

There are number of impurity incorporation mechanisms for industrial growth of crystals in impure conditions. However, in the case of crystallization of sugar from solution containing small amounts of dextran, a reasonable mechanism might be dominated by either liquid inclusions or by surface adsorption (Meenan *et al.*, 2002). Values of the dextran partition coefficient $\left(K_{eff}\right)$ are tabulated in Table 6.2 for the crystallization from 1,000 ppm/Brix dextran solutions and Table 6.3 for crystallization from 2,000 ppm/Brix dextran solutions, and are plotted against the relative supersaturation with two parameters, crystallization temperature and dextran content, in Figure 6.3. It is seen that at the same temperature, the dextran partition coefficient at lower supersaturation is smaller than that at higher supersaturation. This is a result of the growth under high stress conditions generated by a high supersaturation (Myerson and Ginde, 2002). At such conditions the growth is commonly a result of imperfect crystal surface which allows the incorporation of dextran molecules. The temperature also has a significant effect on the partition

coefficient, with higher temperatures resulting in more dextran partitioning into the crystal phase. Previous research has shown that the impurity concentration in the mother liquor has an effect on the partition coefficient (for example the concentrations (about 8-27% W/W in solution) of avermectins A1a, A2a, and B2a, have an effect on their partition during the crystallization of avermectin B1a.) (Liu *et al.*, 2006). However, the result in this experiment shows that although the amount of dextran incorporation into the growing crystal increases with increasing dextran concentration in the solution phase, the dextran concentration does not have a significant effect on the partition coefficient. This result might be due to the fact that the dextran concentration in the current study is very low compared to the previous research. However, since the partition coefficient is the ratio of the mother liquor dextran content (in relation to the total solids content) divided by the dextran content of the crystals, this still indicates that a doubling of dextran content in the liquid phase will also double the amount of dextran included into the crystal product.

Table 6.2 The dextran partition coefficient in sugar crystallization for mother liquor dextran contents of 1,000 ppm/Brix.

Temperature (°C)	**Relative Supersaturation (-)**	**%K_{eff}†**	**SD**	**Rate of crystal growth (µm/min.)**
30	0.05	3.10	1.01	0.17
30	0.07	3.83	0.98	0.26
30	0.09	4.18	0.99	0.36
40	0.05	4.75	1.02	0.41
40	0.07	7.60	0.74	0.61
40	0.09	8.30	0.73	0.85
50	0.05	5.15	0.99	0.80
50	0.07	8.63	0.88	1.24
50	0.09	9.80	1.51	1.71

† All dextran partition coefficient values are an average of 4 determinations

Table 6.3 The dextran partition coefficient in sugar crystallization for mother liquor dextran contents of 2,000 ppm/Brix.

Temperature (°C)	**Relative supersaturation (-)**	**%K_{eff}†**	**SD**	**Rate of crystal growth (µm/min.)**
30	0.05	3.25	0.47	0.16
30	0.07	3.60*	0.88	0.27
30	0.09	3.70	0.57	0.31
40	0.05	4.80	0.60	0.45
40	0.07	7.40*	0.14	0.58
40	0.09	8.65	0.60	0.79
50	0.05	6.10*	0.49	0.87
50	0.07	8.50*	0.28	1.22
50	0.09	9.60*	0.57	1.67

† All dextran partition coefficient values are an average of 4 determinations, except those labeled * which are an average of 2 determinations by the CSR method.

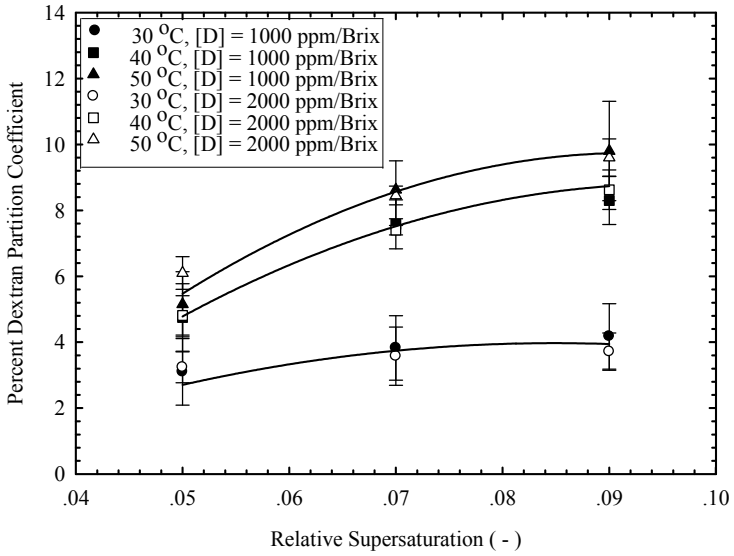

Figure 6.3 Partition coefficients for dextran in sucrose crystallization as a function of temperature, relative supersaturation, and dextran content in the liquid phase.

It is well known that liquid inclusions are a significant source of impurities in crystals obtained from industrial crystallizers (Meenan *et al.*, 2002; Miki *et al.*, 2005; and Saito *et al.*, 2000). Since the partition coefficient results in the present study also showed a strong dependence on supersaturation, and also temperature (another variable strongly correlated with the growth rate), the partition coefficient's correlation with the crystal growth rate was also investigated. This was a simple exercise, since the crystals were grown under constant conditions (temperature, supersaturation, and agitation) and therefore had constant growth rates over the period of the experiment. Growth rates were determined for batches of crystals under each condition used, with the results shown in Figure 6.4. The growth rates determined under the current conditions were compared with those of Shiau (2003), which were determined using a microscopic cell technique and pure sucrose solutions in cell

crystallizer with the syrup flow rate of 6.1 cm/min. Shiau's fit of his growth rate data to equation 6.6 gives,

$$G = 2.68 \times 10^{12} \exp\left(\frac{-66.6}{RT}\right)\sigma^{1.32} \tag{6.8}$$

where the activation energy E_A = 66.6 kJ/mol.

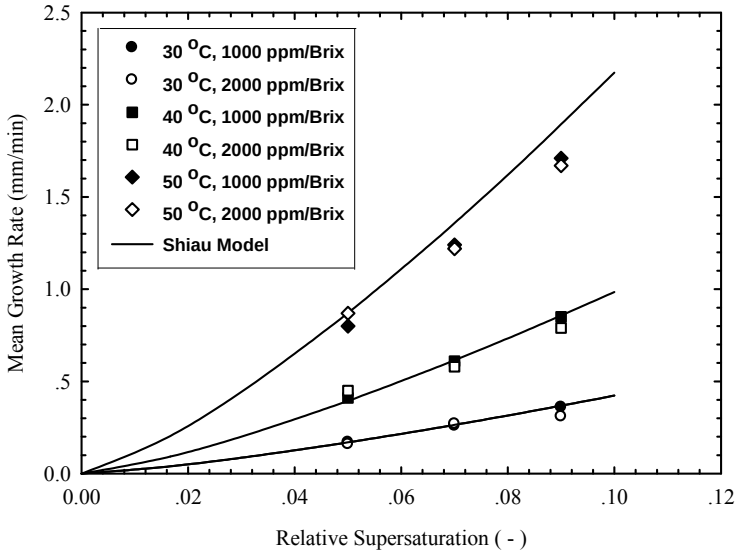

Figure 6.4 Crystal growth rates of sucrose as a function of temperature, relative supersaturation, and dextran content in the liquid phase.

It appears that the dextran concentrations in the current study are not sufficient to lower the growth rate form the model of Shiau (for growth in pure solutions) significantly. It was found that the results agreed very well with shiau model at 30°C and 40°C. Smythe (1967a) also studied the growth rate of sucrose in solutions with dextran as an impurity, and found significant reductions in the growth rate compared to the growth rate of pure solutions. However Smythe used an impurity/water ratio of

7.4 (equivalent to 3.11 dextran/Brix), is much higher than the impurity level in the current experiments. Integration controlled sucrose growth will become diffusion controlled above 40°C, (Mullin, 2001). It can be suggested that there is no significant difference of growth rate controlled by surface integration (which occurs at 30°C and 40°C for this study) of two crystallization systems (the flow cell for Shiau's work, and the batch for the current study) while the difference between the diffusion controlled growth (which occurs at 50°C for this study) supported by agitation and that supported by feed flow rate through the cell are significant. Therefore, at 50°C, the growth rate for the current study were slightly lower than those of the model of Shiau since the growth occurs in an intermediate temperature range where maybe cotrolled either by diffusion or surface integration.

The results of the correlation between the partition coefficient and the growth rate are shown in Figure 6.5. A clear correlation between the partition coefficient and the growth rate (common for the case of crystallization from solution (Mersmann, 2001)) was found, even when results for varying temperature and dextran level are included together. The mean growth rate for 1,000 ppm/Brix of dextran content and 2,000 ppm/Brix of dextran content in solutions for several conditions were plotted to study the effect of dextran concentration on the growth kinetics of sucrose crystallization and to compare with the growth model of Shiau for the growth of sucrose in pure solution. It demonstrates that since the dextran concentration in our case is very small, the concentration does not strongly affect the mean growth rate. In addition, an empirical model for the dextran partition coefficient in sucrose crystallization can be proposed, with data at both 1000 and 2000 ppm/Brix, following the model that:

$$K_{eff}[\%] = (9.8 \pm 1.0) \times \left(1 - \exp^{(-1.7 \pm 0.4)G}\right) \tag{6.9}$$

with G having units of μm/min.

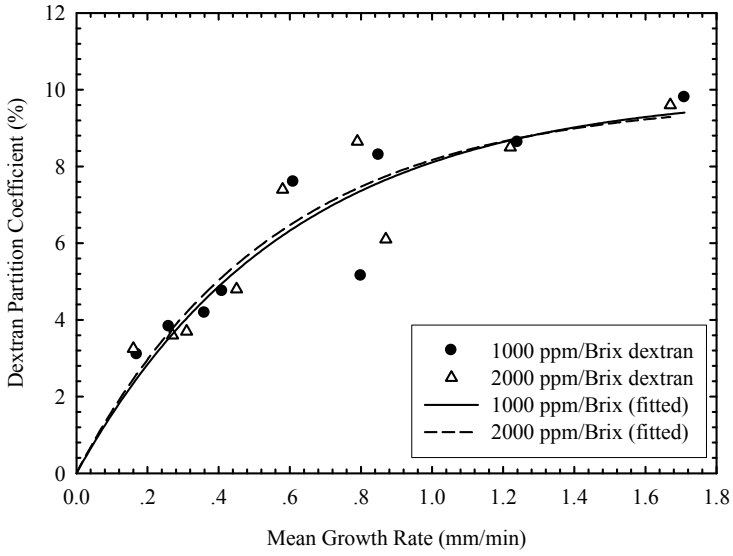

Figure 6.5 Partition coefficients for dextran in sucrose crystallization as a function of the mean crystal growth rate.

The dextran concentration effect on the partition coefficient demonstrates that although the dextran concentration does not have an effect on the partition coefficient, it does have a strong effect on the amount of dextran in the crystal, since the partition coefficient $\left(K_{eff}\right)$ was defined as the ratio of ppm of dextran in crystal product and ppm/Brix of dextran in solution. In addition, there are previous observations at (Rauh *et al.*, 2001; Cuddihy *et al.*, 1999) Midland Research Laboratories involving dextran partition in sugar crystallization process at a commercial sugar factory where the rate of crystal growth seems to be higher than that in a lab-scale crystallization experiment. Their result showed that about 10% dextran partitions from the syrup into commercial

sugar at low dextran concentrations (less than 4,000 ppm/Brix in syrup); this is about the limiting dextran partition determined from our model. They also showed that the partition coefficient did not depend on the dextran content of the syrup for these concentration ranges.

6.5 Conclusions

The study of dextran partition between the syrup and the sugar crystal was performed at relatively low dextran content in solution, with dextran contents of 1,000 ppm/Brix and 2,000 ppm/Brix. The results demonstrate that the 1:1 mass ratio of low fraction and high fraction dextran mixture can be used to represent all ranges of dextran molecular weights in the study.

Although the dextran concentration in solution does have an effect on the amount of dextran incorporation into sugar crystal, it does not strongly affect the dextran partition coefficient. The rate of dextran incorporation from the solution phase to the crystalline phase depends the crystallization temperature as well the supersaturation of the solution. This can be seen by the dextran partition result coefficient increasing significantly with increases in either supersaturation or temperature. Since the growth rate in sucrose crystallization is a function of both supersaturation and temperature, the dextran partition coefficient can be correlated to the growth rate in one curve from which it can be seen that dextran partition coefficient increases strongly with increasing growth rate. An empirical model for the dextran partition coefficient in sucrose crystallization related to the crystal growth rate can be proposed as $K_{eff}[\%] = (9.8 \pm 1.0) \times \left(1 - \exp^{(-1.7 \pm 0.4)G}\right)$. The results could be

applied by sugar manufacturers to reduce the dextran contamination in sugar product by using a low growth rate operation in the crystallization process.

6.6 References

Abdel-Rahman, E. A., Smejkal, Q., Schick, R., El-Syiad, S., and Kurz, T. (2008). Influence of dextran concentration and molecular fractions on the rate of sucrose crystallization in pure sucrose solutions. **Journal of Food Engineering.** 84: 501-508.

Altenburg, W. (1993). Determination of dextran and starch. In J. C. P. Chen and C. C. Chou (eds.). **Cane Sugar Handbook** (12th ed. pp. 904-921). New York: John Wiley and Sons.

Burton, J. A., Prim, R. C., and Slichter, W. P. (1953). The distribution of solute in crystals grown from the melt: Part 1. **Theoretical. J. Chem. Phys.** 21(11): 1987-1991.

Broadfoot, R. and Wright P. G. (1972). Nucleation studies. **Proc. Qld. Soc. Sugar Cane Technol.** 39: 353-362. Quoted in E. T., White. (2000). A review of the crystallization of sugar. In B. S. Gupta and S. Ibrahim (eds.). **Mixing and Crystallization** (pp.329-336). Netherlands: Kluwer Academic Plubishers.

Chou, C. C. and Wnukowski, M. (1981). Dextran problems in sugar refining: A critical laboratory evaluation. In: **Proceedings of the 1980 Technical Session on Cane Sugar Refining Research** (pp. 1-25). LA, USA: Science and Education Administration.

Cuddihy, J. A., Jr., and Donal, D. F. (1999). The process and financial impact of dextran on a sugar refinery. **Sugar Journal.** 3: 27-30.

Dowling, J. F. (1990). Sugar product. In N. L. Pennington and C. W. Baker (eds.). **Sugar: A User's Guide to Sucrose** (pp. 36-45). New York: Van Nostrand Reinhold.

Kelly, F. H. C. and Keng, M. F. (1975). **The Sucrose Crystal and Its Solution** (pp. 6, and pp. 94). Singapore University Press.

Liu, J., Chang, Z., Sun, X., Shen, S., Lei, C., and Liu, H. (2006). Impurity effects on the crystallization of avermectin B1a. **Journal of Crystal Growth.** 291: 448-454.

Martins, P. and Rocha, F. (2006). The role of diffusional resistance on crystal growth: interpretation of dissolution and growth rate data. **Chemical Engineering Science.** 61: 5686-5695.

Martins, P. M., Rocha, F. A., and Rein, P. (2005). Modeling sucrose evaporative crystallization: Part 2. Investigation into crystal growth kinetics and solubility. **Ind. Eng. Chem. Res.** 44(23): 8865-8872.

Martins, P. M., Rocha, F. A., and Rein, P. (2006). The influence of impurities on the crystal growth kinetics according to a competitive adsorption model. **Cryst. Growth Des.** 6 (12): 2814-2821.

Meenan, P. A., Anderson, S. R., and Klug, D. L. (2002). The influence of impurities and solvents on crystallization. In A. S. Myerson (ed.). **Handbook of Industrial Crystallization** (2nd ed., pp. 67-100). USA: Butterworth-Heinemann.

Mersmann, A. (2001). Quality of crystalline products. In A. Mersmann (ed.). **Crystallization Technology Handbook** (2nd ed., pp. 285-322). New York: Marcel Dekker.

Miki, H., Terashima, T., Asakuma, Y., Maeda, K., and Fukui, K. (2005). Inclusion of mother liquor inside KDP crystals in a continuous MSMPR crystallizer. **Separation and Purification Technology.** 43: 71-76.

Mullin, J. W. (2001). Crystal growth. **Crystallization** (4th ed. pp. 216-288). Great Britain: Butterworth-Heinemann.

Myerson, A. S. and Ginde, R. (2002). Crystals, crystal growth, and nucleation. In A. S. Myerson (ed.). **Handbook of Industrial Crystallization** (2nd ed., pp. 33-66). USA: Butterworth-Heinemann.

Priester, R. (1981). Dextran in raw sugar. In: **Proceedings of the 1980 Technical Session on Cane Sugar Refining Research** (pp. 123-124). LA, USA: Science and Education Administration.

Rauh, J. S., Cuddihy, J. A., Jr., and Falgout, R. N. (2001). Analyzing dextran in the sugar industry: A review of dextran in the factory and a new analytical technique. In **Proceedings of XXVII Conference West Indies Sugar Technology** (p. 1). Port of Spain: Sugar Association of the Caribbean.

Reiser, P., Birch, G. G., and Mathlouthi, M. (1995). Physical properties. In M. Mathlouthi and P. Reiser (eds.). **Sucrose Properties and Applications** (pp. 186-222). Great Britain: Blackie Academic and Professional.

Roberts, E. J. (1981). Dextran analysis: Methods and problems. In: **Proceedings of the 1980 Technical Session on Cane Sugar Refining Research** (pp. 128-133). LA, USA: Science and Education Administration.

Saito, N., Yokota, M., and Kubota, T. F. (2000). Liquid inclusions in crystals produced in suspension crystallization. **Chemical Engineering Journal.** 79: 53-59.

Shiau, L. D. (2003). The distribution of dislocation activities among crystals in sucrose crystallization. **Chemical Engineering Science** 58: 5299-5304.

Smythe, B. M. (1967a). Sucrose Crystal Growth. II. Rate of Crystal Growth in the Presence of Impurities. **Aust. J. Chem.** 20: 1097-1114.

Smythe, B. M. (1967b). Sucrose Crystal Growth. I. Rate of Crystal Growth in Pure Solutions. **Aust. J. Chem.** 20: 1087-1095.

Vane, G. W. (1991). Problems arising from the presence of dextran in sugar products. In: **Proceedings of the 1980 Technical Session on Cane Sugar Refining Research** (pp. 125-127). LA, USA: Science and Education Administration.

White, E. T., (2000). A review of the crystallization of sugar. In B. S. Gupta and S. Ibrahim (eds.). **Mixing and Crystallization** (pp.329-336). Netherlands: Kluwer Academic Plubishers.

CHAPTER VII

DEXTRAN INCORPORATION INTO THE SUGAR CRYSTAL

7.1 Abstract

A study on incorporation of dextran into the crystalline phase in sucrose crystallization begins with the determination of the dextran distribution in the crystal phase using a mingling technique. Raw sugar crystal product from the mill was stirred in various compositions and types of solvent mixtures to remove some fraction of the mass from the crystal surface depending on the solubility of sucrose in these mixtures. It has been seen that there is dense dextran contamination present in the region that is closest to the crystal surface while in deeper regions inside the crystal there is a lighter distribution. This is not surprising since the impurity content increases significantly through the batch due to impurity rejection during the crystallization, so the liquid is more impure as the crystals get bigger. From this result, dextran incorporation due to liquid inclusion and surface adsorption are expected to be possible mechanisms for the incorporation. Contamination due to purely to a mechanism of a molasses coating on the surface of the crystal is extremely unlikely. The moisture content of the crystal products grown under various conditions were determined by determination of the mass of liquid evaporation due to heating at 105°C. The results showed that the amount of liquid inclusion inside the crystal product does not depend on the growth conditions. Although the results showed that

there were liquid inclusions in the sugar crystals, the full amount of dextran contamination in the crystal can not be described only by the liquid inclusion mechanism. This can be demonstrated by the volume of inclusions being insufficient to contain all the dextran, and also the liquid inclusion volumes do not depend on growth conditions, whereas the degree of dextran contamination does depend on the growth conditions. The effect of crystal growth rate on the roughness of the crystal surface was investigated using Scanning Electron Microscopy (SEM). The surface of crystal products grown under conditions resulting in the highest and lowest growth rates of this work was observed. The comparison between the two cases showed that the crystal surface of samples from the highest growth rate condition is rougher. It is possible that surface adsorption influences the incorporation of dextran into the crystal since a rougher surface has both additional surface area per area of crystal face, and also additional sites for bonding onto. It is reasonable to describe the increasing amount of dextran contamination to be due to an increasing rate of crystal growth. However there is still evidence of some liquid inclusions from the moisture analysis of the crystal product, and therefore it is apparent that the mechanism of dextran incorporation is partly controlled both by liquid inclusion and surface adsorption.

7.2 Introduction

7.2.1 Growth in Impure Solutions

In many processes involving crystal growth from impure solutions, traces of impurities have significant effects on both nucleation and crystal growth kinetics. Most effects due to impurities are well known, particularly the reduction of the overall growth rate, however some impurities retard the rate of selective faces of

the crystal causing crystal habit variation (Smythe, 1967; Belhamri and Mathlouthi, 2004; Faria *et al.*, 2003). There are previous observations that the active sites on the crystal surface can be blocked by impurities causing a slowing of the growth of that face. In some cases, although some types of impurities cannot interact with the crystal faces directly, they can affect the crystal growth by modifying solution properties, in particular the viscosity (Mullin, 2001a). Rejection of impurities by the crystal surface has an influence on the diffusion of solute from bulk solution to the crystal surface due to obstruction by the rejected impurities (Kaur and Kaler, 2008).

7.2.2 Impurity Incorporation

Incorporation of impurity during the crystal growth process is commonly due to the mechanisms of surface adsorption, liquid inclusion formation, and substitutional incorporation into the crystal lattice or at defect sites. These mechanisms can be significant for impurity incorporation into the crystalline phase depending on many factors. For example, if there are similarities of size and shape between solute and impurities, the crystal lattice incorporation mechanism could be significant. If there is interaction between impurities and the parent crystal due to their similarities of chemical properties or structure, the surface adsorption mechanism could dominate. The effective partition coefficient (K_{eff}) is used for relating dextran contamination in the crystal due to any mechanism. It is defined as

$$K_{eff} = \frac{C_{sp}}{C_m} \tag{7.1}$$

where C_{sp} is dextran concentration in the sugar product (ppm) and C_m is dextran concentration in the mother solution (ppm/Brix). Specific mechanisms are discussed in a little more detail in the sections below.

7.2.3 Adsorption

In the case that there is sufficient interaction between impurities and the parent crystal, the impurities can be adsorbed by the growing crystal surface. In the process of surface adsorption there is competition between impurities and the solute molecules, which usually has a strong effect on the growth kinetics since the movement of solutes is reduced by the presence of the adsorbed impurities (Meenan *et al.*, 2002: Martins *et al.*, 2006). Both the dextran impurity and sucrose are organic material with similar functional group structures, so surface adsorption is possibly a significant mechanism for the incorporation of dextran into the sugar crystal.

7.2.4 Liquid Inclusion

Liquid present inside the crystal is commonly known as an inclusion, and is often a major source of impurity incorporation during the crystal growth process (Mullin, 2001a; Meenan *et al.*, 2002). Crystals grown from aqueous solution can contain as much as 1-2% by mass of included liquid that can significantly affect the crystal product purity (Meenan *et al.*, 2002). When a crystal has a sufficient size, sometimes the face centers have a lower growth rate than the corners or the edges of the crystal, and in consequence a cavity is formed. If the surface growth layer from the corners or the edges grows inwards to entrap a cavity that contains mother liquor, an inclusion is formed inside the crystal. This mechanism creates a crystal product that is contaminated with the impurities that are distributed in the mother liquor. In addition, since there is an impurity rejection mechanism in the surface adsorption

process, the liquid inclusion may be richer in impurities than the bulk mother liquor (Meenan *et al.*, 2002) indicating that the impurity level due to the inclusions maybe higher than expected.

7.2.5 Impurity Incorporation into the Lattice or at Defect Sites

In the case that the solute and the impurities are similar in size and shape, lattice sites may be occupied by the impurity molecules. This mechanism is known as substitutional incorporation of an impurity. However, if there are significant differences between the solute and the impurities, the substitution of impurities always occurs with distortion of the crystal lattice. Since substitution with distortion requires a great deal of energy, it is rare to achieve if the impurities and the parent crystal have no extra interaction. In addition, an imperfect growth of crystal is often induced by any stresses during the growth process. The imperfect growth generates defect sites where numerous impurities may be allowed to incorporate (Meenan et al., 2002; Mullin, 2001).

7.2.6 Objectives of the Study

It is known that in crystal growth from solutions that contain some amount of impurities sometimes leads to product crystals that are contaminated by the impurities. However, the mechanisms of impurity contamination for various systems are normally different. For the study on dextran incorporation into the sugar crystal product, it should be clearly known which mechanisms of dextran incorporation into the growing sugar crystal are most significant. For this purpose, many techniques were used to check for possible mechanisms of dextran incorporation into the sugar crystal.

7.3 Materials and Methods

7.3.1 Materials and Equipment

In the study on impurity distribution in the raw sugar crystal, the crystal is the product from Invicta Sugar Mill where is located in Giru, Queensland, Australia; while in the study of impurity incorporation mechanism, the sugar crystal will be grown from the sucrose solution prepared for the experiment. In the preparation of sucrose solution, a high purity (>99.9%) commercial refined sugar was used as a source of sucrose, and high fraction dextran (approximately 250,000 Da molecular weight) and low fraction dextran (approximately 60,000-90,000 Da molecular weight), both from ACROS Organics were used as an impurity in the ratio of 1:1 dextran mixture. Chemicals required for crystal product separation and the mingling experiment, such as methanol, ethanol, and isopropyl alcohol were absolute ACS grade.

A 2 liter glass crystallizer with stirring by a 45° pitched-blade impeller driven by an overhead stirrer at 1000 rpm was used for the sucrose crystallization process, and is shown in Figure 6.1. Temperature control was provided by a thermostat through a cooling coil. The total dissolved solid (% Brix) in the solution was measured using the PAL-α model digital pocket refractometer (Atago Co., Japan).

7.3.2 Crystallization and Product Separation

Several variables were adjusted to vary the growth conditions in the crystallization experiment. The ranges of the main independent variables are; temperature (30°C to 50°C); relative supersaturation (0.05 to 0.09); and dextran concentration in the solution (1,000 ppm/Brix and 2,000 ppm/Brix). The crystallizer was operated under effectively a constant supersaturation level since the amount of

seed crystal (about 0.5 g) was very small compared with the supersaturation and total volume of the solution (1.8 liter). The seed crystals were prepared by sieving commercial refined sugar through 150-250 μm mesh sizes. The seed crystal size distribution is shown in Figure 6.2 (Chapter VI).

When the crystallization was completed, the majority of the mother liquor was decanted after settling of the product crystals. A large amount of aqueous saturated solution of sucrose was added into the massecuite so that the viscosity of the massecuite is reduced and the dextran content in the liquid phase is diluted approximately 25 times from the initial level. A 47 mm diameter vacuum filter holder (Thermo Scientific Nalgene) with a 51 μm stainless steel mesh was used to separate the crystal product from the mother liquor. This was sufficient to separate crystals from the mother liquor quickly, but did not result in any loss of crystal product since there was no nucleation or breakage occurring in the crystallizer, and since the seed crystals were significantly larger than this size. The crystal product was cleaned by adding saturated methanol, and after all of the methanol passed through the filter, saturated ethanol was added, followed by isopropyl alcohol, in order to clean the crystals of all remaining mother liquor attached to the surface of the crystal. The final step was to dry the crystals in open air at room temperature to remove any remaining alcohol.

7.3.3 Crystal Surface Analysis

In this experiment, the first crystallization process was operated at a temperature of 30°C, 0.05 relative supersaturation, and a dextran content of 1,000 ppm/Brix, and the second was operated at a temperature of 50°C, 0.07 relative supersaturation, and a dextran content 2,000 ppm/Brix. The crystal products of the

two cases were separated to provide the test samples using the sample separation technique described in Section 7.3.2. The dried crystal samples were analyzed using Scanning Electron Microscopy (SEM) with a beam voltage of 20 kV.

7.3.4 Moisture Content

Moisture contents of sugar products grown under various conditions were determined in this study. The moisture contents as a function of three parameters; growth temperature, supersaturation, and dextran content of the solution, were determined. The sugar products were separated from the mother liquor by the method described in Section 7.3.2. A moisture balance (model XM 60, Precisa Instruments Co., Switzerland) was used for the moisture content determination. The moisture content is analyzed by ramping the temperature of the moisture balance to 105°C within 3 minutes, and then maintaining this temperature until the differential weight loss reaches zero. The moisture released in the first five minutes does not account for the moisture content since it releases rapidly in which is considered to be crystal surface moisture.

7.3.5 Impurity Distribution in the Raw Sugar Crystal

Mingling of raw sugar crystals (raw sugar product from the mill) was performed using various solvents such as isopropyl alcohol (IPA), a 95% ethanol-water mixture, methanol, and various methanol-water mixtures. 50 grams of raw sugar crystals (with a sieve size of 1000-1180 μm) were stirred in 70 grams of the solvent mixture at room temperature to dissolve some mass of the crystal surface. The amount of crystal removed by the process varies in relation to the sucrose solubility in the solvent mixture. The remaining crystal from the process was dried at room temperature and then the percent crystal removed was determined by weighing on

four decimal place balance. The dried crystal sample was analyzed by the Roberts test and the CSR technique (as reviewed in previous chapters) to determine dextran content and total polysaccharides content, respectively.

7.4 Results and Discussion

The impurity distribution in the crystal is important evidence which can be used to make deductions about the mechanism of the impurity incorporation in the crystal. The mingling experiments give clear evidence on whether dextran incorporates into the sugar crystal during the growth process, or whether the contamination is due to the mother liquor coating of the sugar crystal product. If the contamination is highly concentrated in the surface layer of the crystal only, it is evident that adsorption of mother liquor is the principal mechanism of the incorporation, and it is not necessary to study other dextran incorporation mechanisms such as adsorption during growth and inclusion. Table 7.1 shows the removal of all polysaccharides including dextran and the percent removal of dextran with respect to the removal of crystal mass.

Table 7.1 Mingling of raw sugar crystal from the mill with various solvents.

Composition of the solvent (mass %) on a sugar free basis	**% Crystal mass removed**	**% Total polysaccharides removed***	**% Dextran removed****
Isopropyl alcohol	0	0	0
95% ethanol-water mixture	0.43	1.39	2.10
100% methanol	1.55	6.09	11.8
95% methanol-water mixture	2.76	27.0	23.6
90% methanol-water mixture	4.40	29.5	26.8
85% methanol-water mixture	7.38	35.2	33.9
80% methanol-water mixture	11.12	47.3	41.7
75% methanol-water mixture	15.75	50.8	48.8
70% methanol-water mixture	23.53	56.4	54.3
65% methanol-water mixture	31.54	62.8	59.0

Note that * The values are an average of 3 determinations from the CSR method

** The values are an average of 3 determinations from the Roberts test

Previous research has shown that dextran not only distributes near the crystal surface region, since although some crystal mass is removed by the washing process there is still a large amount of dextran remaining (approximately 80%) in the washed crystal (Chou and Wnukowski, 1981). From the analysis of the sugar crystals after the mingling process, it was known that dextran and other polysaccharides seem to distribute widely throughout the sugar crystal. According to this result the most likely dextran incorporation mechanisms are liquid inclusion and surface adsorption through the growth process; further experiments in this section are performed to distinguish between these two mechanisms. The distributions of dextran and total polysaccharides in raw sugar crystals can be determined on the plot between dextran and total polysaccharide removals in relation to the removed crystal mass, which is shown in Figure 7.1. It can be seen that the distribution of dextran in the sugar crystal is quite similar to that of the other polysaccharides. Particularly, they have a dense distribution in locations close to the crystal surface, while the distribution in regions deeper within the crystal appears to be smaller. This result shows that a larger amount of dextran and other polysaccharides incorporate into the shallow regions rather than the deep regions. Since the crystal sample is the raw sugar product from the mill, this can be explained by the fact that at the beginning of the vacuum pan batch, the amount of sugar is high, so impurities are a smaller fraction of the total solids. At the end of the batch the amount of sugar left is low, but most of the impurities are still in the liquid phase, so that the relative amount of impurity is much higher than at the beginning of the batch. A more specific mechanism will be explained in more detail later.

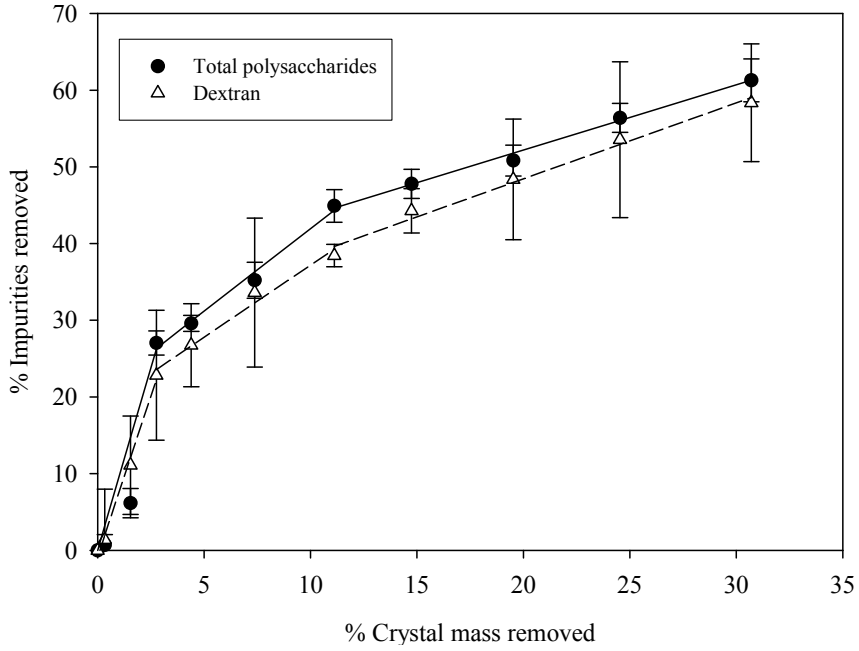

Figure 7.1 The distribution of dextran and total polysaccharide contamination in raw sugar crystal.

Table 7.2 and Table 7.3 show the calculated values of the fraction of the volume of the crystal which is liquid inclusion if all of the dextran contamination in the crystal product was due to the presence of liquid inclusions. The partition coefficient (K_{eff}) is the ratio of dextran concentration in the sugar product C_{sp} (ppm) and dextran concentration in the mother solution C_m (ppm/Brix). If the liquid inclusion is the only source of dextran contamination, the dextran content in the crystalline phase is 0 ppm, and the dextran content in the sugar product on the basis of one unit volume can be written as

$$C_{sp} = \left[\frac{L}{(L+S)} \times C_m \times Brix\right] + \left[\frac{S}{(L+S)} \times 0\,ppm\right] \tag{7.2}$$

$$\frac{L}{(L+S)} = \frac{C_{sp}}{(C_m \times Brix)} = \frac{K_{eff}}{Brix} \tag{7.3}$$

So the volume fraction of the liquid inclusion in the crystal ($L/(L+S)$) was determined by dividing the partition coefficient by the Brix of the initial solution. A reasonable mechanism of dextran incorporation into the crystalline phase can be predicted based on these data.

Table 7.2 The expected volume percent of the liquid inclusion required if all dextran content in the sugar product is due to inclusion. The product is crystallized from mother liquor that initially contains 1000 ppm/Brix dextran.

Temp. (°C)	**Supersat. (-)**	**Brix of initial solution**	**%K_{eff} †**	**The expected volume percent of the liquid inclusion**	**Rate of crystal growth (µm/min.)**
30	0.05	0.694	3.10	4.47	0.17
30	0.07	0.698	3.83	5.49	0.26
30	0.09	0.702	4.18	5.95	0.36
40	0.05	0.712	4.75	6.67	0.41
40	0.07	0.716	7.60	10.6	0.61
40	0.09	0.720	8.30	11.5	0.85
50	0.05	0.731	5.15	7.04	0.80
50	0.07	0.735	8.63	11.7	1.24
50	0.09	0.739	9.80	13.3	1.71

†All dextran partition coefficient values are the average of 4 determinations

Table 7.3 The expected volume percent of the liquid inclusion required if all dextran content in the sugar product is due to inclusion. The product is crystallized from mother liquor that initially contains 2000 ppm/Brix dextran.

Temp. (°C)	Supersat. (-)	Brix of initial solution	$\%K_{eff}$ †	The expected volume percent of the liquid inclusion	Rate of crystal growth (µm/min.)
30	0.05	0.694	3.25	4.68	0.16
30	0.07	0.698	3.60*	5.16	0.27
30	0.09	0.702	3.70	5.27	0.31
40	0.05	0.712	4.80	6.74	0.45
40	0.07	0.716	7.40*	10.3	0.58
40	0.09	0.720	8.65	12.0	0.79
50	0.05	0.731	6.10*	8.34	0.87
50	0.07	0.735	8.50*	11.6	1.22
50	0.09	0.739	9.60*	13.0	1.67

†All dextran partition coefficient values are the average of 4 determinations, except those labeled * which are an average of 2 determinations by the CSR method.

The result of the study of liquid inclusions in the sugar crystal grown from the crystallizations in this research is illustrated in Figure 7.3. Inclusions were observed using optical microscopy with immersion of the crystal in o-dichlrobenzene (a liquid having a refractive index of 1.54, close to the mean refractive index of the crystal (1.56)) after the crystal was separated from the solution by the method discussed in Section 7.3.2. The appearance of the liquid in the crystal is very similar to that in the literature (Vaccari and Mantovani, 1995). There are other results that show the

mechanism of liquid inclusions in sucrose crystallization from solution may be hour-glass patterns or Maltese cross patterns (Mullin, 2001a). In the work of Mantovani (Vaccari and Mantovani, 1995), it was proposed that liquid inclusions prefer to form in the most rapidly growing faces of the sucrose crystal. Since there are significant differences in size and shape between the dextran molecule and the sucrose molecule, the lattice substitution mechanism is very unlikely in this system. However, both sucrose and dextran are organic materials that consist entirely (in the case of dextran) or partly (in the case of sucrose) of the glucose moiety, so the interaction between dextran and the sucrose crystalline phase may be sufficient to induce surface adsorption of dextran.

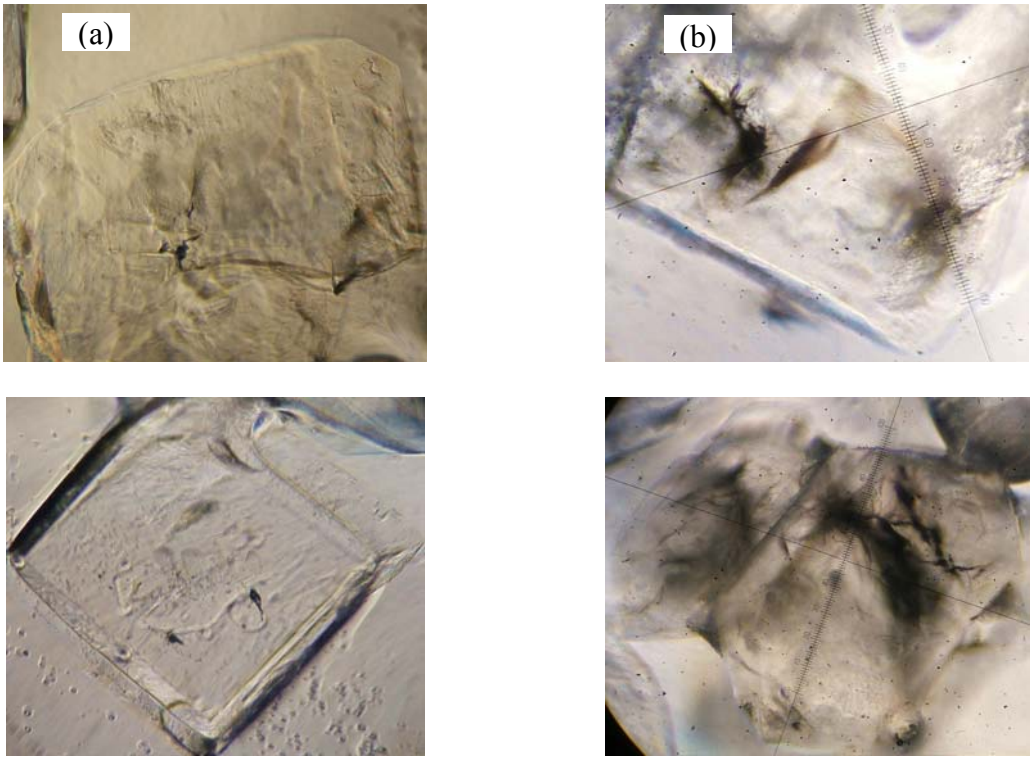

Figure 7.2 Liquid inclusions in sugar crystals grown in the current study (a) at 30°C, supersaturation = 0.05, and [D] = 1000 ppm/Brix; (b) at 50°C, supersaturation = 0.09, and [D] = 2000 ppm/Brix.

For many industrial crystallization processes, inclusions have been known as the main source of impurity contamination in crystal product that was grown from aqueous solution since such crystals can contain a very large amount of impurities in liquid inclusions compared to other mechanisms (Mullin, 2001a). In this work, dextran is the only type of impurity in the process. The expected volumes of liquid inclusion shown in both tables are sufficient to suggest that a significant fraction of the dextran content in the sugar product is incorporated by means of inclusion.

A moisture content analysis for crystal product samples grown under various conditions was undertaken to determine the amount of liquid included in the crystal product. The results of the moisture content determination for various samples are given in Figure 7.4. The results show that the crystal products do have liquid inclusions and that these should be a source of dextran contamination. Since there was no correlation between the amount of dextran contained in the crystal samples (based on the partition coefficient) and the amount of moisture in the crystal, and since the moisture contents, that relate to the inclusion volumes, do not depend on growth conditions, it can be suggested that liquid inclusion does not account for all of the dextran in the crystal, nor do liquid inclusions account for the variation between the dextran content of crystals grown under different conditions. The remaining dextran content variation may be due to other incorporation mechanisms. However, the result is evidence that the dextran incorporation includes the mechanism of liquid inclusion. Since most liquid inclusions prefer to form in a large crystal rather than in a small crystal (Saito *et al.*, 2000) they usually form during the final period of crystallization. This may also be a reason for the tendency of dextran to distribute mainly in the region of the crystal close to the surface.

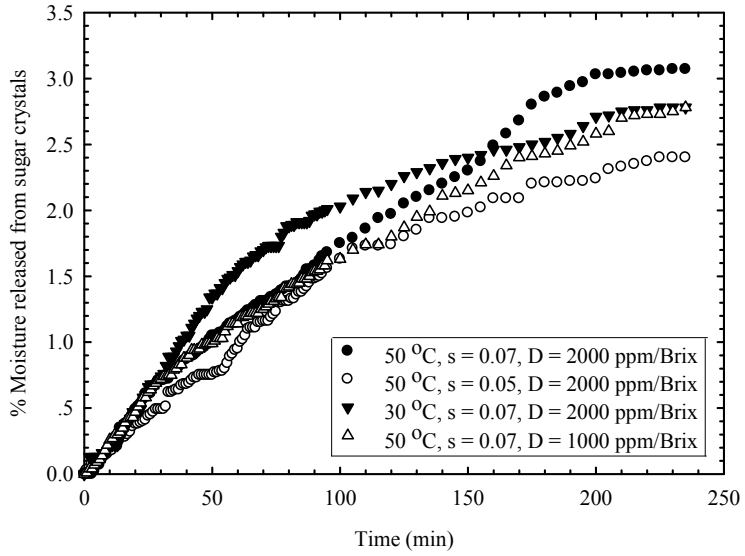

Figure 7.3 The moisture content of sugar crystal products grown under various conditions.

The effect of the growth condition on the dextran partition due to surface adsorption was studied using the SEM technique. The SEM micrographs of sugar crystals grown under the lowest and highest growth rate conditions for this experiment are shown in Figure 7.5 (a) and (b) respectively. It can be conjectured that crystals growing under high growth rate conditions had progressively rougher surface than slow growth crystals. In addition, previous research has shown that the surface of sucrose crystals (Pantaraks and Flood, 2005) (and also a variety of other crystals (Pantaraks *et al.*, 2007)) becomes rough as the growth rate increases past a particular condition. It is possible that growth under these conditions is less selective to the desired solute since the lattice growth is less perfect, which may allow impurities to be adsorbed more easily, and also allow the adsorbed impurity molecules to be grown over more easily. Thus it was decided to characterize the surface of the crystals grown under low and high growth rates to determine if the quality of the surface of

the crystal is likely to have an effect on the incorporation of dextran into the crystal. Since dextran adsorption on the crystal surface is different for various conditions and since the adsorption mechanism can not be a sufficient source of dextran contained in the crystal product, there is a combination of two mechanisms that should be used to describe the dextran incorporation into the crystal. One is dextran incorporation due to the liquid inclusion. Note that the amount of inclusion is effectively unchanged by the different growth conditions evident in the current study: crystals grown under very low growth conditions and very high growth conditions all had moisture content approximately 2.4-3.1% by mass or 7-8% by volume of liquid inclusion (specific gravity values are 1.588 for the sucrose crystal and 1.344-1.375 for the sucrose solutions used in the study (0.69-0.74 Brix)) (Reiser *et al.*, 1995: United States Department of Agriculture, 1981), indicating a relatively constant fraction of liquid inclusion. The second mechanism is dextran incorporation by means of surface adsorption. This mechanism is significantly influenced by the rate of crystal growth that correlates with the condition factors such as temperature, supersaturation, and dextran concentration of the solution. It has been found from the SEM results that crystal growth at a rapid rate gives more surface roughness, so dextran could be adsorbed more into the crystal surface under these conditions.

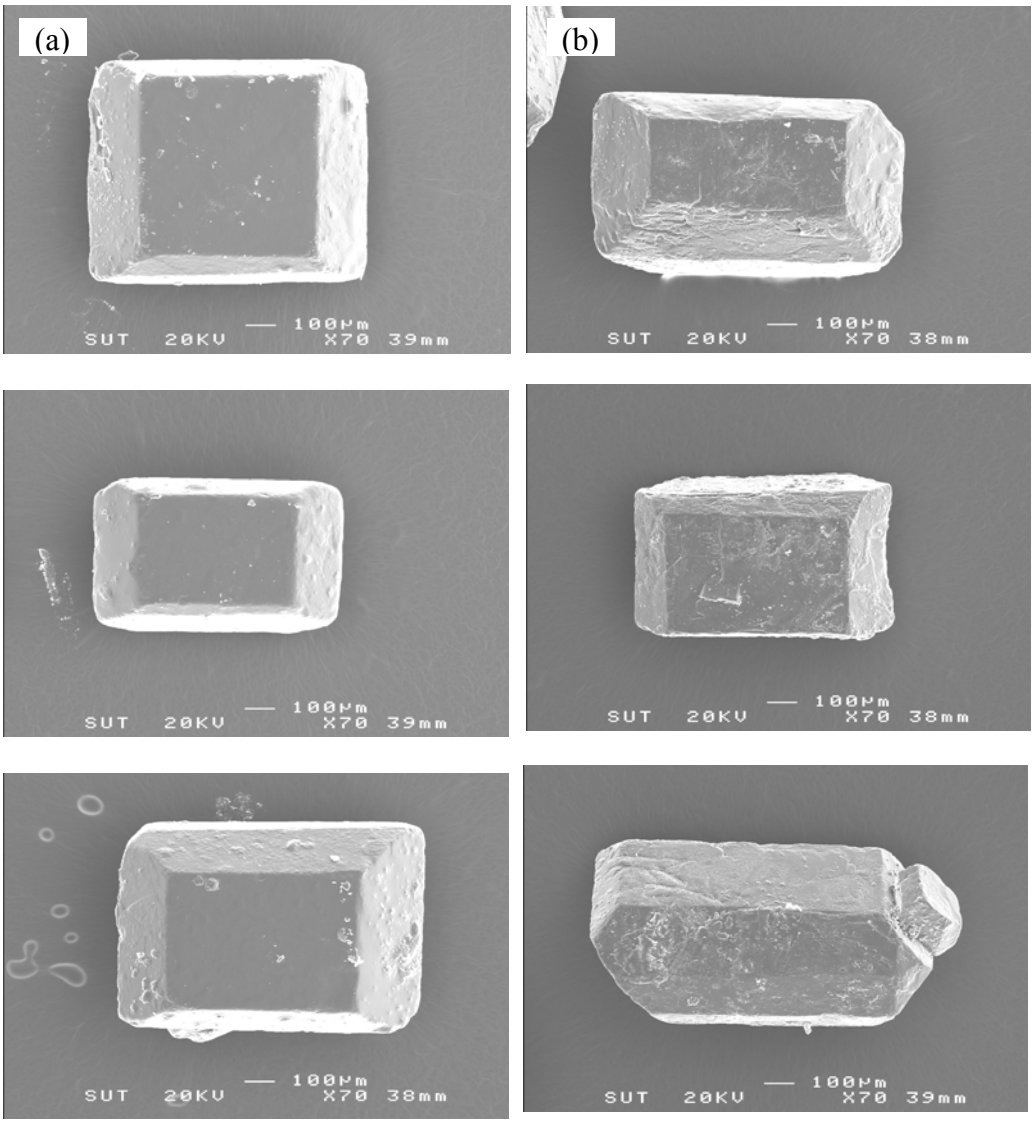

Figure 7.4 Surface roughness of sucrose crystals grown at selected conditions.

(a) 30°C, supersaturation = 0.05, and D = 1000 ppm/Brix;

(b) 50°C, supersaturation = 0.09, and D = 2000 ppm/Brix.

Previous researchers (Ferreira *et al.*, 2008) found that the surface roughness of sucrose crystal increases strongly with residence time and supersaturation. Therefore, a large crystal is likely to have a rougher surface than a smaller one, thus large crystals can adsorb more dextran. Moreover, the relative amount of dextran in solution also increases strongly with the crystallization time as the amount of sucrose is depleted through crystal growth so the crystals that have a longer residence time adsorb larger amounts of dextran due to growth occurring in more impure solution.

7.5 Conclusions

There is a similar distribution profile of dextran and total polysaccharides in the crystal phase of sucrose. The distribution profiles show that either dextran or total polysaccharides initially incorporate into the crystal phase at a slow rate when the crystal size is small, then the rate of incorporation increases through the process of crystal growth. The increase in incorporation can be described by the effect of a combination of liquid inclusion and surface adsorption mechanisms. In the case of liquid inclusion, a crystal product has richer dextran content in the region close to product crystal surface where the most significant amount of liquid inclusion exists. In the case of surface adsorption, dextran can be adsorbed by the crystal surface through the growth process. However the rate of dextran adsorption increases with the residence time in the crystallizer since crystals grown over a long period have rougher surface than crystals in the initial period of crystal growth.

Dextran incorporation during crystallization of sucrose for all conditions observed in this work was controlled by the combination of two mechanisms, liquid inclusion and surface adsorption. The amount of liquid inclusions for each the crystal

products grown in these conditions fall between 2.4-3.1% of crystal mass (7-8% by volume of liquid inclusion). Although the rate of crystal growth under these varying conditions was different, the amount of liquid inclusion does not change with the variation of crystal growth rate. In contrast, dextran incorporation by the surface adsorption is related to the crystal growth rate. The amount of dextran adsorbed on a higher growth rate crystal product is larger than that on crystals grown at a lower rate. Therefore, it can be concluded that the amount of liquid inclusion is effectively unchanged by the different growth conditions, while the amount of dextran incorporated by surface adsorption varies depending on the growth condition, and that this is the reason for the variable amount of contamination in the sugar crystal.

7.6 References

Belhamri, R. and Mathlouthi, M. (2004). Effect of impurities on sucrose crystal shape and growth, **Crystal Growth Research.** 7: 63-70.

Chou, C. C. and Wnukowski, M. (1981). Dextran problems in sugar refining: A critical laboratory evaluation. In: **Proceedings of the 1980 Technical Session on Cane Sugar Refining Research** (pp. 1-25). LA, USA: Science and Education Administration.

Faria, N., Pons, M. N., De Azevedo, S. F., Rocha, F. A., and Vivier, H. (2003). Quantification of the morphology of sucrose crystals by image analysis. **Power Technology.** 133: 54-67.

Ferreira, A., Faria, N., and Rocha, F. (2008). Roughness effect on the overall growth rate of sucrose crystals. **Journal of Crystal Growth.** 310: 442-451.

Kaur, S. and Kaler, R. S. S. (2008). Dextran and its effect on the flow behaviour of molasses and crystallization rate. **Journal of Food Engineering.** 86: 55-60.

Martins, P. M., Rocha, F. A., and Rein, P. (2006). The influence of impurities on the crystal growth kinetics according to a competitive adsorption model. **Cryst. Growth Des.** 6 (12): 2814-2821.

Meenan, P. A., Anderson, S. R., and Klug, D. L. (2002). The influence of impurities and solvents on crystallization. In A. S. Myerson (ed.). **Handbook of Industrial Crystallization** (2^{nd} ed., pp. 67-100). USA: Butterworth-Heinemann.

Mullin, J. W. (2001a). Crystal growth. **Crystallization** (4^{th} ed. pp. 216-288). Great Britain: Butterworth-Heinemann.

Mullin, J. W. (2001b). The crystalline state. **Crystallization** (4^{th} ed. pp. 1-31). Great Britain: Butterworth-Heinemann.

Pantaraks, P. and Flood, A. E. (2005). Effect of Growth Rate History on Current Crystal Growth: a Second Look at Surface Effects on Crystal Growth Rates. **Cryst. Growth Des.** 5(1): 365-371.

Pantaraks, P., Matsuoka, M., and Flood, A. E. (2007). Effect of Growth Rate History on Current Crystal Growth. 2. Crystal Growth of Sucrose, $KAl(SO_4)_2 \cdot 12H_2O$, KH_2PO_4, and K_2SO_4. **Cryst. Growth Des.** 7(12): 2635-2642.

Reiser, P., Birch, G. G., and Mathlouthi, M. (1995). Physical properties. In M. Mathlouthi and P. Reiser (eds.). **Sucrose Properties and Applications** (pp. 186-222). Great Britain: Blackie Academic and Professional.

Saito, N., Yokota, M., and Kubota, T. F. (2000). Liquid inclusions in crystals produced in suspension crystallization. **Chemical Engineering Journal** 79: 53-59.

Smythe, B. M. (1967). Sucrose Crystal Growth. II. Rate of Crystal Growth in the Presence of Impurities. **Aust. J. Chem.** 20: 1097-1114.

United States Department of Agriculture. (1981). Sucrose conversion table [On-line]. Available: www.greenwoodassociates.com/ref/Detailed%20Brix%20Chart.pdf.

Vaccari, G. and Mantovani, G. (1995). Sucrose crystallization. In M. Mathlouthi and P. Reiser (eds.). **Sucrose Properties and Applications** (pp. 33-74). Great Britain: Blackie Academic and Professional.

CHAPTER VIII

CONCLUSIONS AND RECOMMENDATIONS

8.1 Conclusions

Dextran is one of the most significant impurities present in sugar production. It is produced in cane stalk due to deterioration caused by the bacteria of *Leuconostoc* species, mostly prior to the stage of milling. Its problems have been recognized as an increase in viscosity of either cane juices or syrups causing a reduction in the rate of sugar crystallization, sucrose loss due to dextran formation, and false grain (crystal elongation leading to needle-shaped crystals). Furthermore, the contamination of dextran in raw sugar has been a concern of both domestic and overseas customers in purchasing raw sugar as a raw material in the sugar refinery.

This research aims to reduce the dextran contamination in raw sugar production by removing dextran from cane juice by ultrafiltration, and by adjusting the operation in the crystallization stage. The study on the ulrafiltration process can also improve the understanding in the separation of linear macromolecules such as dextran, and in fouling mechanism characterization. The study on the dextran partition coefficient between the solution phase and the crystal phase during crystallization results in important information for designing a suitable condition to reduce dextran content in sugar crystal product, and improves knowledge of dextran incorporation and impurity contamination in crystal product.

In order to achieve the research goal it is necessary to have an accurate method to determine dextran content in a sample. A new technique of dextran

determination was developed using the application of ^{13}C NMR. It was seen that it can be used for quantitative dextran analysis but the detection limit of the NMR method is about 0.2% dextran content in the initial solution sample, which is not suitable for use in the further study concerns dextran reduction for the solution samples containing very low dextran content, in the level of ppm. Therefore, traditional methods such as the Roberts test and the CSR method were considered to use in the membrane separation study and the partition coefficient study.

Dextran separation from a synthetic clarified juice stream that contained a total dissolved solid of 15% Brix (mostly sucrose) was performed on a stirred-cell filtration unit in dead-end mode. It was seen that although the dextran used in the current study has a molecular weight of more than 50,000 Da, there is a low percent rejection by the regenerated cellulose membrane with a 30,000 MWCO. This is a result of the snake movement of linear molecules such as dextran through the membrane. Therefore it was decided to use a lower pore size membrane, such as the regenerated cellulose membrane with a 5,000 MWCO. This is supported by the result that this membrane has a larger percent rejection than that of the other membranes, while its flux is still suitable. Furthermore, it was seen that the flux in the membrane separation of the synthetic solutions can be improved both by operating at a higher agitation speed and increasing transmembrane pressure as much as possible without causing damage to the membrane. In contrast, the percent rejection improvement is more restricted since high transmembrane pressure can induce more dextran passage through the membrane. Thus the rejection improvement can be achieved only by the increasing agitation rate, which is a factor for dispersion of accumulated dextran at the membrane surface. The dextran accumulation is commonly known as

concentration polarization, and has an influence on the probability of passage of dextran through the membrane.

The study on membrane fouling by flux decay observation was performed to characterize the mechanism of the fouling. The k parameters from the flux decay fitting were used for characterization of the fouling mechanism. It was seen that the fouling mechanism in unstirred dead-end filtration is dominated by the cake formation of dextran. By an improved method using k parameters, the determination of the dextran cake compressibility showed that the cake compressibility varied from 0.52 to 0.54. The fouling mechanism in 100 rpm stirred filtration is described by the complete pore blocking model. In addition, the resistances of the polyethersulfone membrane and the regenerated cellulose membrane were determined based on Darcy's Law, which gives membrane resistances of $1.80\times10^{13}\,\mathrm{m}^{-1}$ and $3.36\times10^{13}\,\mathrm{m}^{-1}$, respectively.

In the dextran partition coefficient study, it was found that the partition of dextran from solution into the crystal product increases with either increasing of the crystallization temperature or increasing of the supersaturation of the sucrose solution. However it appears that these are secondary effects, with the partition coefficient correlating almost perfectly with the crystal growth rate alone. The relation between the dextran partition coefficient and the crystal growth rate can be expressed in an empirical form as $K_{eff}[\%]=(9.8\pm1.0)\times\left(1-\exp^{(-1.7\pm0.4)G}\right)$. Knowledge was enhanced on the influence of grow rate on dextran incorporation, and this may be used as basic information in the sugar crystallization process design to reduce dextran contamination in the sugar product.

A study on incorporation of dextran into the crystalline phase in sucrose crystallization showed that there is concentrated dextran contamination present in the region that is closest to the crystal surface, while deeper regions inside the crystal have a lower concentration. Since the moisture content in the crystal product does not strongly relate to the crystal growth condition, the rate of crystal growth does not have a significant effect on the amount of liquid inclusion. Alternatively, the crystal growth at high rate can induce a greater roughening on the crystal surface than apparent for growth at a lower rate. The amount of dextan incorporating into the crystal is too high (varying from 3 to 10% for the current study) to describe with a liquid inclusion mechanism only, it also varies with crystal growth rate, that is controlled by the crystallization condition. Therefore it can be suggested that the mechanism of dextran incorporation is controlled both by liquid inclusion and surface adsorption, with surface adsorption being the more significant mechanism.

8.2 Recommendations

Dextran separation in the current study was conducted in a dead-end filtration cell while most membrane separations in industrial processes are operated using cross-flow filtration applications. The concentration of dextran in feed stream was increasing with operating on dead-end filtration mode so it can be not employed for using in actual industrial membrane processes directly without some modifications. The modification of filtration mode is quite complex both for modeling and operating. However this research was done on the assumption that dextran content in feed solution is very small, and these will not cause a significant change in the solution properties, especially viscosity. The assumption is described in Appendix E.

The growth rate for sucrose crystallization used in this work was determined based on the assumption that number of product crystals is the same as the number of seeds, i.e. no nucleation, agglomeration, and breakage. This can be realized by maintaining the crystallization condition below the secondary nucleation limit. However there is growth rate dispersion effect on the growth rate determination in the research so it is very difficult to measure an accurate the growth rate of an individual crystal. Therefore the crystal growth rate was averaged by mass. The growth rate dispersion would be more evident in actual sugar crystallization in the factory since the growth is commonly performed in a larger system.

Appendix A

Dextran Elimination Methods in the Review of Literature

A-1 Dextran Elimination Methods

In the sections below are the details of experimental procedures used for laboratory scale simulation of refinery processes discussed for dextran elimination methods in the review of literature (Chou and Wnukowski, 1981).

1. *Affination*

300 mL of 64% Brix sugar syrup at room temperature was slowly added into 1000 g of sugar sample at a uniform rate for 5 min. The sugar sample and the syrup were mixed by agitation at low speed for one more minute making the total mingling time 6 min. The sugar crystals were separated by a centrifuge at 3,000 rpm for exactly two minutes and the crystals were dried to air for approximately one hour.

2. *Clarification Processes*

Carbonation: CaO was added into 500 g of washed sugar liquor in various amounts from 0.70 to 0.76% on a solid basis. The liquor was heated to approximately 80°C allowing CO_2 gas to dissolve into the liquor to adjust the pH to about 8.2. The liquor was then paper filtered through a vaccum filter. Treated and untreated liquors were collected for later analysis.

Phosphatation: 500 g of washed sugar liquor was heated to approximately 75°C then 0.025% of phosphoric acid solution was added into the liquor. The pH of the liquor was then adjusted to approximately 7.2 by the addition of calcium saccharate solution, and 8 ppm on a sugar solids basis of polyacrylamide was added to aim the flotation of scum. 100mL Nessler tubes with bottom outlets were used to contain the liquor then they were heated in a water bath at 90°C for approximately 30 minutes to float scum to the top. The clear bottom liquor was then drained off and filtered through a filter paper to remove suspended impurities.

Phosphatation plus Cationic Surfactant Additives: The procedure of phosphatation plus cationic surfactant additives is similar to the phosphatation process as in the above described procedure except for the addition of 350 ppm of a cationic surfactant before the polyacrylamide addition.

3. *Adsorption Processes*

Bone Char and Granular Carbon: A 60% Brix feed liquor was prepared from washed raw sugar. A column filled with an adsorbent granular carbon or bone char was prepared. The column was maintained at 80°C by temperature controlling with a jacket. The liquor was flowed through the column at a constant rate of 1.2 mL/min. The effluents were collected approximately in fraction 24 mL every 20 min. Two sample composites, one made by collecting fractions 7-12 and the other made by collecting fractions 47-52, were prepared for later analysis.

Powdered Activated Carbon: A 60% Brix feed liquor was prepared from washed raw sugar. The pH of the liquor was adjusted to 7.0 ± 0.05 then the liquor was split into five equal 250 g portions. The liquor portions were heated in a water bath to 80°C. At this point four liquor portions were treated with about 0.3% of activated carbon from various sources for 20 min of total contact time. One liquor portion was set as the blank. At the end of the contact process, the liquors were filtered through a vacuum filter to remove suspended carbon.

4. *Crystallization*

A rotary flask was used as a vacuum pan for sugar crystallization process. 1,000 g of liquor was transferred to the flask then the liquor was concentrated to 76.5% Brix by evaporation at 155°F. Refrigeration was used to condense the vapor from the flask at 40°F. One gram of seed was placed into the

concentrated liquor and continued boiling the liquor to grow the seed for one additional hour. The sugar product was then separated from the liquor by a centrifuge at 3,000 rpm for 15 minutes. The crystal product was dried to air and stored for later analysis.

A-2 Reference

Chou, C. C. and Wnukowski, M. (1981). Dextran problems in sugar refining: A critical laboratory evaluation. In: **Proceedings of the 1980 Technical Session on Cane Sugar Refining Research** (pp. 1-25). LA, USA: Science and Education Administration.

Appendix B

Peak Integral Data for NMR Method Calibration

Table B-1 Dextran precipitation in 57.5% Brix sucrose solution by adding ethanol.

Final Ratio of Ethanol : solution sample	**C6 peak integral of dextran**
0.5	0
1.0	0.66
1.5	0.67
2.0	0.76
2.5	0.76
3.0	0.74
3.5	0.73

Note: the solution containing 6% by mass dextran,

Table B-2 C6 peak integral of dextran for four replicates in the NMR method calibration.

% Dextran content in sample solutions	**C6 peak integral of dextran**				**Average peak integral**	**SD**
	Run#1	Run#2	Run#3	Run#4		
2	0.50	0.36	0.34	0.46	0.42	0.077
9	1.33	1.35	1.35	1.33	1.34	0.012
15	1.98	1.96	1.93	1.92	1.95	0.028

Appendix C

Dextran Molecular Weight Distribution

C-1 The Molecular Weight of Dextran Used in the Current Study

Report for molecular weight determination of polymer, performed using GPC with the following conditions:

Eluent: 0.1 M sodium nitrate

Flow rate: 0.6 mL/min.

Injection volume: 20 μL

Temperature: 30°C

Column set: Ultrahydrogel linear

(MW resolving range = 1,000-20,000,000)

1 column + guard column

Polymer standard: Polysaccharide (Pullulan: MW 5,900-788,000)

Calibration method: Polysaccharide standard calibration

Detector: Refractive Index Detector

Sample preparation: Samples (2mg/mL) were dissolved in eluent and filtered with nylon 66 membrane with pore size 0.45 μm before injection.

Polydispersity index: the polydispersity index (PDI), is a measure of the distribution of molecular weight of polymer sample. The PDI can be calculated by dividing the weight average molecular weight by the number average molecular weight.

Number average molecular weight: Number average molecular weight $\overline{M}_n$ is determined by measuring the molecular weight of n polymer molecules, summing the weight, and dividing by n.

$$\overline{M}_n = \frac{\sum_i n_i M_i}{\sum_i n_i} \tag{C.1}$$

Weight average molecular weight: Weight average molecular weight $\overline{M}_w$ can be defined as

$$\overline{M}_w = \frac{\sum_i n_i M_i^2}{\sum_i n_i M_i} \tag{C.2}$$

Table C-1 Molecular weight of dextrans.

Sample description	$\overline{M}_n$ **(Da)**	$\overline{M}_w$ **(Da)**	M_p **(Da)**	**Polydispersity**
Low fraction dextran	3.8×10^4	7.0×10^4	5.3×10^4	1.9
High fraction dextran	3.7×10^4	2.3×10^5	1.4×10^5	6.2
1:1 mixture of low and high fraction dextran	4.0×10^4	1.4×10^5	5.4×10^4	3.5

Table C-2 Molecular weight of polysaccharides contained in samples.

Sample description*	$\overline{M}_n$ **(Da)**	$\overline{M}_w$ **(Da)**	M_p **(Da)**	**Polydispersity**
Polysaccharides in raw sugar	2.8×10^4	9.7×10^4	2.3×10^4	3.5
	1.7×10^3	2.2×10^3	1.7×10^3	1.3
	$<1.0\times10^3$	$<1.0\times10^3$	$<1.0\times10^3$	1.1
Polysaccharides in clarified juice	2.4×10^4	4.4×10^4	5.6×10^4	1.8
	1.5×10^3	1.8×10^3	1.6×10^3	1.2
	$<1.0\times10^3$	$<1.0\times10^3$	$<1.0\times10^3$	1.1
Polysaccharides in raw syrup	3.4×10^4	5.1×10^4	6.2×10^4	1.5
	1.4×10^3	1.7×10^3	1.6×10^3	1.2
	$<1.0\times10^3$	$<1.0\times10^3$	$<1.0\times10^3$	1.1

* The samples collected from the factory

Appendix D

Flux Decay Fitting

D-1 Fouling Model for Stirred Dead-End Filtration in Dilute Solution System Assumption.

Both unstirred and stirred dead-end filtration was used in the current study. The flux fitting model for unstirred dead-end can use flux decline without cross-flow removal given by Hermia (1982). On the other hand, for the flux fitting model for stirred dead-end it is necessary to consider cross-flow removal due to stirring. For the dilute solution system, the removal rate of the fouling molecules, *B,* may be considered to be constant so that the stirred cell filtration can be described by the cross-flow filtration model that is based on classical constant pressure dead-end filtration equation

Hermia equation (Hermia, 1982)

$$\frac{d^2t}{dv^2} = k\left(\frac{dt}{dv}\right)^2 \tag{D.1}$$

where v is the volume of filtrate collected from $t = 0$ up to t

k and n are constants and depend on the mechanism of fouling

Since J is a flux at time t (m^3/m^2s)

AJ is the flow rate at time t (m^3/s)

$$\therefore AJ = \frac{dv}{dt} \tag{D.2}$$

$$\therefore \frac{dt}{dv} = \frac{1}{AJ} \tag{D.3}$$

$$\therefore \frac{d^2t}{dv^2} = \frac{d(1/AJ)}{dv} \tag{D.4}$$

Since $A \neq f(v)$

$$\frac{d(1/AJ)}{dv} = -\frac{1}{AJ^2}\frac{dJ}{dv} = -\frac{1}{AJ^2}\frac{dJ}{dt}\frac{dt}{dv} \tag{D.5}$$

And from (D.3)

$$\therefore \frac{d^2t}{dv^2} = -\frac{1}{A^2J^3}\frac{dJ}{dt} \tag{D.6}$$

Hence, from (D.1)

$$-\frac{1}{A^2J^3}\frac{dJ}{dt} = k\left(\frac{1}{AJ}\right)^n \tag{D.7}$$

Comparison between unstirred dead-end filtration and stirred dead-end filtration

(A) Dead-end with complete pore blocking: n=2

The equation becomes

$$-\frac{dJ}{dt} = kJ \tag{D.8}$$

$$J = J_0 e^{-kt} \tag{D.9}$$

(B) Cross-flow filtration with complete pore blocking

For complete pore blocking, each fouling molecule reaching the surface fully blocks a pore: in cross-flow there is a mechanism which removes the particles from the pore

mouth also. Flow through unblocked pore is unchanged. Therefore, fractional reduction in J is equal to the fractional reduction in the open pore area a. Derivations of Field *et al*. (1995)

At $t = 0$, $J_0 = ca_0$

where a_0 is the open area at $t = 0$ and J_0 is the flux at $t = 0$

[Note that J, J_0 are fluxes relative to the total membrane area, A, rather than to the open area, a].

$$J = ca \tag{D.10}$$

If the flux reduction in Δt is $J_0 - J = \Delta J$, and the area reduction in the same time is

$$a_0 - a = \Delta a \tag{D.11}$$

then $$\frac{\Delta J}{J_0} = \frac{\Delta a}{a_0} \tag{D.12}$$

dividing by the relevant Δt

$$\frac{(\Delta J / \Delta t)}{J_0} = \frac{(\Delta a / \Delta t)}{a_0} \tag{D.13}$$

and taking the limit as $\Delta t \to 0$

$$\frac{(dJ / dt)}{J_0} = \frac{(da / dt)}{a_0} \tag{D.14}$$

If there is no molecule removal from the surface, then

$$a = a_0 - A_b v \tag{D.15}$$

where A_b is the blocked area per unit volume of filtrate passed through the membrane

From (D.14) and (D.15), can achieve

$$\frac{dJ}{dt} = \frac{J_0}{a_0}\frac{da}{dt} \tag{D.16}$$

$$\frac{da}{dt} = -A_b \frac{dv}{dt} \quad \text{and} \quad \frac{dv}{dt} = AJ \tag{D.17}$$

so $$\frac{da}{dt} = -A_b AJ \tag{D.18}$$

$$\therefore \frac{dJ}{dt} = -\frac{J_0 A_b AJ}{a_0} \tag{D.19}$$

but $a_0 = \varepsilon_0 A$, so

$$\frac{dJ}{dt} = -\frac{J_0 A_b J}{\varepsilon_0} \tag{D.20}$$

If flow across the membrane surface removes particles from the surface then we need to modify equation (D.18) to account for this

$$\frac{da}{dt} = -A_b AJ + Ba_0 \tag{D.21}$$

where B depends on the removal rate, and ε_0

It can be substituted into equation then gives

$$\frac{dJ}{dt} = \frac{J_0}{a_0}\left(-A_b AJ + Ba_0\right) \tag{D.22}$$

Since $a_0 = \varepsilon_0 A$, the above equation becomes

$$\frac{dJ}{dt} = -\frac{A_b J_0 J}{\varepsilon_0} + BJ_0 \tag{D.23}$$

Equation (D.23) is first order-inhomogeneous ODE that can be solved to be

$$J = \frac{B\varepsilon_0}{A_b} + Ce^{-\left(\frac{\alpha J_0}{\varepsilon_0}\right)t} \tag{D.24}$$

Since the second term reaches to be zero for infinite time, $J_{\lim} = \frac{B\varepsilon_0}{A_b}$ can be defined

$$\therefore J = J_{\lim} + Ce^{-\left(\frac{\alpha J_0}{\varepsilon_0}\right)t} \tag{D.25}$$

Determine C by using the initial condition $J(0) = J_0$

$$C = J_0 - J_{\lim} \tag{D.26}$$

$$J = J_{\lim} + \left(J_0 - J_{\lim}\right)e^{-\left(\frac{\alpha J_0}{\varepsilon_0}\right)t} \tag{D.27}$$

D-2 References

Hermia, J. (1982). Constant pressure blocking filtration laws. Application to power law non-Newtonian fluids. **Trans. Inst. Chem. Eng.** 60: 183-187.

Field, R. W., Wu, D., Howell, J. A., and Gupta, B. B. (1995). Critical flux concept for microfiltration fouling. **J. Membr. Sci.** 100: 250-272.

Appendix E

Crystal Growth Rate and Dextran Partition Coefficient

Table E-1 Dextran partition coefficeint for crystallization in the solution containing 2,000 ppm/Brix of various dextrans.

Compositions	**Dextran partition coefficient K_{eff} for CSR method replicates (%)**				**%$K_{eff,ave}$**	**SD**
	Run#1	Run#2	Run#3	Run#4		
100% low fraction dextran	6.8	7.2	6.3	7.7	7.0	0.6
100% high fraction dextran	7.3	7.6	8.0	7.1	7.5	0.4
1:1 mass ratio of low and high fraction dextrans	7.5	7.3	-	-	7.4	0.1

Note:The crystallization was performed at temperature of 40°C and 0.07 relative supersaturation.

Table E-2 Crystal growth rate determination for crystallization in the solution containing 1,000 ppm/Brix of dextran.

Temperature (°C)	**Relative supersaturation (-)**	**Product mass (grams)**	**Resident time (hours)**	**Mean growth rate by mass (μm/min.)**
30	0.05	8.15	30	0.17
30	0.07	11.13	23	0.26
30	0.09	8.92	15	0.36
40	0.05	11.60	15	0.41
40	0.07	11.12	10	0.61
40	0.09	8.07	6	0.85
50	0.05	9.63	7	0.80
50	0.07	11.69	5	1.24
50	0.09	8.21	3	1.71

Table E-3 Crystal growth rate determination for crystallization in the solution containing 2,000 ppm/Brix of dextran.

Temperature (°C)	**Relative supersaturation (-)**	**Product mass (grams)**	**Resident time (hours)**	**Mean growth rate by mass (μm/min.)**
30	0.05	8.54	32	0.16
30	0.07	11.43	23	0.27
30	0.09	8.23	16	0.31
40	0.05	13.76	15	0.45
40	0.07	10.33	10	0.58
40	0.09	9.35	7	0.79
50	0.05	11.21	7	0.87
50	0.07	11.35	5	1.22
50	0.09	13.53	4	1.67

Table E-4 Dextran partition coefficeint for crystallization in the solution containing 1,000 ppm/Brix of dextran.

Temp. (°C)	**Relative supersat. (-)**	**Dextran partition coefficient K_{eff} for CSR method replicates (%)**				**Average %K_{eff}**	**SD**
		Run#1	Run#2	Run#3	Run#4		
30	0.05	4.2	2.4	2.1	3.7	3.1	1.01
30	0.07	3.7	2.9	5.2	3.5	3.8	0.98
30	0.09	5.5	4.3	3.7	3.2	4.2	0.99
40	0.05	3.7	4.9	6.1	4.3	4.8	1.02
40	0.07	8.5	7.8	6.8	7.2	7.6	0.74
40	0.09	9.1	7.4	8.1	8.6	8.3	0.73
50	0.05	6.4	4.1	5.4	4.7	5.2	0.99
50	0.07	7.5	8.4	9.1	9.5	8.6	0.88
50	0.09	11.6	9.4	8.0	10.2	9.8	1.51

Table E-5 Dextran partition coefficeint for crystallization in the solution containing 2,000 ppm/Brix of dextran.

Temp. (°C)	**Relative supersat. (-)**	**Dextran partition coefficient K_{eff} for CSR method replicates (%)**				**Average %K_{eff}**	**SD**
		Run#1	Run#2	Run#3	Run#4		
30	0.05	3.2	3.8	3.3	2.7	3.3	0.47
30	0.07	4.2	3.0	-	-	3.6	0.88
30	0.09	4.4	3.1	4.0	3.4	3.7	0.57
40	0.05	4.6	5.6	4.2	4.9	4.8	0.60
40	0.07	7.5	7.3	-	-	7.4	0.14
40	0.09	9.3	9.0	8.4	7.9	8.7	0.60
50	0.05	5.8	6.5	-	-	6.1	0.49
50	0.07	8.7	8.3	-	-	8.5	0.28
50	0.09	9.2	10.0	-	-	9.6	0.57

Table E-6 Total polysaccharides distribution data in raw sugar crystal made from three replicates of CSR method.

Sugar-free mixture of solvents by mass percentage	**%Crystal mass removed**	**Total polysaccharides in crystal remains from mingling (ppm)**			**Average %TPS removed**
		Run#1	Run#2	Run#3	
Isopropyl alcohol	0	845	838	829	0
95% ethanol-water mixture	0.43	828	837	811	1.39
100% methanol	1.55	777	786	794	6.09
95% methanol-water mixture	2.76	632	604	597	27.0
90% methanol-water mixture	4.40	602	593	574	29.5
85% methanol-water mixture	7.38	544	525	558	35.2
80% methanol-water mixture	11.12	455	426	443	47.3
75% methanol-water mixture	15.75	414	396	425	50.8
70% methanol-water mixture	23.53	386	362	348	56.4
65% methanol-water mixture	31.54	336	312	285	62.8

Table E-7 Dextran distribution data in raw sugar crystal.

(Three replicates of Roberts test).

Sugar-free mixture of solvents by mass percentage	**%Crystal mass removed**	**Dextran in crystal remains from mingling (ppm)**			**Average % Dextran removed**
		Run#1	Run#2	Run#3	
Isopropyl alcohol	0	120	124	136	0
95% ethanol-water mixture	0.43	114	127	132	2.10
100% methanol	1.55	107	118	112	11.8
95% methanol-water mixture	2.76	96	104	92	23.6
90% methanol-water mixture	4.40	95	85	98	26.8
85% methanol-water mixture	7.38	93	77	81	33.9
80% methanol-water mixture	11.12	68	73	81	41.7
75% methanol-water mixture	15.75	66	71	58	48.8
70% methanol-water mixture	23.53	69	55	51	54.3
65% methanol-water mixture	31.54	59	52	46	59.0

BIOGRAPHY

Mr. Arwut Promraksa was born on the 4th of April 1981 in Loei province. He earned his Bachelor's degree (Second Class Honours) in Chemical Engineering from Suranaree University of Technology (SUT), Nakhon Ratchasima, in 2003. He has received a scolararship for his Ph.D. study in Chemical Engineering at SUT from the Thailand Research Fund (TRF) through the Royal Golden Jubilee (RGJ) program since 2003. He has been an occupational trainee in the Division of Chemical Engineering at James Cook University (JCU), Townsville, Australia during 2007. His expertise includes the fields of sugar crystallization and fouling in membrane separation of impure sucose juice.